Examiner's copy

THE DEVELOPMENT AND APPLICATION OF A REAL-TIME ELECTRICAL RESISTANCE TOMOGRAPHY SYSTEM

Peter Ayotola Adigun

A dissertation submitted to the School of Electrical, Electronic & Computer Engineering,

University of KwaZulu-Natal, in fulfilment of the requirements for the degree of Master of Science in Engineering.

Declaration

I ..... declare that

(i) The research reported in this dissertation/thesis, except where otherwise indicated, and is my original work.

(ii) This dissertation/thesis has not been submitted for any degree or examination at any other university.

(iii) This dissertation/thesis does not contain other persons' data, pictures, graphs or other information, unless specifically acknowledged as being sourced from other persons.

(iv) This dissertation/thesis does not contain other persons' writing, unless specifically acknowledged as being sourced from other researchers. Where other written sources have been quoted, then:

a) their words have been re-written but the general information attributed to them has been referenced;

b) where their exact words have been used, their writing has been placed inside quotation marks, and referenced.

(v) Where I have reproduced a publication of which I am an author, co-author or editor, I have indicated in detail which part of the publication was actually written by myself alone and have fully referenced such publications.

(vi) This dissertation/thesis does not contain text, graphics or tables copied and pasted from the Internet, unless specifically acknowledged, and the source being detailed in the dissertation/thesis and in the References sections.

Signed:

To my family

Acknowledgement

A heartfelt thank you goes to all the people who have contributed to the completion of this research in one way or another:

1. Dr Leigh Jarvis, my supervisor, for the chance to do a M.Sc. under your supervision, for always being available to point me in the right direction and for the innumerable sponsored lunches.
2. Jonathan Archer, Brett Swann, Neil Hendry, Jonathan Turck, Roland Harrison, Darryl Daniel and Sergio Babet, fellow postgrads and Material science Lab colleagues, for always being available to run ideas past you and for the constant distractions (you know who you are).
3. SMRI and Tongaat Huletts our industry partners and sponsors of the research.
4. Mr Anthony Lester, for all your help with the technical side of things.
5. Mr Moonsamy Naidoo, for your constant willingness to go above and beyond when I need to purchase equipment.

Please note that the contents of this dissertation are considered confidential.

Abstract

This dissertation focuses on the application of tomography in the sugar milling process, specifically within the vacuum pan. The research aims to improve the efficiency and throughput of a sugar mill by producing real-time images of the boiling dynamic in the pan and hence can be used as a diagnostic tool. The real-time tomography system is a combination of ruggedized data collecting hardware, a switching circuit and software algorithms. The system described in this dissertation uses 16 electrodes and estimates images based on the distinct differences in conductivities to be found in the vacuum pan, i.e. a conductive syrup-like fluid (massecuite) and bubbles.

There is a direct correlation between the bubbles produced during the boiling process and heat transfer in the pan. From this correlation one can determine how well the pan is operating. The system has been developed in order to monitor specific parts of a pan for optimal boiling. A binary reconstructed image identifies either massecuite or water vapour.

Each image is reconstructed using a modified neighbourhood data collection method and a back projection algorithm. The data collection and image reconstruction take place simultaneously, making it possible to generate images in real-time. Each image frame is reconstructed at approximately 1.1 frames per second. Most of the system was developed in LabVIEW, with some added external drive electronics, and functions seamlessly. The tomography system is LAN enabled hence measurements are initiated through a remote PC on the same network and the reconstructed images are streamed to the user.

The laboratory results demonstrate that it is possible to generate tomographic images from bubbles vs massecuite, tap water and deionized water in real-time.

Table of Contents

List of Figures

List of Abbreviations

ADC: Analogue to digital converter.

CCM: Current control module.

CCS: Constant current source.

cDAQ: Compact data acquisition chassis.

CFD: Computer fluid dynamics.

cRIO: Compact reconfigurable input output chassis.

CT: computerized tomography.

ECT: Electrical capacitance tomography.

EIT: Electrical impedance tomography.

ERT: Electrical resistance tomography.

FEM: Finite element method.

HTTP: Hypertext transfer protocol.

LabVIEW: Laboratory virtual instrument engineering workbench.

MATLAB: Matrix laboratory.

MRI: Magnetic resonance imaging.

MUXA: Multiplexer A.

MUXB: Multiplexer B.

OS: Operating system.

PCB: Printed circuit board.

PDIP: Plastic dual inline package.

PSU: Power supply unit.

SMRI: Sugar milling research institute.

SPST: Single pole single throw

TSSOP: Thin shrink small outline package.

UKZN: University of KwaZulu Natal.

USFF PC: Ultra-small form factor personal computer.

VI: Virtual instrument.

VSP: Vacuum sugar pan.

List of Variables

ρ: Resistivity distribution

V: Voltage distribution

f: Current distribution

V_0: Voltage density measured on the boundary surface

J_0: Current density measured on the boundary surface

∂A: Surface area of the object

$c = c(x,y)$: is the conductivity distribution within the medium

R: Log resistance

X_{coord}: X-coordinate

Y_{coord}: Y-coordinate

r: is the radius of the unit circle

t : is the electrode number

ρ_0: is the resistance value when the medium is uniform or homogeneous

$g_m(\theta)$: is the boundary profile taken from a region with a non-uniform (but isotropic) distribution of resistance within the region

$g_u(\theta)$: is the boundary profile taken from a region of uniform resistance

$(V_i\text{-}V_j)$*measured*: $g_m(\theta)$

$(V_i\text{-}V_j)$*expected*: $g_u(\theta)$

w_p: is the weighting factor of each pixel

d: is the distance between the injection point and pixel P

l: is the distance between the centre pixel O and pixel P

1. Introduction

Tomography is a method of reconstructing a cross sectional image of an object. The root word 'tomos' is Greek and is translated to mean a slice. The reconstructed image is referred to as a tomogram and the equipment used in this process is called a tomograph. Although tomography was initially limited to fields like medicine and biology; it is now being used in industry [**1**]. To the best of our knowledge, prior to the work done by the University of Kwazulu-Natal (UKZN) tomography research group, no work involving the application of tomography to vacuum pans has been done.

In this chapter an introduction to the sugar milling industry is presented, followed by previous tomography research conducted in the sugar industry with a focus on sugar pans. A literature review of some relevant real-time tomography systems is presented. The chapter concludes with a discussion of the objectives of this work and the results achieved.

1.1 Sugar Milling

Sugar is the end product of a long process known as sugar milling. This process starts with sugar cane, which is grown in tropical and sub-tropical areas. The harvested sugar cane undergoes the milling process, which includes washing, crushing and rolling, the result of which separates the cane fibres (bagasse) from sugar juice. Once separated the bagasse is used as fuel to power the sugar mill, making the mill independent of the electric grid while, the sugar juice is passed through a gravitational tank (clarifier) to remove soil, stray fibres and excess solids. The juice is then mixed with lime which, apart from maintaining a pH of 7, prevents decomposition into glucose and fructose while precipitating impurities.

The sugar juice then exits the clarifier and passes through a series of evaporators on its way to the vacuum sugar pan (VSP). A high temperature and low pressure environment is created in the VSP. This enables the growth of sugar crystals. The juice is seeded with crystallized sugar in the VSP and undergoes the boiling process via steam pipes embedded in the VSP. The syrup produced by this process is called 'massecuite'. This is then transferred to a crystallization tank where it cools down and its crystals continue to mature. The massecuite is then passed through a series of centrifuges where the crystals are separated from the massecuite, leaving behind a liquid substance known as molasses. The molasses is then sent back to the VSP where they are used to seed new massecuite.

Figure 1-1 shows a cross sectional drawing of the VSP. Massecuite flows up through the calandria tubes and is heated by steam (blue) flowing through the tube walls. The heat eventually spreads through the entire VSP and crystallization occurs when low pressure is combined with the heat, i.e. the evaporation of water.

The heating process through the calandria tubes produces vapour (bubbles) in the tubes. The formation of bubbles affects the conduction of heat through the VSP. Monitoring the boiling dynamics would give chemical engineers a better understanding of their pan designs. Too many bubbles hinder the amount of thermal conduction taking place and too few bubbles cause rapid thermal conduction which leads to hot spots in the pan.

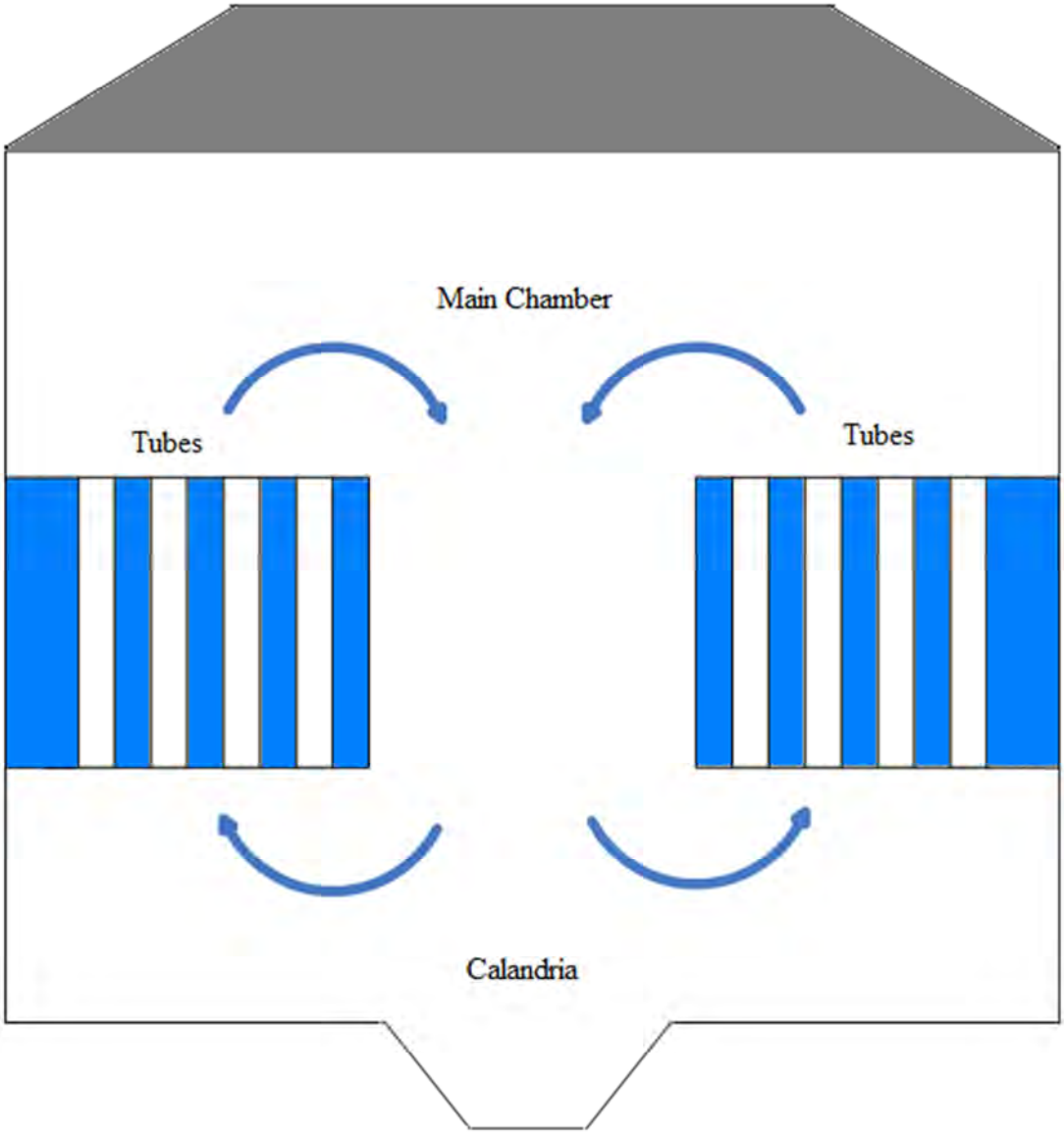

Figure 1-1: Cross sectional view of the Vacuum Sugar Pan

Steam (blue) heats the tubes' walls, which heat the massecuite. The tubes are positioned vertically and are made up of brass, steel or stainless steel 100 *mm* in diameter, 1.5 *mm* wall thickness and approximately 1m in height. The hydrostatic head supresses boiling at the bottom of the tube; vapour generated by the steam inside the tube wall drives the massecuite upwards. As heated massecuite is carried upwards through the tube by bubbles, fresh massecuite enters the tube from the bottom; hence the circulation shown in Figure 1-1.

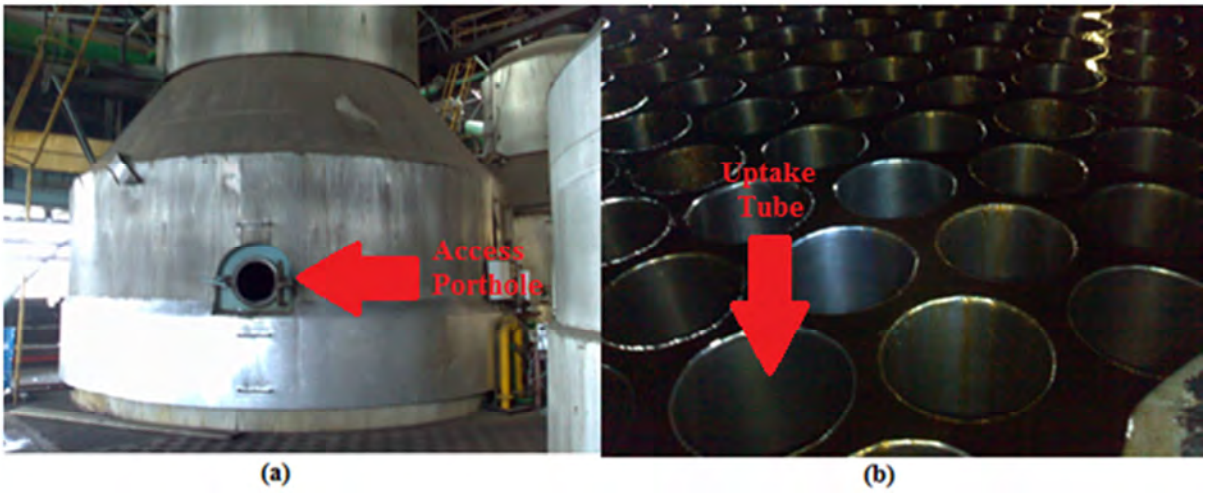

Figure 1-2: (a) Outside view of a vacuum pan, approximately 8metres in diameter (b) uptake tubes inside the vacuum pan.

Figure 1-2a shows the outside view of a VSP with the access porthole visible. The circulation of massecuite in a vacuum pan occurs through steam-generating tubes which heat and transport pockets of massecuite from the base of the pan to the top. Figure 1-2b shows an array of uptake tubes. Massecuite flows from the top to the base of the pan through the hole referred to as the 'down-take' tube. The 'down-take' tube is located at the centre of the VSP.

Due to high operational temperatures and low pressure in the VSP, observing and collecting data from the VSP has been difficult. In order to understand boiling dynamics, laboratory prototypes have been constructed. For example, Echeverri "et al." [**2**] built a lab-scale test rig to replicate uptake tubes and the circulation occurring in a VSP. They managed to reproduce a behaviour referred to as 'slug' or 'slugging'. 'Slugging' occurs at high viscosity values ranging from 0.7 to 110 Pascal-seconds (Pa.s). As viscosity is decreased so does the 'slug' behaviour. 'Slug' is defined as the behaviour where gas congregates into a single large bubble, resulting in strong vibrations and pulsating circulation.

1.1.1 Tomography as a solution

Boiling and crystal growth in pans is considered in part as an art rather than a science. The sugar mills therefore rely on handed-down skills of pan boilers. There is therefore a need to better understand pan boiling as it is from a better understanding that improved pan designs can be introduced. One possible route to better understanding of pan boiling could be real-time observation of the boiling process. Viewing portholes on the pan walls offer a limited view of the internal boiling dynamics of the pan since the opaque massecuite level often rises above the height of the viewing potholes.

As mentioned, the conditions in the VSP are harsh and must be taken into account when planning experiments. It is also vital that all equipment used in the pan study must not interfere with the functioning of the vacuum pan itself.

To this end electrical resistance tomography (ERT) offers an interesting solution in the observation of the boiling dynamics of a VSP. ERT generates images based on different resistances; in this case water vapour in the form of bubbles and massecuite.

1.2 Previous work

Previous tomography work done at UKZN in conjunction with the Sugar Milling Research Institute (SMRI) involved both a study of a clarifier (unpublished work by a member of the UKZN tomography group, Adrian Boutelje) and vacuum sugar pan (VSP) [**3**]. This dissertation focuses on tomography of VSP.

The purpose of the VSP research was to investigate tomography as a possible tool for detecting areas of high and low conductivity in a vacuum pan. This is because water vapour, produced during the boiling of massecuite in a VSP, has low conductivity while massecuite is highly conductive in comparison. A prototype was designed and tested at the sugar mill and proof of principle was shown. It formed the basis of knowledge which this research aims to builds on.

1.2.1 Design

Prior to this work, an off-line tomography system was designed by Daniel Sanderson [**3**] to perform experiments at the sugar mill. The design was split into two main components: data collection and image reconstruction.

The data collection part included a collar, which is a structure that secures sensor electrodes above one of the uptake tubes (shown in Figure 1-2b), switching circuit and a data collecting module. Data collecting was achieved by use of IOtech's DAQBOOK 2001 which was controlled through a software package known as DASYLab. This formed the data collection portion of the tomography system.

The image reconstruction portion was achieved offline with the help of MATLAB by using the partial differential equation (PDE) tool to model images. The PDE tool generates a mesh of the interior of the object and uses the data recorded by the electrodes on the boundary of the collar to solve the mesh.

Before the development of the real-time tomography system a number of experiments were conducted at a sugar mill on three different occasions, August 2008, November 2008 and October 2009.

In August 2008, measurements were taken during the following activities at the sugar mill: steaming the pan prior to being filled with massecuite, during initial syrup + steam run (creates a foamy mixture), with pan full of massecuite prior to boiling and while the pan was 40% full, at 61^{o}C, -89.6kPa.

In November 2008 three collars were placed at different zones within the VSP so as to gain insight into the boiling actions taking place at different zones within the pan. One collar was placed near the

down-take tube another placed near the pan wall and the third collar was placed between the down-take and the pan wall.

Measurements were taken while the pan was being filled to capacity. They were taken at 1%, 5%, 18%, 53% and 87% capacities.

In October 2009 three collars were again placed at the same points in the pan. Measurements were taken at different times during the boiling process. From the initial steaming to the striking (a forceful emptying of the VSP by opening the exit at the bottom of the pan) that takes place after boiling.

The results collected during the three mill experiments were taken back to the laboratory to be processed. The results showed different boiling behaviour, including the 'slug' mode. The results were considered successful as they could give the boiler of the pan an indication of the pan state and engineers insight into the behaviour of their new possible designs. A major problem identified was the fact that the tomography images were produced sometime after the boiling.

1.3 Real-time tomography systems

Previous work done in the vacuum pan was successful as it achieved its main objective which was to show that tomography could be used as tool for detecting high (massecuite) and low (water vapour) conductivity areas in a VSP [**3**]; resulting in the detection of different boiling dynamics.

There was also a mechanical contribution, notably a 'collar' which was fixed above a tube of interest. The collar was semi-permanently fixed to the top of an uptake tube; which secured the collar during boiling or striking processes.

However, the limitation is the fact that the design can only collect data at the mill and requires post-processing in order to reconstruct the images of the boiling process. A real-time system would be more useful in understanding pan boiling dynamics i.e. measured data is reconstructed into an image almost immediately thus requiring no post-processing. The real-time implementation would be more beneficial, for example, if a zone within the VSP is not performing as it should, hence the 'live' reconstructed images can be used as a diagnostic tool. There is therefore a case to be made for the research and development of a real-time tomography system for a VSP. Another contribution would be the fact that theoretical computer fluid dynamics (CFD) predictions of pans can be confirmed.

LabVIEW is a National Instruments (NI) software package which allows for fast development of applications due to its user friendly, block diagram, programming interface. It is also easily interfaced with custom hardware produced by NI. This means the entire real-time system can be designed on one software package. This is a better design since it will be easier to debug such a system than a system which runs software and hardware across different platforms. There is therefore a case to be made for the research and development of a real-time tomography system for the VSP.

There are a number of real-time tomography systems in use. High speed x-ray and ultrasound systems have made it possible to produce two and three-dimensional images. These have been extremely useful in medical imaging ([**4**], [**5**]) and in security checks at airports and train stations [**6**].

The EIT work done by Smith *"et al."* [**5**] was of particular interest as there were similarities between their system design and the design of the offline VSP research on which this work is based. The design is specifically for observing lung ventilation and lung perfusion in real-time. It produces images at 25frames per second. The design uses 'transputers', which can be used to perform parallel computing resulting in an increase in processing speed. More processing power can be added to the system by adding more transputers to the system network without needing a system redesign. The image reconstruction algorithm used was a weighted back projection whose advantage over some other reconstruction algorithms is that it is not iterative. The in vivo and in vitro results presented show that ventilation and perfusion were successfully observed.

There are several other real-time EIT systems that have been developed, for example Briggs [**7**] and Heikkinen [**8**]. Brigg's group built a real-time three dimensional EIT system which allowed for interactive manipulation of the user's view of the image. This was done because the typical monitor is a two dimensional display and would not adequately display the depth cues of a three dimensional image. The system was built due to the need to track patient events and view the effect of certain procedures in real-time.

Heikkinen *"et al."* discarded the method of combining several layers of two dimensional images to form a three dimensional image as it can be erroneous and does not produce an actual three dimensional image since there is no real three dimensional information used in the image reconstruction. Instead a difference imaging scheme for image reconstruction was introduced along with an efficient data collection protocol which increases sensitivity and reduces data collection time. It is estimated that the system can produce 15 three dimensional EIT images per second. Three dimensional images of air and liquid in a stirred vessel were successfully reconstructed in real-time. This research would have been very useful if the objective was to reconstruct three dimensional images.

1.4 Research objectives

The objectives of this research were:

i.) Develop a real-time tomography system.
ii.) The system must be a compact, portable and standalone solution.
iii.) Must be able to detect changes in conductivity due to the bubbling of massecuite, deionized water and tap water.

After consultation with sugar experts including the SMRI it was agreed that the processing of one frame must be less than two seconds minimum, i.e. 0.5 frames per second.

The problem with this reported research was access to a sugar mill. At the time of system testing it was impossible to access a sugar mill; this was mainly due to internal pressures at the sugar mill. Previous offline work [**3**] had at least proof of principle that EIT was indeed a method that could be used to monitor pan boiling.

1.5 Implementation overview

The system developed for this research is based around an ultra-small form factor (USFF) PC and NI equipment. The USFF PC controls the entire implementation. It runs both the data collection and image reconstruction portions of the design while also acting as a web server for remote access from users in the same local area network. The USFF PC communicates with the compact DAQ chassis (which contains the analogue to digital converter and digital output modules) through a USB port.

The power supply and switching circuit, which forms part of the data collection hardware, were designed and constructed in-house. The switching circuit injects an AC current source (0 – 39 V); this voltage range ensured good performance in an electrically noisy environment like the sugar mill. The system also uses high voltage multiplexers with a small footprint. This helps to keep the board design compact which is a research objective. The software is packaged into an installer and can be installed on any windows operating system from Windows XP upwards without the need for LabVIEW to be installed on those PCs. The final implementation is neat and compact.

1.6 Experiment and result overview

This section is divided into two parts. The first part briefly discusses experiments that were performed and the second contains results obtained from the experiments.

1.6.1 Experiment overview

All tests were carried out in the laboratory as access to a sugar mill proved impossible during the time of testing with the sugar mill in 2011; it is costly and there are certain requirements that made access difficult.

In the design of a real-time system it is important to investigate the limitations that could affect the system's speed i.e. how much the capacitive medium of massecuite will affect image quality.

Since a mill test was not possible, modifications were made to the collars by fitting a base and a tube to the bottom of the cylindrical collar. Tests were performed on the collars by filling them with a synthetic massecuite, deionized water and tap water. The synthetic massecuite was used during the lab test so that the exact conditions in a VSP during boiling would not have to be recreated; instead the

synthetic massecuite has been designed to have the same electrical characteristics at room temperature as real massecuite does at boiling temperature.

Proof of principle would be achieved by tracking the movement of a non-conducting PVC rod in the tomography sensing zone. Finally bubbles of compressed air would be forced from the bottom of the collar and detected when they move through the sensing zone.

1.6.2 Result overview

What is crucial to a real-time tomography system is the maximum speed it can generate a frame. It was thought that the massecuite's capacitive nature may be a limiting factor, and hence this was measured. A voltage of 39V was injected into massecuite of approximately 52 mm^3 (collar radius=55 *mm* and massecuite height=150 *mm*). A 3τ settling time of 31.2μs was measured and proved not to be a limiting factor in the system because the fastest speed the USB compact DAQ chassis can sample the ADC is 35 samples per second, which is equivalent to one sample every 28.6ms. This gives the signal more than enough time to settle and there is no danger of sampling a signal before it has reached its final value.

The USB compact DAQ chassis severely limits the speed at which data is sampled. The chassis sampling rate cannot be set dynamically as it is a hardwired setting only available during the setup of the ADC's profile. The ADC modules on the chassis are capable of 60kilo-samples per second and the chassis is setup to sample on demand. However, the speed at which the LabVIEW application accesses the samples from the ADC severely limits the system speed. This was only discovered during the implementation as none of the compact DAQ's quoted specifications states this. Further investigations show that the slow sampling rate is a feature of the USB version of the compact DAQ. The Ethernet version of the compact DAQ was not considered initially as the Ethernet port is needed to allow users remote access to the system.

Ultimately, the mediums will definitely play a part in the data collection speeds. It is expected that data can be reliably sampled at higher frequencies when the medium is tap water and deionized water but the capacitive nature of massecuite means that a delay period will have to be implemented before data can be collected.

The experiments carried out to test if the number of collars enabled by the user affects the data collection rate showed that as more collars are added to the system the rate at which data is collected decreases. This makes sense since adding more collars means the chassis is sampling more channels simultaneously while its sampling frequency is fixed at 35Hz. This means the system is fastest when one collar is enabled and slows down as more collars are added.

The experiments to test if conductivity changes can be detected in the three different mediums (massecuite, deionized water and tap water) successfully detected the change in conductivities at the

centre and the periphery of the collar when the PVC rod was moved around inside the sensing zone confined by the collar. Bubbles were also successfully detected in all three mediums.

This chapter discussed previous work and other EIT systems that laid the foundation for this research. The problem requiring the research was also presented. The need for a real-time system was outlined and the summary of some real-time systems that have been developed were also given. The research objectives were listed and explained while a brief overview of the design, experimental method and results are also included.

1.7 Structure of dissertation

The structure of this dissertation is the following:

Chapter 2 introduces electrical impedance tomography and discusses some common data collection methods.

Chapter 3 discusses the tomography theory in general. It also contains an explanation of the theory that governs the reconstruction algorithm (back projection) and the weighting method.

Chapter 4 is the design and implementation chapter and involves the design decisions taken involving the hardware and software used in the implementation. It includes an implementation discussion.

Chapter 5 discusses the results obtained from the laboratory.

Chapter 6 discusses some future improvements.

Chapter 7 is the conclusion of the dissertation.

2. Tomography techniques

There are a number of techniques that rely on the science of tomography e.g. x-ray imaging, magnetic resonance imaging and computerized tomography [**9**]. Electrical impedance tomography is the technique focused on by this dissertation.

2.1 Electrical Impedance Tomography (EIT)

EIT is an imaging method that estimates the electrical properties at the interior of an object using measurements made on the surface of the object. EIT focuses on both the resistive and reactive properties of an object. However, there are applications which require only the resistive or reactive component of an object's impedance to reconstruct an image. When only the reactive component is taken into account the method is referred to as electrical capacitance tomography (ECT). When only the resistive component is taken into account the method is referred to as electrical resistance tomography (ERT).

2.1.1 Electrical capacitance tomography (ECT)

ECT is a technique for measuring and reconstructing a cross sectional image of the permittivity distribution in an object. Extra care is required for equipment design as electronic components can add extra capacitance to that being measured from the object. This makes ECT more suited to applications when the tomogram of a nonconductive object is desired.

2.1.2 Electrical resistance tomography (ERT)

ERT is a technique for taking measurements to generate a cross sectional image of the resistivity distribution in an object. The technique involves applying currents to electrodes on the surface of the object and measuring voltages from the other (non-current) electrodes. They are referred to as data collection methods. Reconstruction algorithms are applied to the measured voltage in order to produce a cross sectional image which represents a resistance distribution in the object.

2.2 Data collection methods

There are a number of data collection methods in existence and each has its benefits and drawbacks. The tomography research group in UKZN has successfully implemented the adaptive (unpublished work) and neighbourhood methods [**3**] on different software packages.

2.2.1 Adaptive method

First proposed by Gisser "et al." [**10**], the adaptive method requires that each electrode has its own current source while a control algorithm is also required to adjust the current magnitude until optimal current is reached. This method is also known as the optimal current method because almost any desired current distribution can be obtained by applying specific current magnitudes simultaneously through all the electrodes. The main advantages of the adaptive method are that it is the most versatile and has the best distinguishability (a measure of the ability of patterns of current to distinguish between different conductivities). The complexity involved in the design of an adjustable current

source per electrode as well as the need for a control algorithm to find the optimal current are disadvantages of the Adaptive method.

2.2.2 Neighbourhood method

This method involves applying or injecting current through two neighbouring electrodes and measuring voltage from the other adjacent pairs of electrodes. Compared to the adaptive method, only one current source is required for this method as multiplexers can be used to select the relevant electrode pairs to a current source.

Figure 1-3 shows current simultaneously applied to electrodes 1 and 2. The voltages are then measured differentially through electrode pairs 3-4, 4-5, 5-6 … 15-16. Current is then applied to electrodes 2 and 3 with the voltage measurement starting from electrodes 4-5 and ending at 16-1. This process is repeated until current has been applied to all 16 electrodes. Each current injection produces 13 voltage measurements. For a 16 electrode system used in this research, 208 (16 x 13) measurements are taken to produce a single image frame. The current distribution derived by this method is non-uniform as most of the currents travel near the periphery of the object. This leads to the area near the electrodes being more sensitive to resistance changes than the area at the centre of the object [**9**].

The neighbourhood method is the most common data collection method in Tomography. It is also less complex than the Adaptive method.

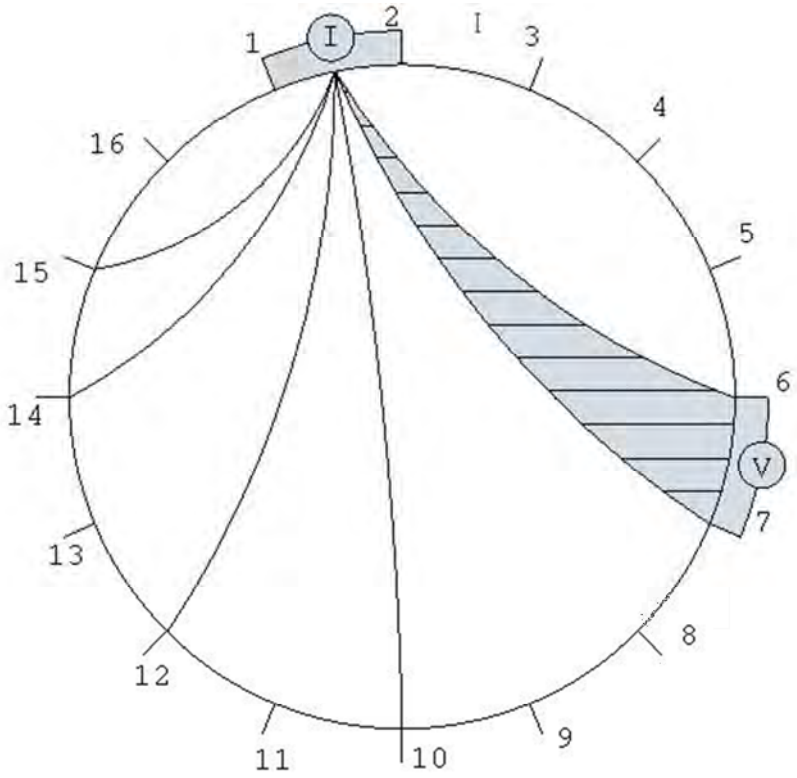

Figure 2-1: Neighbourhood Method; equipotential lines in an homogeneous medium

2.2.3 Cross method

The cross method is more suited when electrodes are separated by large dimensions. The method applied by Hua "et al." [**11**] was as follows: Assuming a 16-electrode system, make electrode 1 the current reference electrode and electrode 2 the voltage reference electrode. Current is then successively applied to electrodes 3, 5, 7 … 15. Voltage is then measured, with respect to the voltage reference electrode, at each electrode except the current electrode. The references are then shifted and the process is repeated until current has been applied to all the electrodes. The cross method is less sensitive on the periphery than the neighbourhood method. However, it has an advantage in that it has a more uniform current distribution, which leads to a more balanced sensitivity across the object. Figure 1-4 shows the equipotential lines obtained when the cross method is applied.

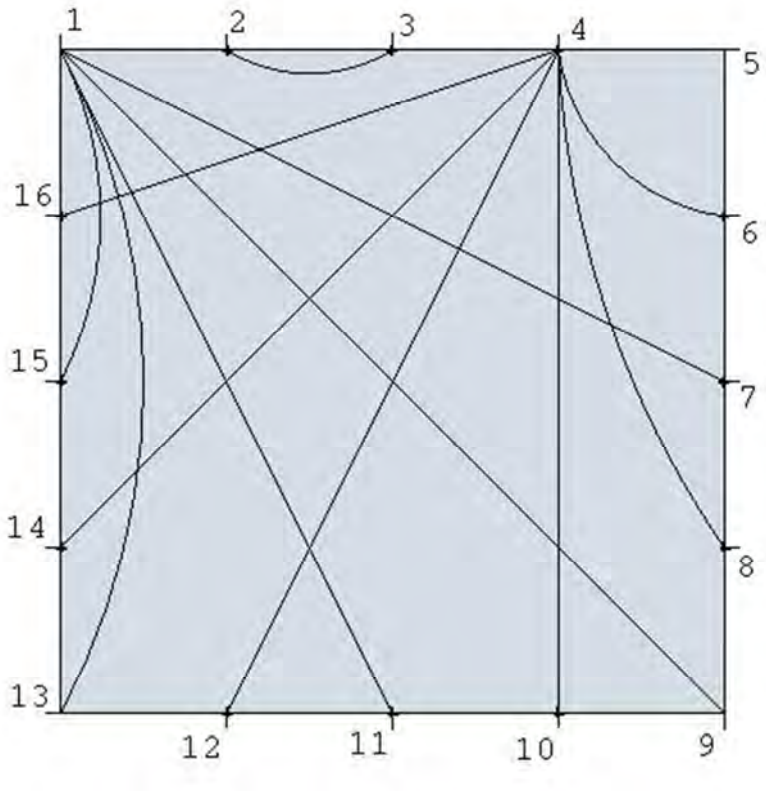

Figure 2-2: Diagram of the equipotential lines generated by the cross method.

2.2.4 Opposite method

This method is also known as the 180 degree method and involves injecting current through diametrically opposed electrodes and setting a voltage reference electrode adjacent to the current injecting electrode. Measurements are then taken from all other electrodes with respect to the reference electrode. The current injecting and reference electrodes are then shifted to obtain the next set of measurements. This is repeated until current has been applied to all electrodes. This method has the distinct advantage in that the number of measurements taken is only half of the measurements taken in the neighbourhood method. This is because only 8 injections are possible as compared to the 16 injections required for the neighbourhood method. The current distribution derived from this method means it has greater sensitivity in the centre and less on the boundary. This is a disadvantage as its overall sensitive area is smaller than in the neighbourhood method. Figure 1-5 shows the current pattern induced by the opposite method for an homogeneous medium.

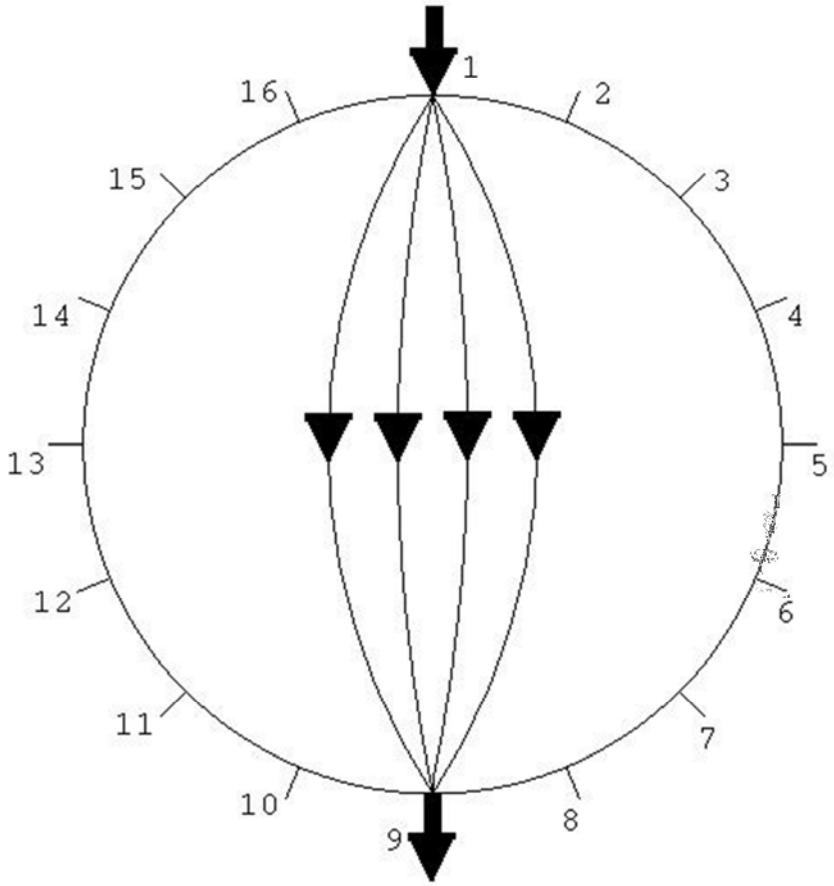

Figure 2-3: Opposite method, equipotential lines (source at electrode 1 and sink at electrode 9).

3. Tomography Theory

Electrical Resistance Tomography (ERT) differs in complexity from x-ray tomography in that electrical current is not confined to a straight line when injected into the phantom. X-Ray beams are considerably easier to work with because they do not spread across the medium of interest but have a straight line trajectory from the source to destination.

The chapter starts with an introduction of the theory governing electric field potentials at the interior and boundary of a circular medium. The more specific forward and inverse problems are also introduced as well as the theory and implementation of back projection, an image reconstruction technique.

As stated in Chapter 1 the reconstructed image must distinguish between two states i.e. boiling and non-boiling. Based on this, the studied medium is assumed to be binary in nature. A quantization method is included with the weighted back projection method.

3.1 Background

ERT images are essentially a map of the potential distribution in the object being imaged (phantom). The electrical potentials at the boundary of the phantom are obtained by applying a current to the medium. The electric field created as a result is governed by Poisson's Equation [**9**]:

$$\nabla . \rho^{-1} \nabla V = f, \tag{3.1}$$

with the boundary conditions:

$$V = V_0 \text{ on } \partial A, \tag{3.2}$$

$$\rho^{-1} \partial V / \partial n = J_0 \text{ on } \partial A\,, \tag{3.3}$$

where $\rho, V \; and \; f$ are respectively the resistivity, voltage and current distribution within the phantom, A is the boundary surface area of the electrode. V_0 on ∂A and J_0 on ∂A are respectively the voltage and current densities measured on the boundary surface of the object with *n* electrodes uniformly placed around the phantom boundary. Voltage at the boundary is measured differentially across adjacent electrodes. We can further simplify Poisson's equation by assuming that no AC current sources exist within the phantom, hence $f = 0$. Equation 3.1 therefore reduces to

$$\nabla . \rho^{-1} \nabla V = 0. \tag{3.4}$$

3.2 The Forward and Inverse Problem

The forward problem solves for the internal voltage and current densities given the resistivity distribution, boundary current density J_0 and the boundary voltage density V_0. The inverse problem

solves for the resistivity distribution ρ given either the internal voltage and current density distributions or the boundary voltage and current density distributions.

For ERT the inverse problem is encountered during image reconstruction. The voltage and current measurements are taken on the boundary and applied to a reconstruction algorithm to produce an image which is the resistivity distribution.

Equation 3.4 is an impossible differential equation to solve; numerical methods are usually applied to arrive at a solution. The most common numerical method used in this case is the Finite Element Method (FEM) and is used to convert the calculus problem into an algebraic problem. FEM involves dividing up the phantom into smaller finite elements thus converting a continuous problem into one with a finite number of unknowns. FEM provides a large amount of spatial resolution depending on how closely knit the mesh nodes are defined. Imaging the boiling process in a vacuum pan does not require a large amount of spatial resolution or definition as the requirements is simply to detect the presence or absence of bubbles. Therefore the image reconstruction method chosen is the back projection method. However, the back projection method does not yield images with uniform sensitivity across all pixels hence a quantized-weighted method is introduced. This is combined with the back projection method to form a weighted back projection method.

3.3 Weighted Back Projection

The weighted back projection first involves back projecting data measured at the boundary of the phantom. A weighted value used to even out each pixel's sensitivity is calculated. The weighted value of each pixel is then multiplied with the value of the corresponding pixel in the back projected image to produce the weighted back projection image. This image is then quantized to simplify the image into a binary format. The 'quantized-weighted back projection' algorithm can be divided into the following steps:

2 Back project data along equipotential lines.
3 Calculate the weight factor for each pixel in the image.
4 Adjust corresponding pixels of back projected image by the weight factor.
5 Quantize the weighted image into binary form.

3.3.1 Back Projection

This method gains its name due to the potential difference between two equipotential lines (measured on the boundary) which is back projected as the resistance value. Back projection can be divided up into the following steps:

- Computation of equipotential lines.
- Back projection of potential difference on the boundary.

3.3.1.1 Computation of equipotential lines

Consider a medium that is circular, homogeneous, isotropic and resistive in nature. When current is injected through a pair of electrodes at its boundary; current will flow in that medium. The potential distribution in that medium is given by Barber and Brown [**12**] as:

$$c.\nabla^2 V + \nabla c.\nabla V = 0, \tag{3.5}$$

where $c = c(x,y)$ is the conductivity distribution within the medium. Replacing c with R where R is a log resistance. $R = -\ln(c)$ reduces Equation 3.5 to

$$\nabla^2 V = \nabla R.\nabla V. \tag{3.6}$$

If the resistance within the medium is uniform then Equation 3.6 simply becomes Laplace's Equation

$$\nabla^2 V = 0. \tag{3.7}$$

Analytically solving Equation 3.7 using the given boundary conditions the equipotential lines can be calculated.

However, Barber and Brown [**12**] used a different approximate method to find the equipotential lines and develop the back projection reconstruction algorithm. This method is called conformal transformation.

In order to relate the boundary profile to the distribution of resistance in the object the problem is transformed from the z(x, y) plane to the t(u, v) plane. For ease of theoretical analysis, it is convenient to assume that the distance between two adjacent current injecting electrodes is very small (2τ), the drive pair can then be considered to be a current dipole.

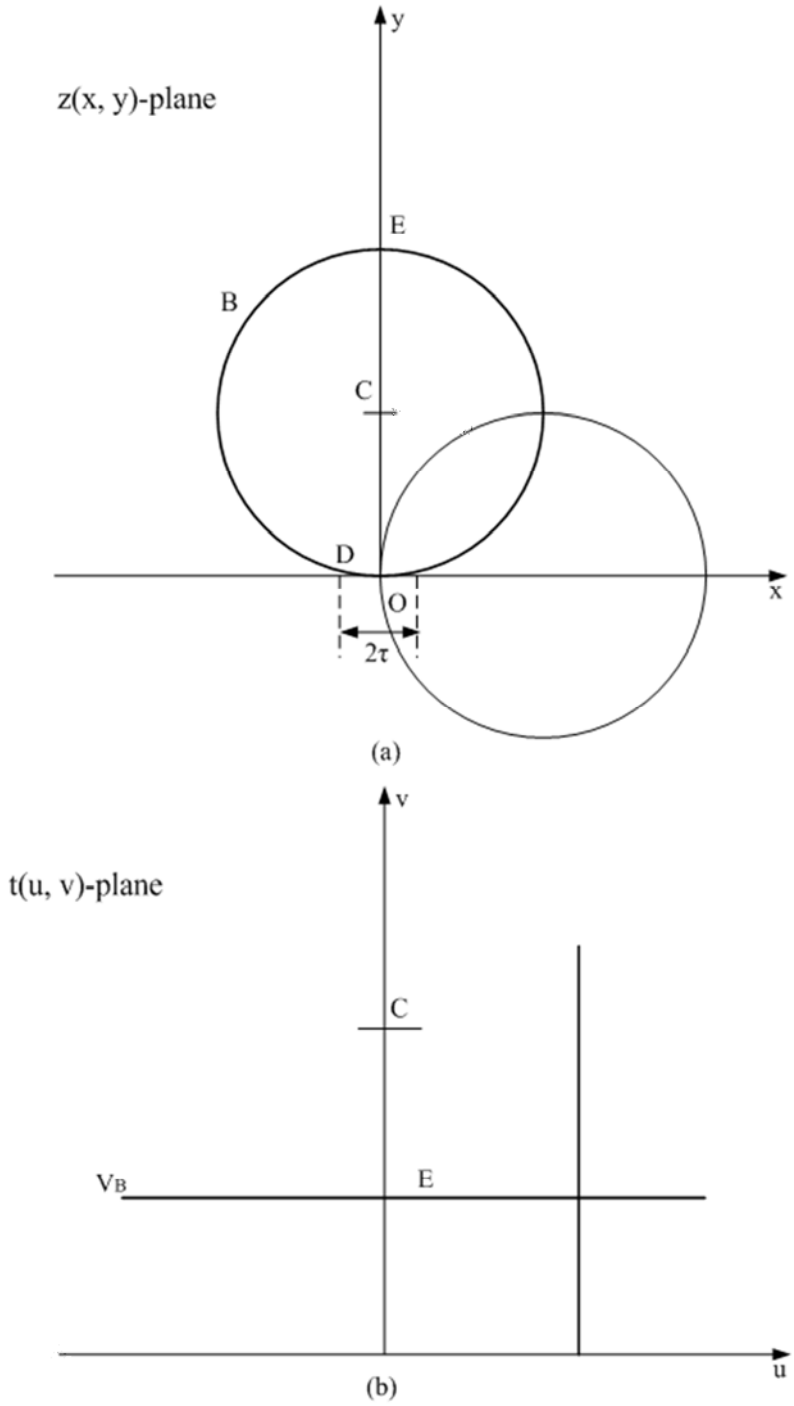

Figure 3-1: Conformal transformation between; (a) a circular region and (b) a semi-infinite region. The points C and E are identified in both the z(x, y) and t(u, v) planes. V_B is the boundary of the circular region transformed into the t(u, v) plane. Redrawn from [9].

Using the conformal transformation, z(x,y) plane in Figure 3-1(a) above is transformed into the t(u, v) plane in Figure 3-1(b).

$$x = \frac{u}{(u^2+v^2)}, \tag{3.8}$$

$$y = \frac{v}{(u^2+v^2)}, \tag{3.9}$$

$$u = \frac{x}{(x^2+y^2)}, \tag{3.10}$$

$$v = \frac{y}{(x^2+y^2)}. \tag{3.11}$$

In Figure 3-1(a) Circle B in the z-plane is transformed into the straight line (v=E) in Figure 3-1(b). The two end points of the current dipole, 2τ apart, are transformed into points at -∞ and +∞ on the u-axis. Straight lines parallel to the u-axis become field lines and are transformed into circles tangential to the x-axis at the point O in the z-plane. Similarly, equipotential lines perpendicular to the u-axis in the t-plane are transformed into circular lines passing through point O in the z-plane

$$V = \frac{mx}{(x^2+y^2)}. \tag{3.12}$$

For a dipole strength m; the equipotential lines are passing through points where equation 3.12 is constant.

To implement the conformal transformation the circular medium is represented by a unit circle. There are 16 equally spaced electrodes on the boundary of the circle. The x and y coordinates of each electrode position on the boundary of the unit circle is obtained by first dividing the circle into 16 equal portions. Each portion will be 22.5 degrees apart hence the x and y coordinates of each electrode will be given by:

$$X_{coord} = r * cos(t * 22.5),$$

$$Y_{coord} = r * sin(t * 22.5), \tag{3.13}$$

Where r is the radius of the unit circle and t is the electrode number. For a 16 electrode system t ranges from 1-16. Once the electrodes coordinates have been calculated the 2 x 16 matrix containing the X_{coord} and Y_{coord} pair is substituted into Equation 3.12 while keeping m=1 (unit circle). This results in a matrix of 16 Vs. known as *V[1-16]*

The path of each equipotential line starts at the injection point and terminates at an electrode on the boundary (see Figure 3-2). To obtain the x and y coordinates which make up these equipotential lines, the elements of matrix *V[1-16]* are substituted into v in Equations 3.8 and 3.9 while u is incremented. The incremental steps used for u determines how close successive x and y coordinates will be from each other.

When all 16 elements in the *V[1-16]* matrix have been substituted into Equation 3.8 and 3.9 and the incremental u matrix has also been substituted then the equipotential line can be plotted from the current dipole to each electrode.

A sample MATLAB code of the entire conformal transformation routine is included in Appendix A4.

Once the equipotential line's coordinates are known. They can be plotted along with the unit circle (see Figure 3-2) and the back projection along equipotential lines may begin.

3.3.1.2 Back Projection of potential difference along equipotential lines

In practice it is more useful to measure the voltage difference between adjacent electrodes than to measure the voltage of each electrode with respect to a common reference. This is because measuring voltage difference is easier but also because reconstruction algorithms require the former rather than the latter.

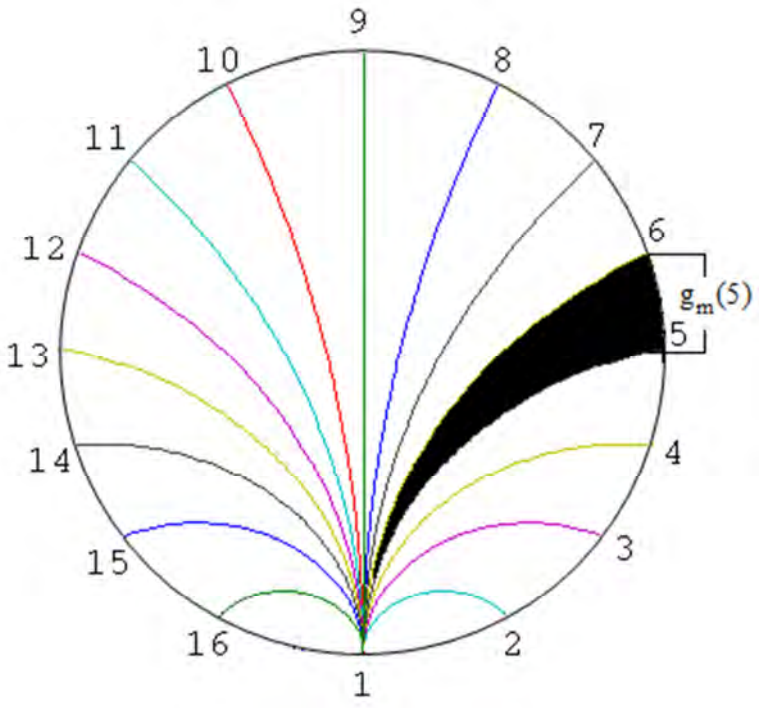

Figure 3-2: Equipotential lines for neighbourhood method. Equipotential lines diverge from injection point 1. Potential difference is measured between adjacent electrodes on the boundary

Given a g_u which is the potential difference measured on the boundary of a region of uniform resistance and a g_m which is the potential difference measured on the boundary of a region of non-uniform resistance. θ denotes the electrodes across which the potential difference is measured e.g. $\theta=4$ when potential difference is measured between electrodes 4 and 5 and $\theta=5$ when potential difference is measured between electrodes 5 and 6. Now, consider a boundary profile $g_u(\theta)$ taken from a region of uniform resistance and a second boundary profile $g_m(\theta)$ taken from a region of the same boundary shape but with a non-uniform (but isotropic) distribution of resistance within the region. The two profiles will certainly differ from each other. To back project $g_m(\theta)$ we take the view that a back projection is the simplest distribution of the property being measured, in this case resistance, which can describe the observed measurements. Figure 3-2 shows the equipotential lines

for the neighbourhood method with current injection between two adjacent electrodes assumed to be a very small distance apart, hence resolved down to a single point. It also shows the simplest distribution of resistance that explains why $g_m(5)$ is different to $g_u(5)$. The resistance between the equipotential lines ending on points 5 and 6 is altered in the ratio $g_m(5)/\, g_u(5)$ or the log resistance is altered to $ln(g_m(5)) - ln(g_u(5))$. The boundary profile g_m/g_u or $ln(g_m/g_u)$ is back projected between the equipotential lines as resistance. The back projected resistance is

$$\rho = \rho_0 \frac{(V_i\text{-}V_j)measured}{(V_i\text{-}V_j)expected}, \tag{3.14}$$

Where $(V_i\text{-}V_j)expected$ is represented as g_u and $(V_i\text{-}V_j)measured$ is represented as g_m. ρ is the overall resistance of the medium and ρ_0 is the resistance value when the medium is uniform/homogeneous i.e. when the measured voltage and the expected voltage are the same.

Since the equipotential lines have been calculated and the theory behind back projection along equipotential lines are known the first step in implementing the theory is to obtain $(V_i\text{-}V_j)expected$. This is done by taking measurements at the boundary of a homogeneous medium. It is important to note that $(V_i\text{-}V_j)expected$ differs with mediums i.e. $(V_i\text{-}V_j)expected$ for water is different from massecuite. The $(V_i\text{-}V_j)expected$ is measured when the medium is homogeneous. A number of readings are taken and the average is calculated and stored by the system. Every measurement is then compared to this averaged homogeneous case as shown in Equation 3.14.

There are 13 voltage readings per current injection. These voltages are substituted into Equation 3.14 as $(V_i\text{-}V_j)measured$ while the stored homogeneous voltages are substituted as $(V_i\text{-}V_j)expected$. ρ_0 will be the resistance value of a homogeneous medium. This was chosen to be 0.5 since the resistance values are normalised to range from 0-1.

To back project a resistance ρ calculated for the highlighted region in Figure 3-2 along equipotential lines. The measured data corresponding to $(V_i\text{-}V_j)measured$ i.e. $(V_5\text{-}V_6)measured$ and the stored expected data i.e. $(V_5\text{-}V_6)expected$ are substituted along with ρ_0=0.5 into Equation 3.14. The resistance value obtained is then assigned to every pixel between the equipotential lines 5 and 6. This is done 13 times per current injection and successive injections are rotated at increments of 22.5 degrees. The images produced are shown Figure 3-3 (homogeneous state) and Figure 3-4 (non-homogeneous state).

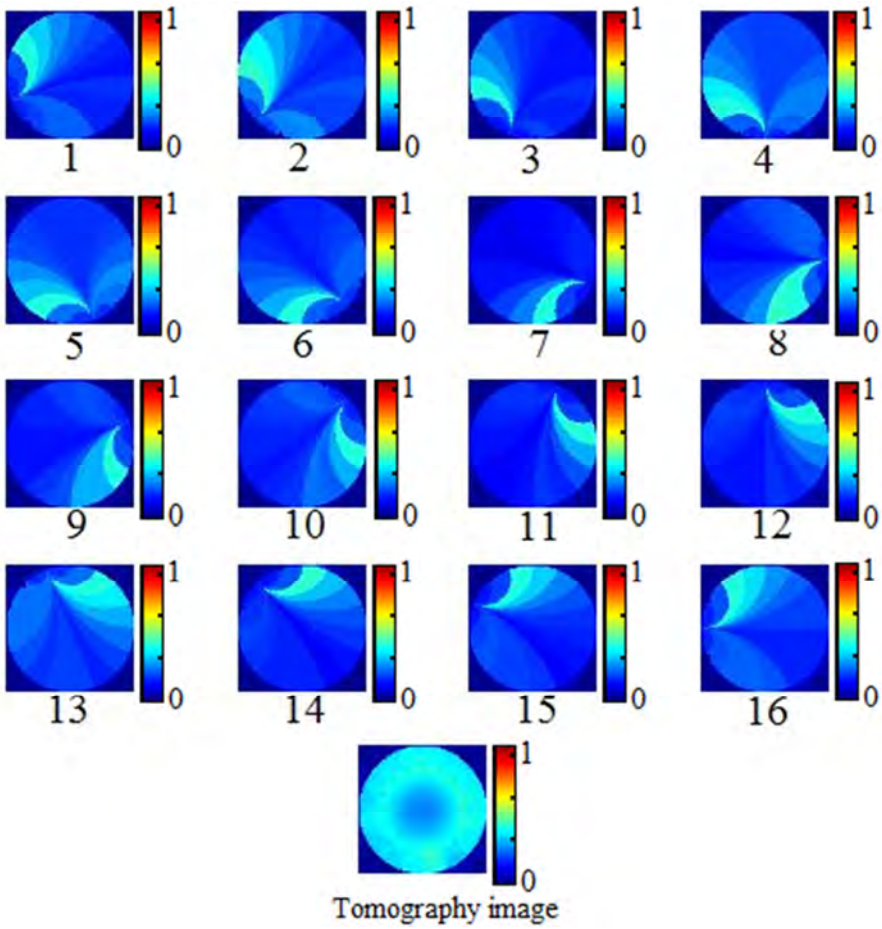

Figure 3-3: 16 back projected images required to form one tomography image frame for a homogeneous medium.

The 16 image frames shown above represent the measured boundary potentials compared with an expected value. Each frame is rotated 22.5 degrees from the previous image. The tomography image is a result of the superimposition of the 16 image frames.

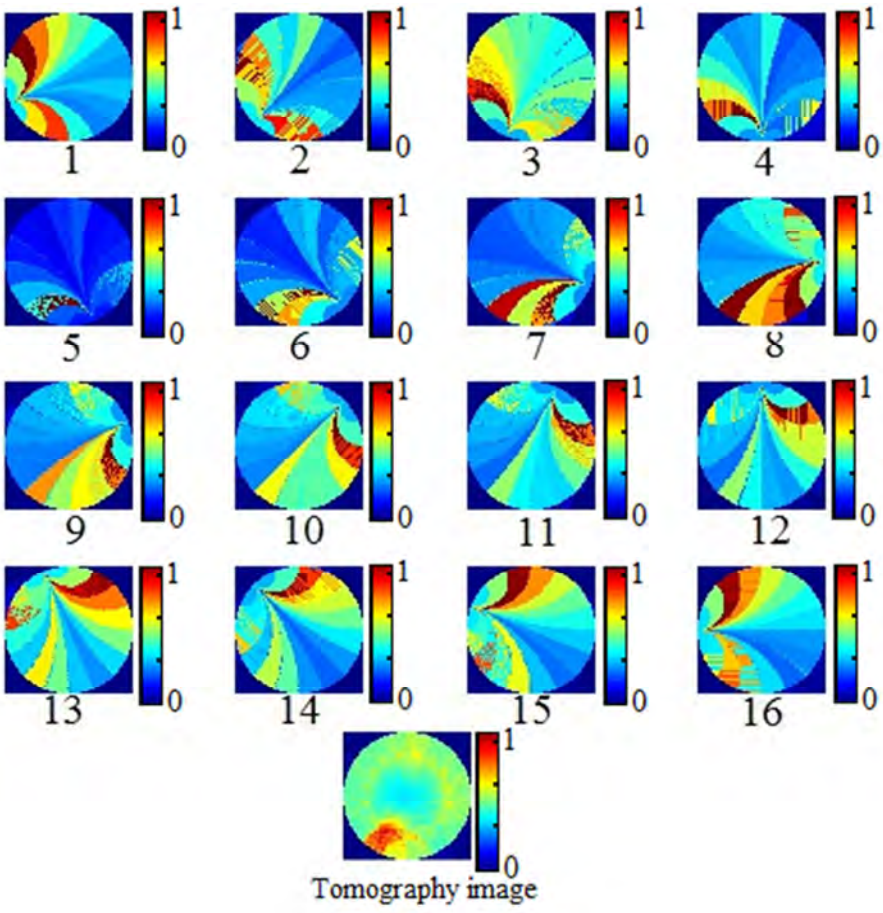

Figure 3-4: 16 back projected images required to form one tomography image frame for a non-homogeneous medium.

Figure 3-4 shows the 16 resistance distributions for a non-homogeneous medium. Each of the frames shown is superimposed to form the tomography image. Each resistance distribution shown in Figure 4-15 is also shifted by 22.5 degrees from the previous image.

The neighbourhood method used in collecting the data yields images which are sensitive to resistance changes on the periphery of the object but which have little or no sensitivity at the centre of the object. In order to have uniform sensitivity across the pixels of the reconstructed image a weighting factor is implemented.

3.3.2 Weight Factor

The inverse problem is ill-posed in that, large changes in impedance at the interior of the object can result in small voltage changes at the boundary. Hence sensitivity is not uniform across the object. It is required that each pixel in the reconstructed image have even sensitivity. Therefore based on the conformal transformation Seagar “et al.” [**13**] proposed a weighting factor for even sensitivity across all pixels. The weighting factor is computed as follows.

Assuming equally spaced electrodes, equipotential lines are not circularly symmetric for all pixels except the centre pixel. Therefore the weight each equipotential line carries must be different for all pixels except the centre pixel.

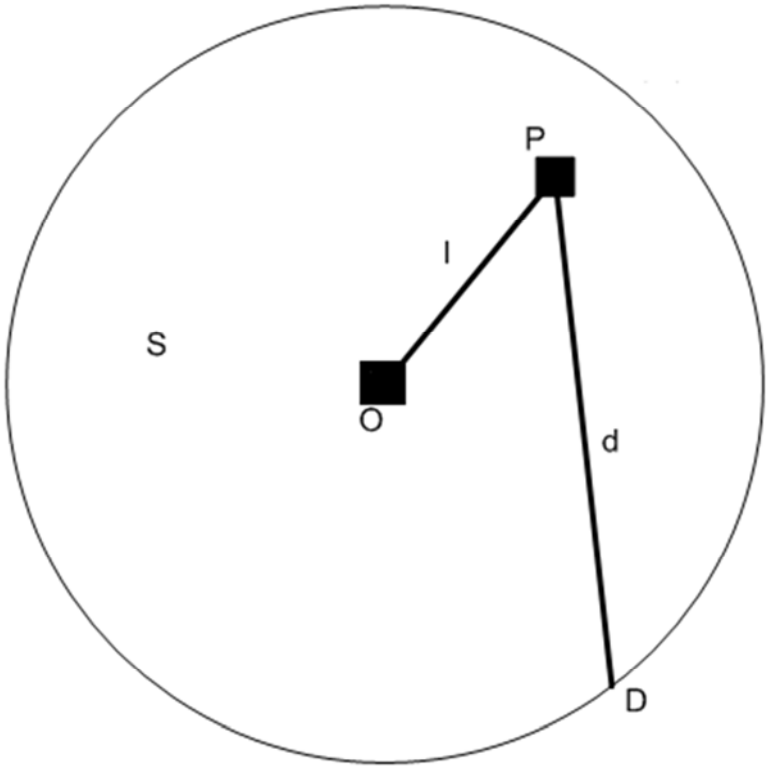

Figure 3-5: Illustration of the parameters used in the computation of back projection weight [9**]**

Figure 3-5 illustrates the parameters used to compute the weighting factor w_p based on how far pixels are from the centre and from the point of injection. In Figure 3-5 Circle S represents the circular phantom, O is the centre pixel of the reconstructed image, D is the point of injection, P is the pixel whose weight is to be calculated, d is the distance between the injection point and pixel P and l is the distance between the centre pixel O and pixel P. The weight factor for w_p is given by [**9**]

$$w_p = \frac{d-l^2}{l^2}. \tag{3.15}$$

The sensitivity plot resulting from Equation 3.15 is shown in Figure 3-6. The weighting factor of each pixel, w_p, depends on the injection point. A 16 electrode phantom will have 16 injection points and hence 16 weighting plots. The plot shown in Figure 3-6 is the sum of the 16 weighting plots. The colour bar to the right of the sensitivity plot shows that the pixels closest to the electrodes have the least weighting so as to even out the sensitivity. The weighting increases the further away the pixels are from the boundary. This reduces the sensitivity to resistance changes around the boundary and enhances resistance changes that occur towards the centre of the image.

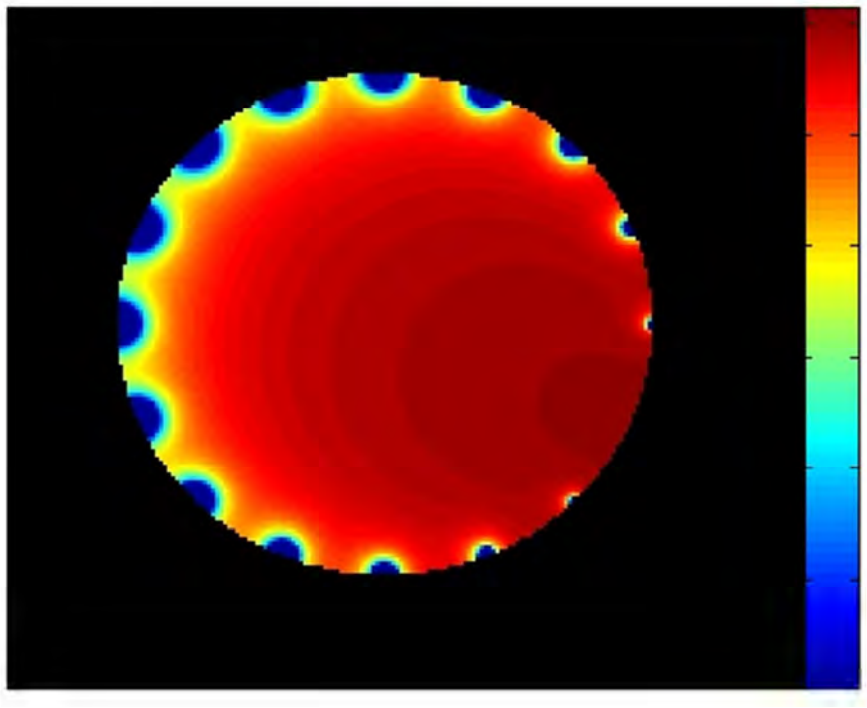

Figure 3-6: Sensitivity plot of weighting factor w_p for 16 injection points superimposed on each other.

An obvious offset which covers one of the electrodes is visible in the Figure. The trade-off created by the sensitivity plot is that the region covered in red are more sensitive than the region immediately surrounding most of the electrodes. Experiments reveal that placing a non-conducting PVC rod on the periphery of the medium yields little or no change to the reconstructed image. A method of dynamically adjusting the sensitivity of the medium was therefore implemented. This method dampens the sensitivity of the whole medium by modifying Equation 3.15 to

$$w_p = \left(\frac{d-l^2}{l^2}\right)^m, \tag{3.16}$$

where *m* has a range [0, 0.1]. Experiments show that bubbles can still be detected when *m* is as low as 0.1 but the PVC rod could only be accurately detected at *m*>0.3The range is controlled (see labels 4, 7 and 9 in Figure A14 in the appendix) at run time to adjust the overall sensitivity and hence make the

periphery of the medium more sensitive to changes. The test results shown in Chapter 5 where the non-conducting PVC rod is used requires that the sensitivity of the medium be adjusted at run time.

Let $w_{tot}[P]$ be the matrix plotted in Figure 3-6 and $BP_{tot}[P]$ be the matrix whose elements are the pixels of a tomography image (see Figure 3-4). Let *P* be the total number of pixels in the matrix. The weighted back projection will therefore be

$$Weight_{BP}[P] = w_{tot}[P] * BP_{tot}[P]. \tag{3.17}$$

Corresponding elements/pixels from $w_{tot}[P]$ and $BP_{tot}[P]$ are multiplied with each other to give $Weight_{BP}[P]$.

A quantization method is introduced after the weighted image has been obtained. The quantization minimizes the effect of the offset in the sensitivity plot and also transforms the weighted back projection image into a binary image.

3.3.3 Quantization Method

One of the objectives stated in the introduction is that the final image must be able to distinguish between two massecuite states, a homogeneous state (no bubbles) and a low conductivity state (bubbles). The weighted back projection method is quantized so that the final image is binary.

The quantization routine is implemented in software by comparing each pixel in the image. The pixel values in the image range from 0 to 1. Each pixel in an image is compared to a threshold (0.75). If the comparison is true i.e. the pixel value is less than 0.75 then the pixel is assigned the value 0.5 otherwise the pixel is assigned the value 1.

The 0.75 threshold was obtained through tests conducted by placing various non-conducting materials in the medium (water, massecuite and deionized water). The quantized-weighted back projection method was successfully implemented.

The theory behind tomography image reconstruction in general and weighted back projection in particular is presented in this chapter along with a method of quantization which has the effect of filtering the image into binary form. The results which show the implementation of the theory discussed in this chapter are presented in Chapter 5.

4. Design and Implementation of a Real-time Tomography System

The design and implementation of the real-time tomography system is described in this chapter. Each component used in the design is discussed in detail.

The system was designed around the compact DAQ (hardware), a data acquisition device with removable I/O slots and LabVIEW (software), both of which are National Instrument products. This is an advantage over custom designed equipment as it ensures that parts of the system can be easily replaced should the need arise, while making software and hardware interfacing a seamless process. The design objective was to implement a real-time tomography system that runs as fast as possible i.e. collect data and reconstruct images in real-time while being as compacted as possible.

4.1 Overview

A stepwise overview of the implementation is given below:

i.) Collar design
ii.) Electronic hardware design
iii.) Image reconstruction software implementation
iv.) Final boxed system

The tomography system was designed to produce real-time images and therefore was required to collect data and process images in parallel. The system is controlled by a LabVIEW application running on an ultra-small form factor (USFF) PC. The USFF PC interfaces with the compact DAQ (cDAQ) chassis through a USB port. The cDAQ chassis essentially houses the analogue to digital converters (ADC) and digital output modules and provides a compact interface with the PC through a USB port. A switching circuit which contains multiplexers, a constant current source, a bi-polar switch and a relay for isolating electrodes from the current source was designed in-house. Three test collars, which housed electrodes and positioned them above the area of study, were constructed for laboratory tests.

4.2 Collar

The term ‘collar’ refers to the support structure that encases the current injection and voltage measurement electrodes. The structure is able to withstand the heat and vacuum conditions that occur during the boiling process in a vacuum pan for up to two months. A collar is made from 110 *mm* PVC pipe, stainless steel bolts and plates for injecting and sensing current and voltage signals respectively. Figure 4-1 shows the test collar built for laboratory testing. The major difference between the collar used at the mill and the test collar is that the collar (used at the sugar mill) does not have a base with a

pipe protruding. This allows the collars to fit on top of the calandria tubes in the vacuum pan as shown Figure 1-2b. The collar and test collar are not susceptible to corrosion as the electrode plates, bolts and nuts are stainless steel while PVC is a noncorrosive material..

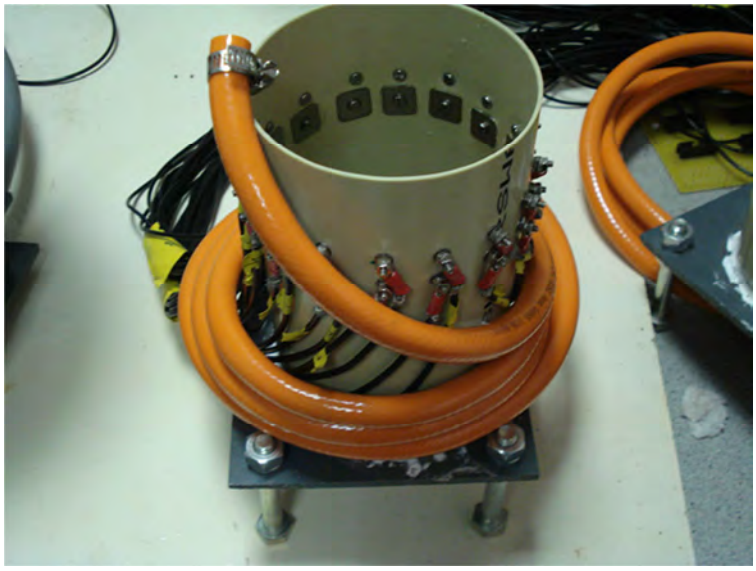

Figure 4-1: Test collar showing the current injection (bottom row), voltage sensing (top row) electrodes and an orange gas pipe to transfer compressed air into the medium. The pipe is not normally wrapped around the collar.

For testing purposes a tube was fitted to the base of the collar. Air was pumped through the base of the collar in order to simulate boiling.

Figure 4-2: Shielded coaxial cables transfer signals to and from collar

Due to the electrically noisy environments of the sugar mill, shielded coaxial cables were necessary and connected the collar to the electronic part of the tomography system. Shielding each cable helped prevent cross-talk between cables. Cables used during testing were 10meters in length and minimal interference was observed between them with shielding. Figure 4-2 shows the coaxial cables attached to the exterior of the PVC pipe. They are connected to the electrodes which are inside the pipe by 3*mm* stainless steel bolts. A 2.7% signal attenuation was measured across the cables when applying an AC signal (with a frequency of 35Hz and an amplitude of 39V) across the cable while it was connected to the collar filled with massecuite which acted as load resistance. The applied signal was then compared to the measured signal.

Impedance decreases as electrode area increases [**9**]. Therefore, in order to have as little contact impedance as possible, the aim was to make the electrode plates as large as possible while ensuring they are not in direct contact as this would cause an electrical short. For a PVC pipe with diameter D = 110 *mm*, the circumference of the pipe is $\pi * D$ = 345.58 *mm*. Dividing this into 16 equal parts, we obtain the maximum length each electrode must have in order to fit 16 electrodes in the collar. This length L = 345.58 *mm*/16, L = 21.60 *mm*. It was therefore decided to choose stainless steel plates to be15 *mm* x 15 *mm* so as to leave enough clearance between electrodes while also ensuring that potential difference measured across adjacent sensors have a large enough variance. The stainless

steel plates used for injecting current into the medium are equal surface area electrodes; this ensures equal contact resistance. Construction of the electrodes was outsourced to a laser cutting specialist[1]. Dimensioned drawings and manufacturing instructions for the electrodes and brackets are included in Appendix A4 to A12. Figure 4-3 shows two rows of electrodes fixed to the interior of the PVC pipe. The top row of stainless steel bolts are used for voltage sensing while the bottom row of stainless steel plates are for current injection. The bolts are kept fixed to the PVC tube by 3 *mm* stainless steel nuts.

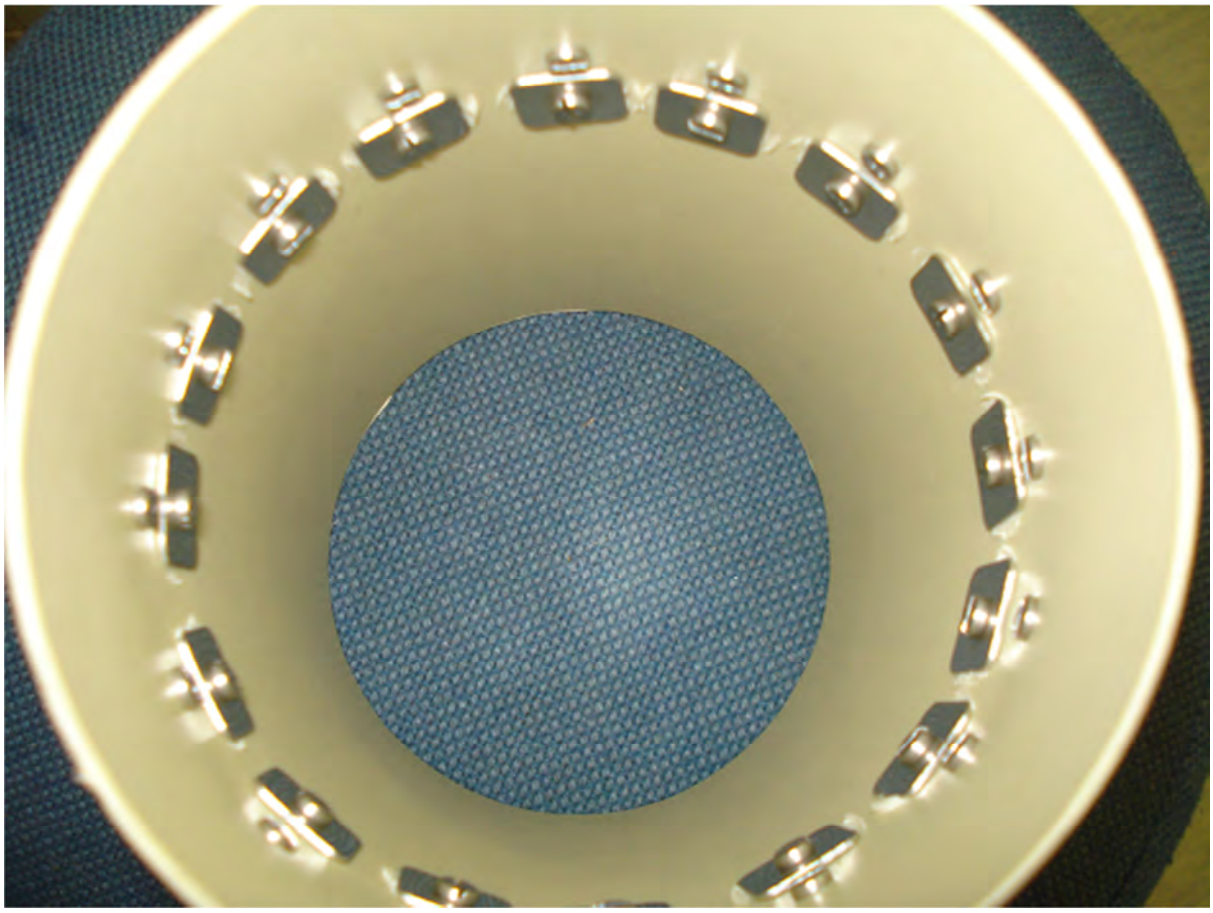

Figure 4-3: Laser cut stainless steel plates (bottom row).

For the laboratory test, three test collars were constructed. Collar 1 contained massecuite, Collar 2 tap-water and collar 3 deionized water. This was done to test the effect of different liquids (resistances) would have on the system's speed and image quality. This is discussed further in Chapter 5, the results chapter. Each of the collars was constructed to be waterproof. They must also be strong enough to withstand the pressure from the gas being pumped from their base. Figure 4-4 shows the gas tube attached to the base of the collar.

[1] Construction of the L-shaped brackets which hold the collars upright while in the vacuum pan was also outsourced.

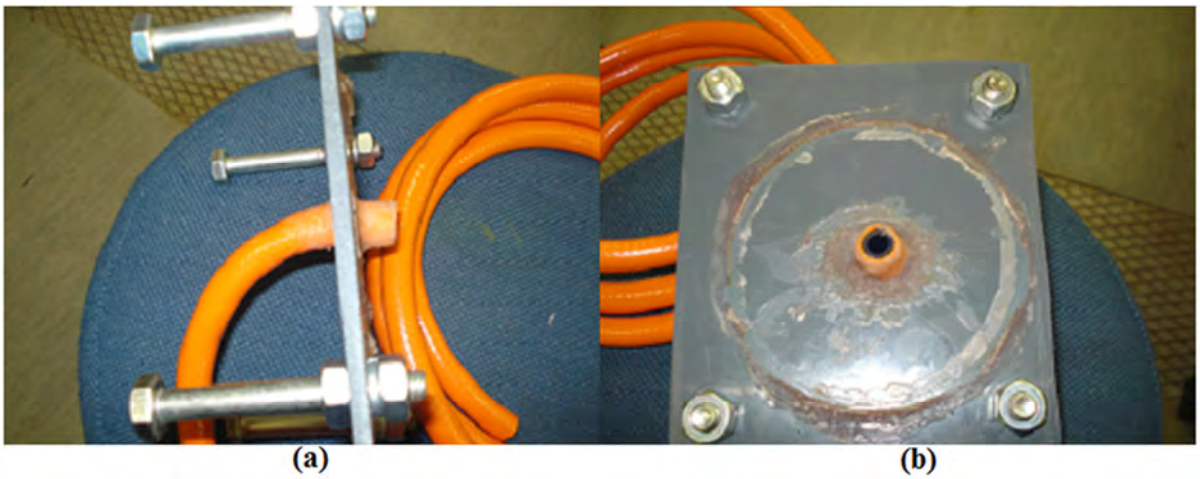

Figure 4-4: Test collar's base with the gas pipe protruding: (a) Side view (b) Top view.

4.3 Electronic Hardware

The main control of the system is housed in a small form factor PC. It communicates with the National Instrument compact DAQ (cDAQ) and the Current Control Module (CCM). Measurements are transferred from the collar to the National Instruments compact DAQ using RG174 shielded co-axial cables. The CCM contains a current source, a relay switch, a single pole single throw (SPST) IC switch and multiplexers.

4.3.1 Overview

Unknown impedances exist between an electrode and the medium it is in contact with. This is known as contact impedance and its value depends on the medium to be imaged. In order to minimize the effect of contact impedance on the signal applied to the electrodes it is crucial that the signal source has high output impedance. A constant current source (CCS) has high output impedance while a voltage source has low input impedance. Similarly, a voltmeter (ADC) has high input impedance thus making the contact impedance negligible while an ammeter has low input impedance which will allow contact impedance to degrade any measurements taken. This is why a current source is used to supply signal to the electrodes (rather than a voltage source) and a voltmeter (ADC) is used to measure the resulting voltage.

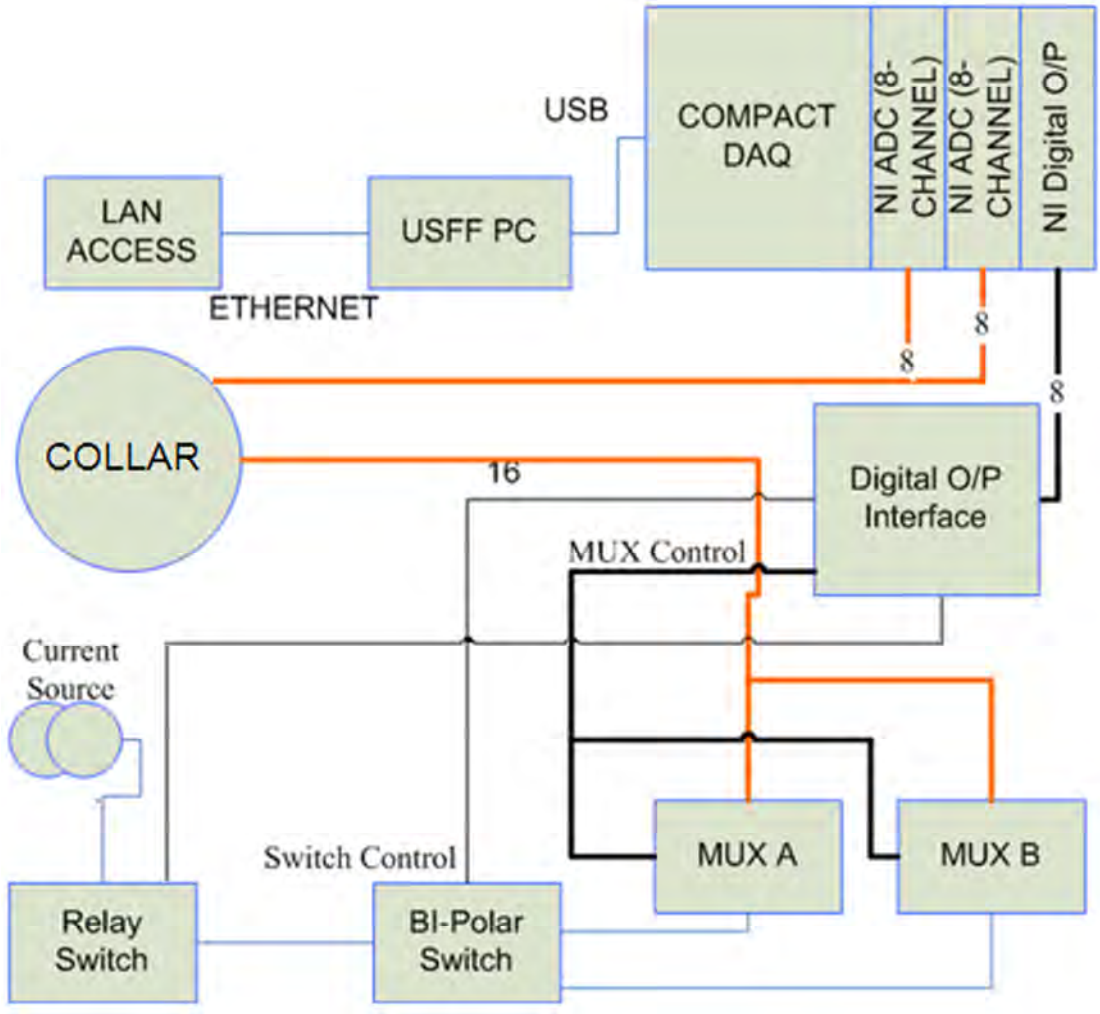

Figure 4-5: Electronic Hardware Overview

Figure 4-5 shows a block diagram of the tomography system connected to one collar. Adding one more collar requires (i) 2xNI ADC channels and (ii) 1xCCM. This is because each collar has 16 ADC channels to measure the potential difference generated as a result of the applied current and a separate CCS.

The data collection process begins by enabling the relay switch, so that the current source is connected to the bi-polar switch and no longer isolated from the electrodes. The switch control signal is a square wave generated in software and output through the digital O/P module on the cDAQ. The bi-polar switch uses the square wave and the CCS signals to generate two AC square wave signals which are out of phase with each other. These signals are connected to the inputs of MUX A and MUX B. Electrodes are connected to each multiplexer such that even numbered electrodes are connected to the outputs of MUX B while odd numbered electrodes are connected to the outputs of MUX A. This ensures that any pair of adjacent electrodes will have signals that are out of phase with each other. Therefore at any given time during the data collection process one electrode will source current while the adjacent electrode will be the sink. The relevant electrode pairs are selected through

the line labelled MUX control. The voltages are measured through the 2 ADC modules on the compact DAQ chassis. The USFF PC, via LabVIEW, controls the data collection process and constructs the tomography image. Remote access to the USFF PC is possible for computers on the same local area network; therefore measurements can be remotely initiated and the reconstructed image displayed.

Power Supply

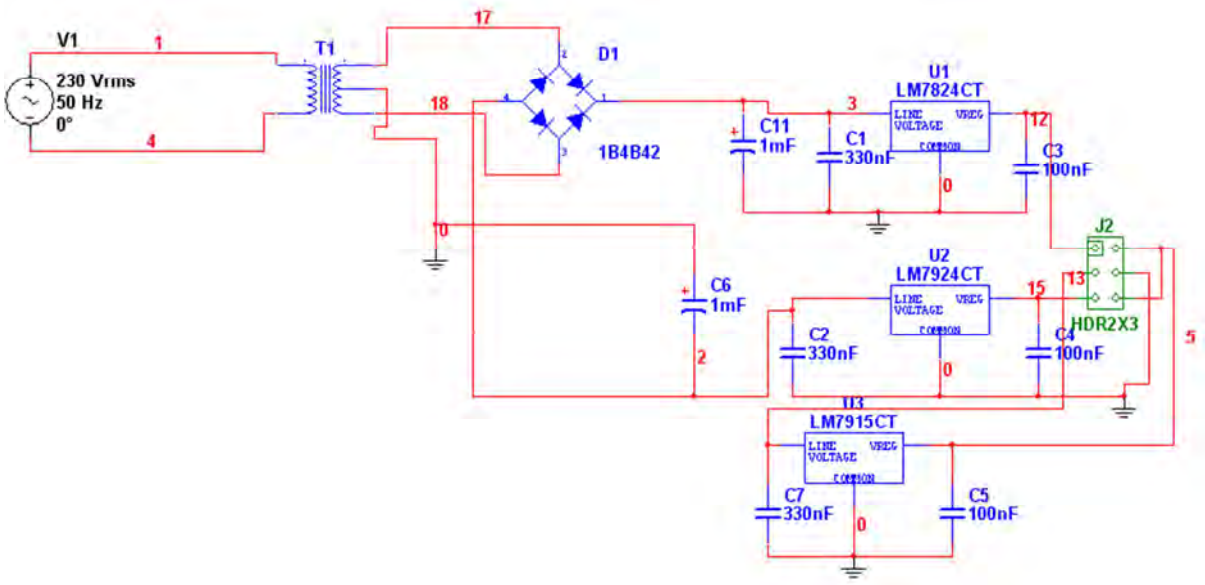

Figure 4-6: Power Supply Schematic

The power supply schematic is shown in Figure 4-6. The function of the power supply is to supply a high enough current and voltage (power) to the CCS so that data collected is not corrupted by noise and cable length is less of a factor in the attenuation of the current source signal. The power supply output rails are +23.8V with a voltage ripple of 50mV and -15.4V with a voltage ripple of 75mV. This gives 39.2V across the supply rails. According to the datasheet the LM7824, LM7924 and LM7915 ICs are capable of supplying a maximum current of 1.5 A. It is important to keep the voltage ripple as small as possible as large voltage ripples will cause fluctuations in differential voltage measured from adjacent electrodes. This can lead to data collected from certain electrodes being unreliable.

Constant Current Source

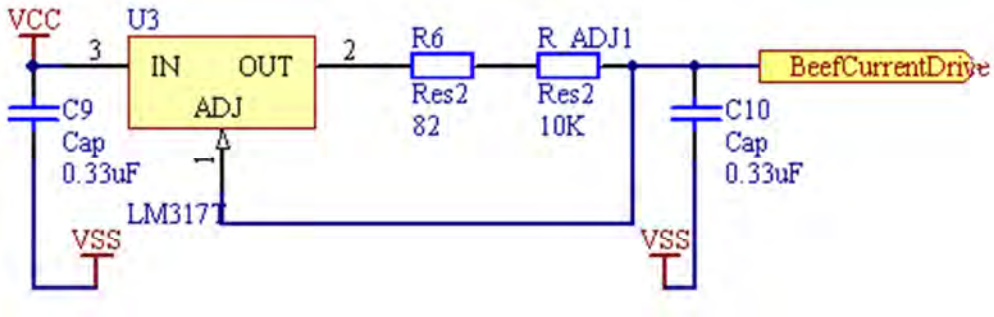

Figure 4-7: Constant Current Source

The constant current source schematic is shown in Figure 4-7. The LM317 regulator maintains 1.25V potential difference between its V_{out} and V_{adj} pins [**14**]. A resistor across both pins sets up a constant current across them. In this case a variable 10kΩ resistor is used in series with an 82Ω resistor making this an adjustable CCS. The 82Ω resistor is added to set the maximum current to be $I = \frac{V}{R} = \frac{1.25\ V}{(82+1)\Omega} =$ 15mA when the variable resistor is at its minimum value. The minimum current is set when the 10kΩ pot is at its maximum and is therefore $I = \frac{V}{R} = \frac{1.25\,V}{(82+10\text{k})\Omega} = 0.12\text{mA}$.

Bi-Polar Switching and Multiplexing

When current is injected through an electrode pair into the medium of interest, one electrode will be at ground potential and the other will be at a higher potential. One electrode will therefore always be the anode and the other the cathode. This causes reduction and oxidation which can inhibit the flow of ions in the medium; hence the need for a bipolar switch. The bi-polar switch produces two signals which are opposite in polarity to each other thus ensuring that the anode and cathode keeps switching so that any reduction or oxidation effect created during a half cycle is reversed in the following half cycle.

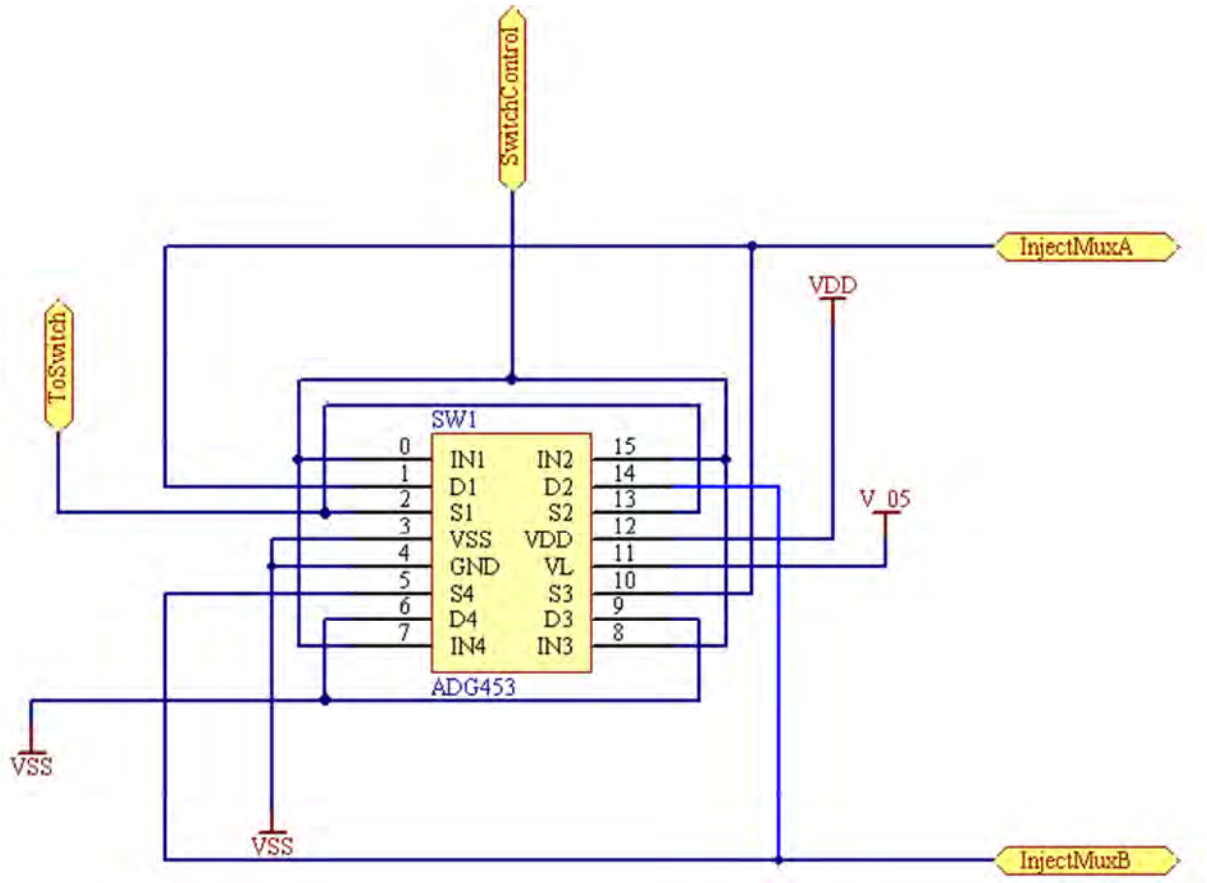

Figure 4-8: Bi-polar Switch (H-bridge) Configuration

Figure 4-8 above shows a circuit for a solid state SPST switch based on the ADG5408 device manufactured by Analogue Devices. It is connected in Figure 4-8 to function as an H-bridge, i.e. at any given time the signals labelled "InjectMuxA" and "InjectMuxB" will always be opposite in polarity but equal in magnitude. The AC signals from "InjectMuxA" and "InjectMuxB" are multiplexed into the electrodes of the collar. Its low 'on' resistance (4Ω), fast switching times (t_{on}=70nS and t_{off}=60nS), continuous current rating (100mA), supply ratings (44V) and power dissipation (18µW) make it an ideal device for implementing a real-time system that can handle increased current source specifications while dissipating ultralow power.

The "SwitchControl" label is an input to the bi-polar switch. It carries the square wave signal generated in software and output through the digital output module. The "ToSwitch" label contains the DC output signal of the CCS. The "InjectMuxA" and "InjectMuxB" signals are the output of the bi-polar switch and are square wave signals which are always opposite in polarity to each other. They oscillate between the switch's ground potential and the CCS's potential.

In a past prototype the CD4051 was used to de-multiplex the CCS to the electrodes. However, the prototype limited the magnitude of the current source signal that was used. The ADG5408 is a high voltage latch-up proof multiplexer. Its capacity for higher voltage and current has helped to further

reduce the effect of noise on the measurements made from the collar. The ADG5408 has an added advantage as it has a much smaller TSSOP footprint compared to the CD4051 which has a PDIP footprint. This reduced the physical size of the CCM board.

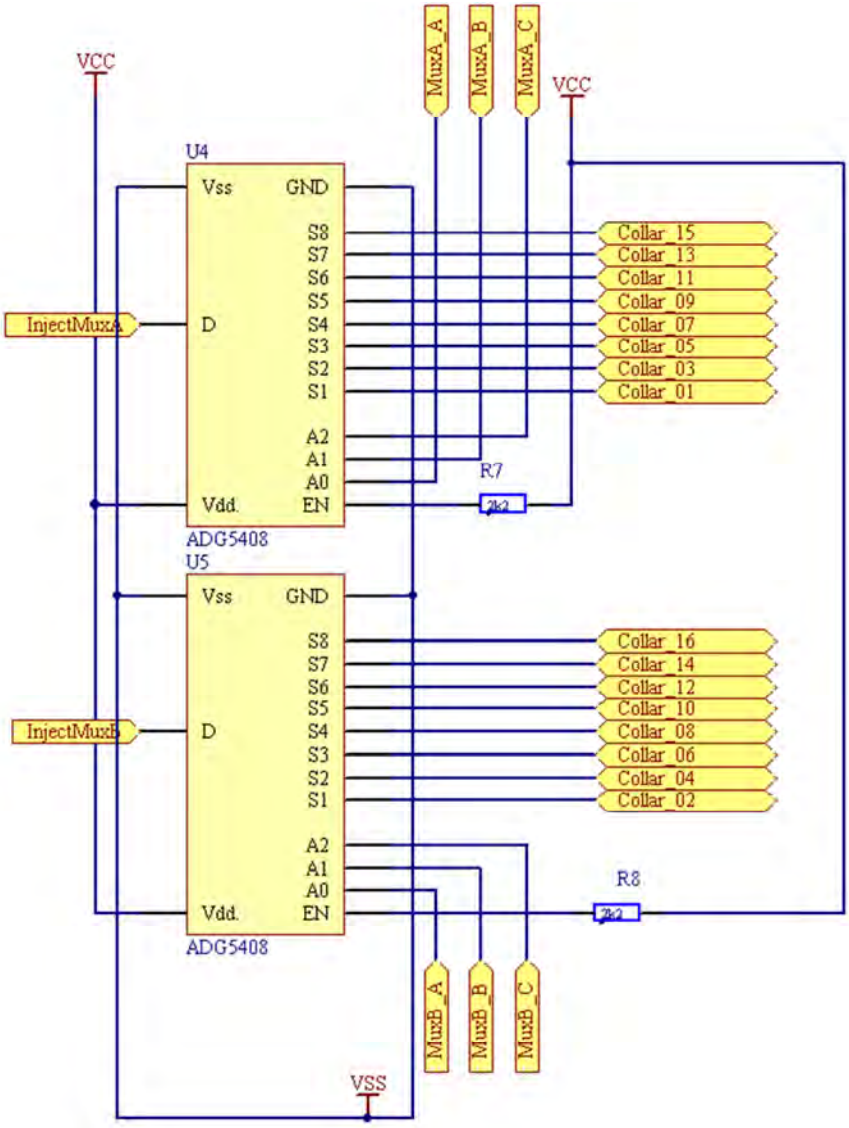

Figure 4-9: Current Injection Multiplexers

Figure 4-9 shows two multiplexer circuits. The “InjectMuxA” and “InjectMuxB” labels are the two outputs of the bi-polar switch. The multiplexer, labelled “U4”, is connected to the odd numbered electrodes. Its outputs are labelled as “Collar_01” to “Collar_15”. The multiplexer, labelled “U5”, is connected to the even numbered electrodes and its outputs are labelled as “Collar_02” to “Collar_16”. The select lines A0, A1 and A2 operate at 5V logic. The enable pin, EN, must be at the same potential as the supply voltage for the multiplexer to function.

An added advantage of increasing the magnitude of the injected CCS signal is that a differential amplifier is no longer required to amplify the signal before it is measured by the ADC. This has reduced the complexity and size of the design.

4.3.2 NI Compact DAQ

The compact DAQ (cDAQ) is a chassis manufactured by National Instrument. It allows for easy interfacing of NI C-series modules, such as ADC and Digital I/O, to a PC. It is available in USB or Ethernet addressable versions. There are two chassis sizes: 4-slot and 8-slot chassis. A number of different modules can be used with the chassis slots depending on design requirements. As can be seen in the system block diagram, Figure 4-5, 16-channel ADC and one digital output module are required to collect data from a collar with 16 electrodes.

Modules are automatically detected by the cDAQ and are hot swappable. The chassis is designed to be robust, ruggedized (for use in harsh environments) and is constructed from A380 cast aluminium. It is capable of operating at temperature ranges from -20 to 55 degrees Celsius. This makes it perfect for the mill environment.

A major problem encountered during implementation was that the cDAQ does not allow its sampling speed to be modified within an application. All sampling speed related settings are only available pre-run time when the ADC module's measurement profile is set and stored in memory. It later became apparent that the fastest speed which the application can access the cDAQ's ADC module measurements was 35Hz. The ADC is setup to sample on demand but the speed which the LabVIEW application can access data through the USB port has limited the capabilities of the system.

A picture of the actual cDAQ chassis with two Analogue input modules and one digital output module inserted into the chassis is shown in Figure 4-10. The analogue input modules are inserted into the first two slots and the digital output module is inserted into the third slot.

Figure 4-10: NI Compact DAQ with Analogue inputs (NI9221) and Digital Output (NI9403) used for data collecting directly from the collar and control

Analogue Input

The NI 9221 Analogue input module is used to sample electrode voltage in the phantom. Each module consists of 8-channels where each channel is isolated from the next. The input signals are first scanned, buffered, conditioned and then sampled by a 12-bit ADC. The NI 9221 has an adjustable +-60V measurement range and can operate at extreme temperatures ranging from -40 to 70 degrees Celsius. The module's voltage range is large enough to measure the signal being injected into the phantom (0V to 39V). This module has been designed with spring loaded latches that lock into place once the module is installed into the chassis.

Digital Output

The NI 9403 digital output module, as seen in Figure 4-10, has 32 channels each internally referenced to ground and operates at 5V TTL. It contains overcurrent/short-circuit protection such that a maximum of 64 mA can be drawn from each channel. Any current in excess of 64 mA will drive the device into a high impedance state to protect its internal circuitry. This module is used to control the select lines of the current injecting multiplexers as well as to control the switch and enable the relay.

Like the analogue input this module is also designed and fitted with spring load latches that lock into place once the module is installed into the chassis.

4.3.3 Ultra Small Form Factor PC

An ultra-small form factor PC (USFF PC) was selected to run the software of the real-time tomography system due to its physical size. It is 23.7cm in height, 6.5cm width and 24cm in depth and has a high end Intel i5-2400s processor. Its sole purpose is to run the tomography LabVIEW application and function as a web server. The application automatically runs once the PC's operating system initializes. The PC controls both the data collection and the image reconstruction and interfaces with the cDAQ through a USB port and requires an Ethernet connection to a local area network so that real-time tomography images can be viewed by any PC connected to the local area network. The cDAQ chassis is simply an end device used to interface the USFF PC to the collars and the CCM and does not execute any of the software written in LabVIEW. All controls are issued from the USFF PC.

The development work was done in LabVIEW on a Windows XP Operating System (OS), but the USFF PC running the application uses a Windows 7 OS. This has made the transition to the USFF PC a more challenging prospect as there are major and minor changes between the OSs. One of the important changes is the characters allowed in a filename. For example, Windows XP allows the comma character to be inserted in a filename of a text file while Windows 7 does not. This was discovered as the problem after debugging the system.

4.3.4 Printed Circuit Board Design

The Printed Circuit Boards (PCBs) were designed using two different PCB packages, Ultiboard and Altium. Ultiboard is a product of National Instruments Electronic Workbench and was used to make the first set of PCBs, which were the power supply (Figure 4-6) and Digital Output Interface boards. The Altium software was used to make the more complex CCM board which contained the CCS, bi-polar switch and multiplexers. A total of three PCBs are required for one collar to be imaged. They are the power supply, the digital interface and the CCM PCBs; an extra CCM board is required for each additional collar as each collar has a separate current source and control circuit. The circuit diagram of the CCM is shown in Figure 4-11. The other PCBs are shown in Appendix A1, A2 and A3.

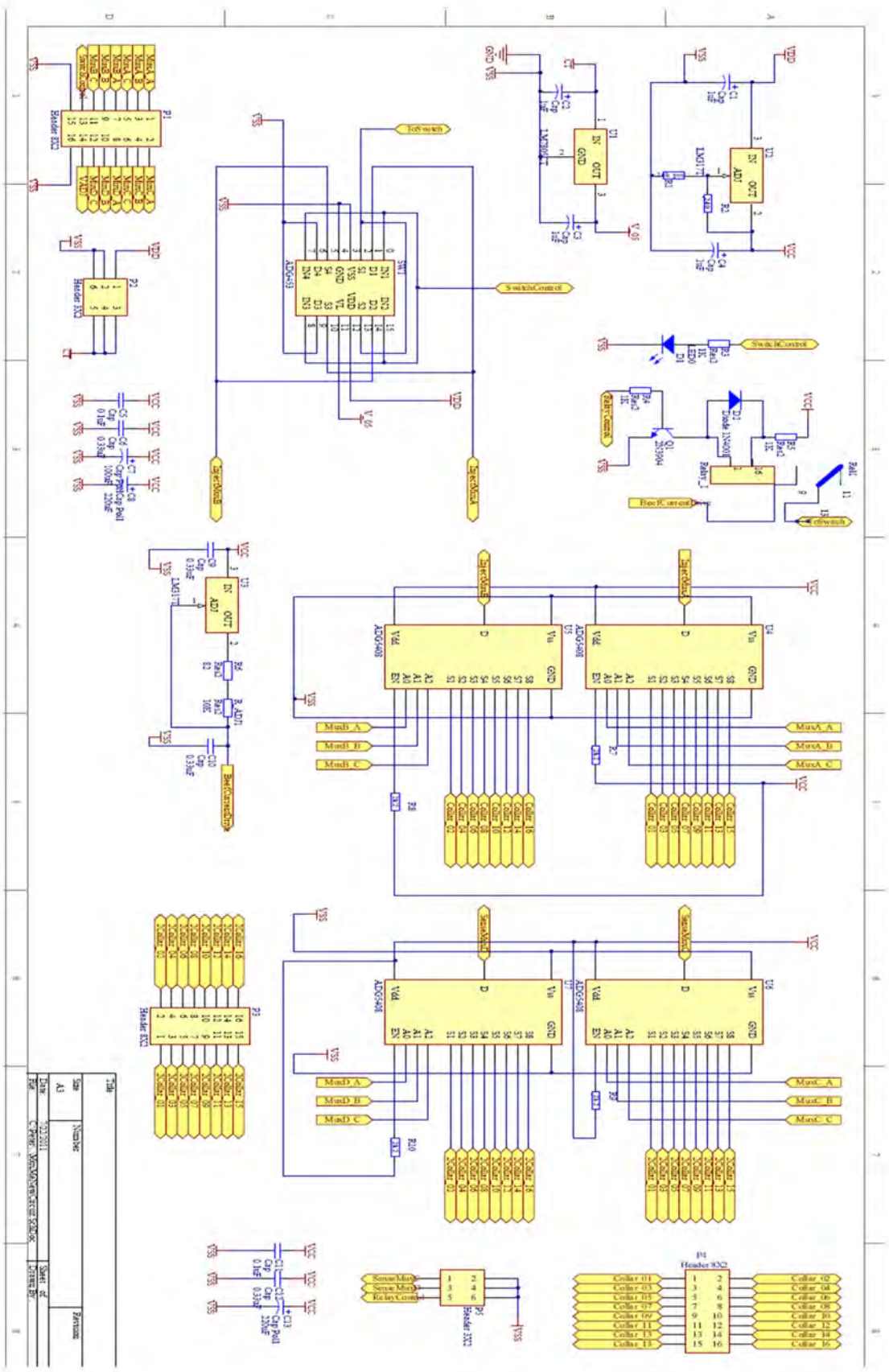

Figure 4-11: Circuit diagram of the current control module (CCM) which contains the CCS, multiplexers, relay and bi-polar switch

4.4 Image Reconstruction Software Implementation

Initial image reconstruction software was developed using MATLAB as it is an excellent software package for prototyping. Previous tomography research done in order to achieve images from a sugar pan made use of MATLAB's partial differential equation tools for image reconstruction, which was done offline [**3**]. This research focus is real-time tomographic imaging and it makes use of a back projection technique.

Proof of principle image reconstruction algorithms were initially developed in MATLAB and then ported to LabVIEW so that it could be implemented on NI hardware. Retrospectively, initial development should have taken place by use of LabVIEW as this prevents cross platform synchronisation issues which were encountered while using MATLAB for image reconstruction, the DASYLab (software) and the DAQbook as the data collecting hardware used by [**3**] as explained in Section 1.2 of Chapter 1.

4.4.1 Laboratory Virtual Instrument Engineering Workbench

Laboratory Virtual Instrument Engineering Workbench (LabVIEW) developed by National Instruments, is a powerful programming language that uses a GUI block diagram interface. This graphically based programming language is ideal for test and measurement, instrument control, data acquisition and data analysis applications, resulting in less design and programming time when compared to text-based programming languages. LabVIEW allows a huge amount of flexibility to programmers as its libraries contain numerous functions allowing the programmer to design very complex applications with relative ease [**15**].

LabVIEW also allows programmers to compile a stand-alone executable or to package an installer for their application once the design process is completed. This means LabVIEW applications can be used on PCs that do not have LabVIEW installed on them, a very useful feature as it frees the end user of licensing costs.

Programming in LabVIEW is done through Virtual Instruments (VIs). Virtual Instruments comprises two windows through which applications are created. The first window is called the 'front panel' and contains the graphical user interface. Front panels would usually contain text boxes, graph indicators for plotting, command buttons, toggle switches etc. The second window is known as the 'block diagram'. The program is constructed in the block diagram window by placing objects from the components library into the block diagram window and connecting them together using virtual connector wires. Loops are created by dragging and dropping these components from the library into the block diagram window [**15**].

Data Collection

Figure 4-12 shows the flow diagram of the data collection process.

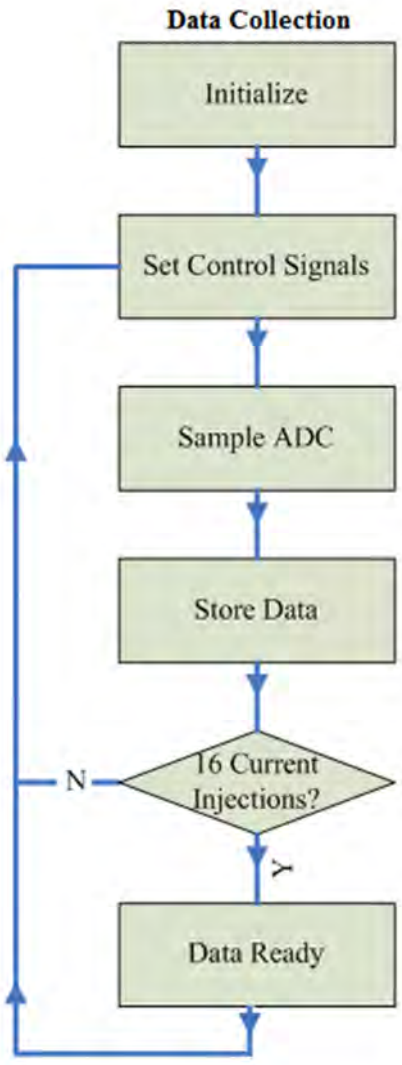

Figure 4-12: Flow diagram of the data collection process.

The neighbourhood method is the preferred data collection method as it is less complex than the adaptive method, more suitable to the medium than the cross method (electrodes in this medium are not separated by large dimensions) and has a larger sensitive area than the opposite method. Control signals for selecting electrodes are preloaded via the VI, while in standby mode. In standby mode the data collection VI waits for the user to enable it. Once enabled the VI begins taking measurements. To increase the accuracy of the measured voltages, an average of four voltage samples is taken per electrode, i.e. two measurements each on the positive half and negative half cycle.

When a complete frame's worth of data is captured (208 data samples), it is transferred to the image reconstruction VI.

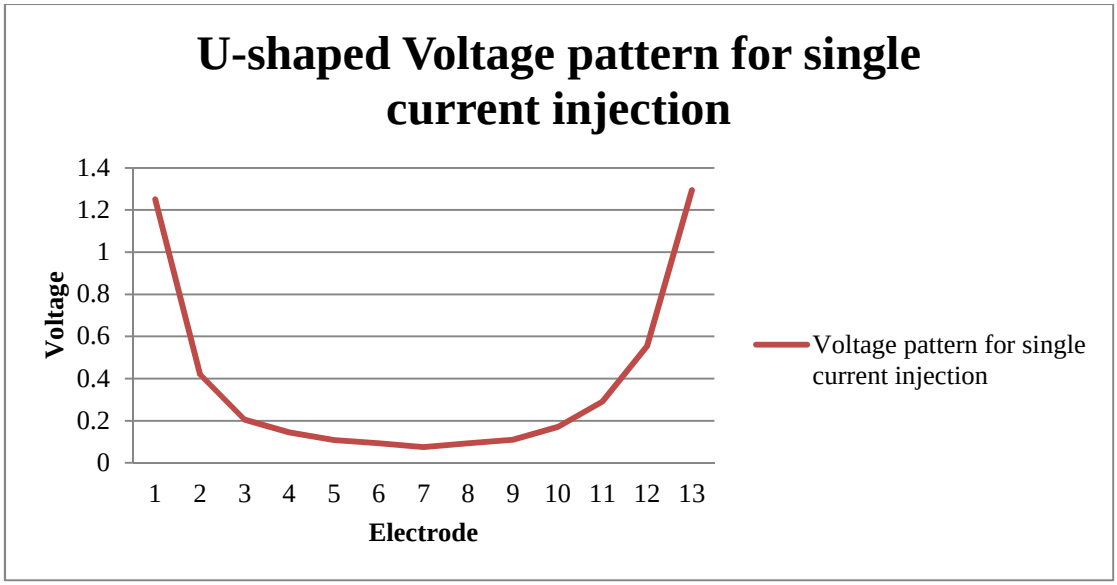

Figure 4-13: Data collected for a single current injection

When the AC current signal is applied to an adjacent pair of electrodes, the data collected for the applied current injection is 13 (voltage) samples. The pattern forms a U-shape shown in Figure 4-13. This is the characteristic shape of data collected in an homogeneous medium. The U-shape is to be expected as the first measurement is taken from the adjacent electrode pair closest to the point of injection (electrodes 1 and 2 in this case); the voltage measurement is then rotated around the phantom as described in Section 2.2.2 of Chapter 2. As the measurement is rotated around the phantom the measured voltage will decrease since the measurement is being taken further and further away from the point of injection. It then starts to increase again (from electrode 8) as the measurement gets closer to the point of injection from the other side of the phantom. The lowest voltage is recorded at the electrode pair opposite the point of injection as it is the farthest point from the point of injection thus the injected signal would have been attenuated due to the resistance of the medium.

Data collected is updated to a VI in real-time. This VI consists of a graph indicator used to plot the data collected from the phantom. This is done as a debugging tool to help confirm that the data collected is correct. If an electrode, multiplexer or connector wire, such as between the CCM and the collar is faulty, the data plotted on the VI will not have the U-shape as shown in Figure 4-13. Figure 4-14 shows 16 U-shaped curves; each 'U' represents a current injection. Due to different contact resistances in the collar electrodes, measured data differs for each electrode current injection pair. This affects the reconstructed image and has been compensated for through the use of tank controls (labelled '4', '7' and '9') shown in Figure A-14, so that only relevant changes are shown in the reconstructed image.

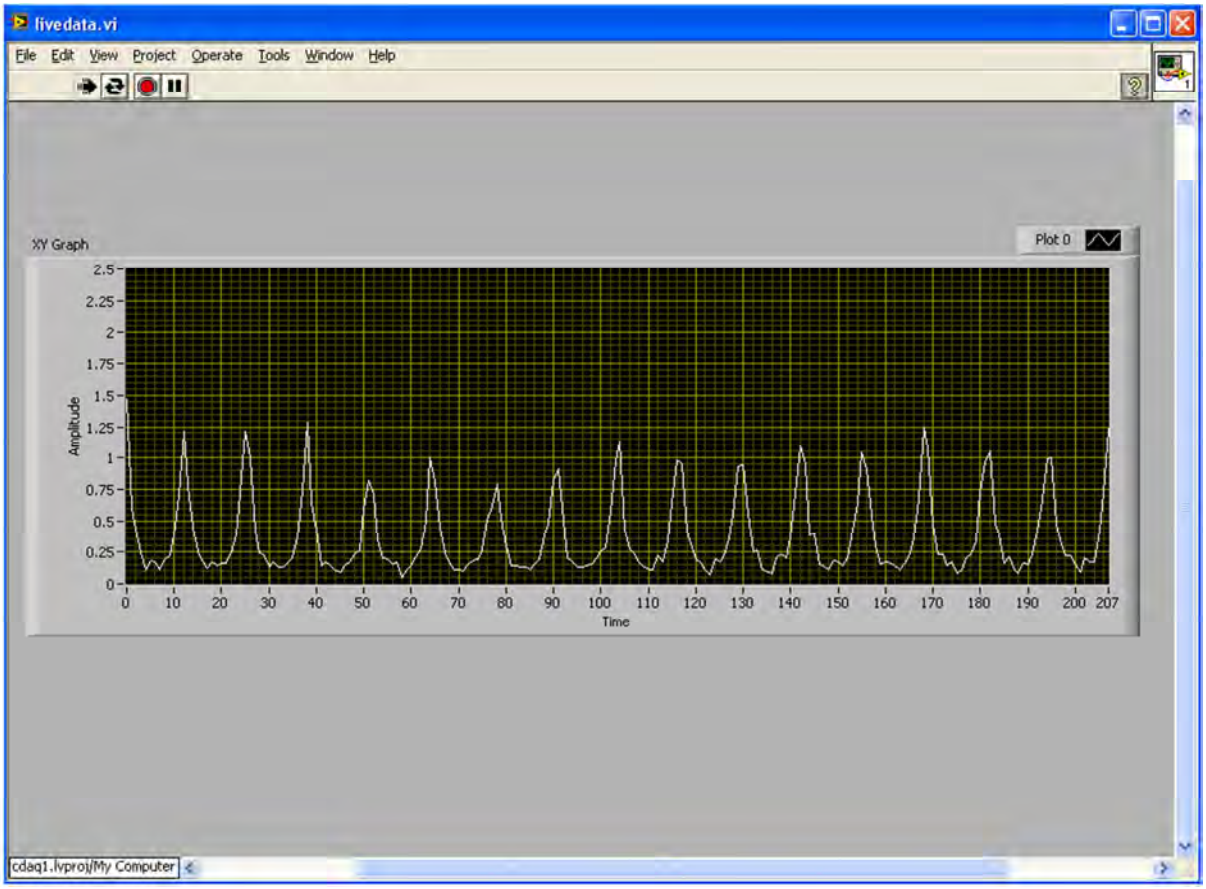

Figure 4-14: Front Panel of the live data VI showing raw data collected for a single tomographic image in an homogeneous medium.

Image Reconstruction

A high level flow diagram of the image reconstruction process is shown in Figure 4-15. The back projection algorithm described in Section 3.3.1 was ported to LabVIEW. Equipotential lines and weighting factor calculations are pre-computed during the initialization process. The image reconstruction VI then waits until enough data needed to reconstruct an image has been collected. Once the data has been collected, the back projection algorithm is executed and the reconstructed image is multiplied (pixel-wise) with the weighting factor to even out the sensitivity of each pixel in the image. The quantization process then takes place before the image is displayed on the VI. The image reconstruction VI executes faster than the data collection VI. This ensures that all data collected is reconstructed into an image before it is overwritten by a new data set.

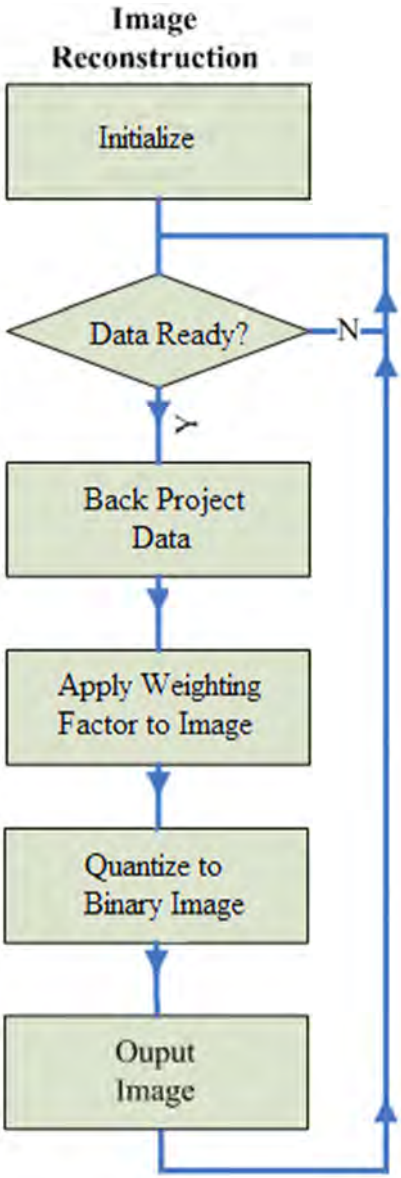

Figure 4-15: High level flow diagram showing the image reconstruction process.

A trade-off exists in the system between sensitivity in the centre and on the boundary. The system weighting factor improves overall sensitivity of the image in the centre but the decreased sensitivity on the periphery of the collar is obvious on the sensitivity plot shown in Figure 3-6 and through initial experiments performed.

As explained in Section 3.3.2 of Chapter 3, a modification was made to the weighting factor equation which helps to make the sensitivity more uniform across all pixels within the image. The sensitivity region depends on a user controlled tank control which is shown in Figure A-14. The reconstructed images produced using LabVIEW are presented in Chapter 5, the results chapter.

LabVIEW Web Services

LabVIEW web services allow communication with LabVIEW applications from remote devices that do not have LabVIEW by using a standard web based communication protocol via the web/LAN. A web service requires the following components:

- Server
- Client
- Standard Protocol
- Network

A server contains the main application where the requests and commands are processed. The server in this case is the USFF PC which runs the application that processes requests and sends back the processed image. The client is the web browser from which the user sends a request through HTTP standard protocol over a network such as Firefox or Google chrome.

A VI built as a web service must have methods through which it accepts requests, known as input methods or controls. A web service VI must also have a method through which it returns information; these are called indicators. Indicators are output methods the web service VIs use to respond to the client. Figure 4-16 is an overview of the flow of information from a LabVIEW application to the web service.

Figure 4-16: LabVIEW web services overview [16**]**

Once the Web service has been developed a thin client application is needed. Thin client applications typically run through a web browser and are the front end or user interface that a client uses to access a server. National Instruments Web UI Builder allows developers to build thin client user interfaces using graphical programming. The thin client allows LabVIEW applications that have been built as a web service to be accessed through a web browser. Figure 4-17 details the flow of information between a web service and a thin client.

Figure 4-17: Thin Clients and LabVIEW VIs [16,17**]**

The tomography application was built as a web service and a thin client application was developed for the web service. The thin client application simultaneously monitors 3 phantoms and updates images to a remote web browser.

Figure 4-18: Web page through which remote user may access the tomography system

Figure 4-18 shows the web interface of the real-time system seen from a browser on the client side. A manual is included in Appendix A16 explaining how the web interface is to be operated.

4.5 Final Boxed System

The real-time tomography system will be used as a diagnostic tool in the sugar mill hence it is required that the final solution be compact, portable and easy to use. A manual of the entire system (included in the Appendix) will accompany the tomography system. This will allow users to easily familiarise themselves with the system setup.

The boxed system, shown in Figure 4-19 is well ventilated through holes on its sides. This is necessary to keep the various parts of the system within operating temperatures. Precautions have been taken to ensure the safety of all users. The system contains a fuse to protect against any power surge or unexpected hazard that may occur. The USFF PC automatically powers up when the on/off switch is switched on. The entire system is pictured and labelled in Figure 4-19.

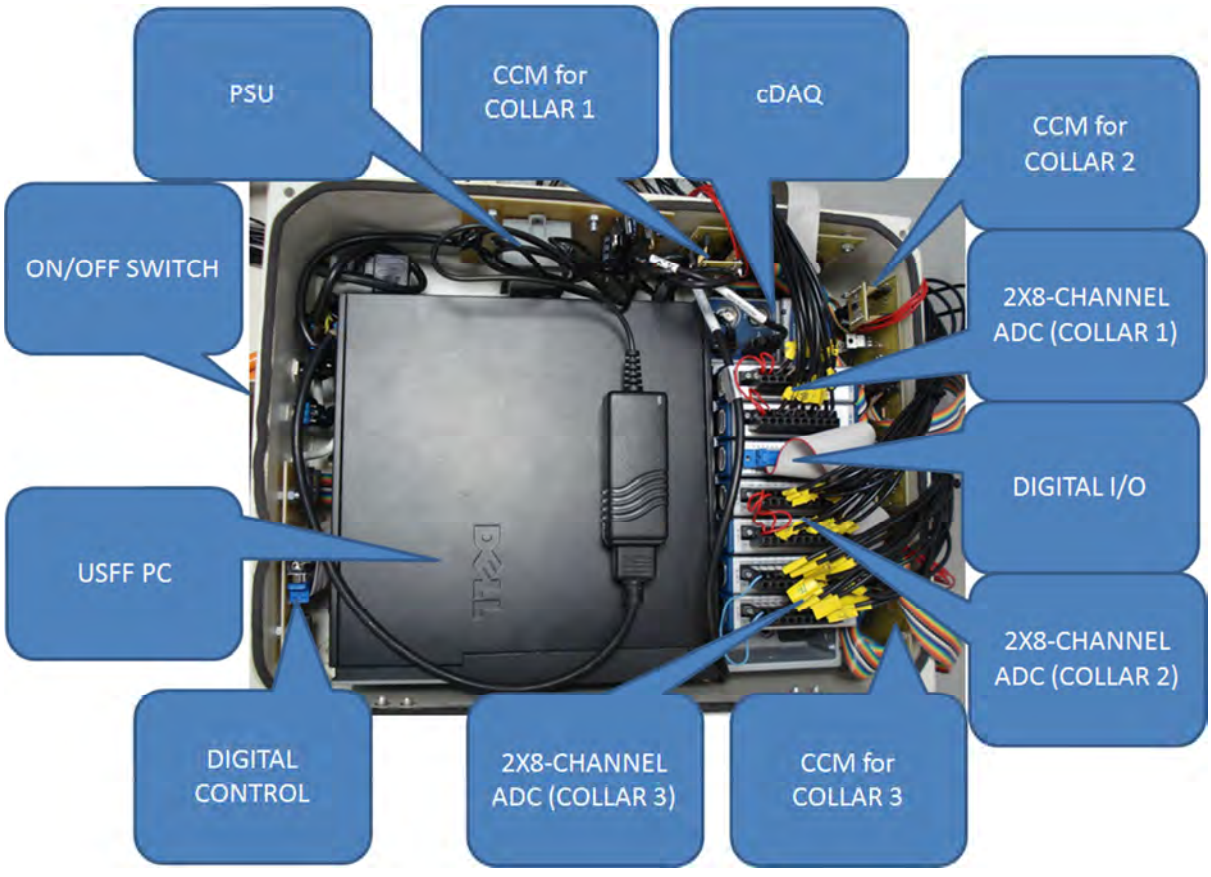

Figure 4-19: Real-time tomography system

The PSU is the power supply unit board. There are three CCM boards labelled, one for each of the collars. The digital control is the interface between the digital I/O module and the CCM boards.

In conclusion several improvements have been made on previous work [**3**]. The system now operates at a higher voltage than was previously designed this was to ensure that the data collected is less noisy than the previous design. The collection of data and reconstruction of image frames is now a seamless process which is one of the design objectives. The boxed system shown in Figure 4-19 is compact, which is also a research objective.

5. Results

In this chapter the results of tests performed in the laboratory are presented and analysed. Tests were performed on the capacitive massecuite to determine a suitable settling time i.e. the length of time which the system must wait before reliable data can be collected. The performance of the system under different collar loads is tested. The parameter *m* introduced in Chapter 3, the theory chapter, is varied to ascertain the system's operating conditions. Tests are performed over three conductive mediums i.e. 'pseudo' massecuite, water and deionized water.

The results of experiments done in the following areas are shown and discussed:

1. Optimum data collection speed
2. Image reconstruction speed.
3. Operating limits of the weighting factor and its impact on image reconstruction speed

5.1 System performance

The real-time tomography system comprises of two main parts; data collection and image reconstruction, which run in parallel. To test the data collection speed the mediums to be imaged must first be characterized.

5.1.1 Characterizing the massecuite medium

The highest sampling frequency of the tomography system is 35Hz therefore a 35Hz AC signal was applied to a massecuite filled collar to measure its response to a step input. The settling time of the massecuite response to this input must be calculated so as to determine a suitable sampling frequency. Deionized water and tap water were not characterized as they have minimal capacitive components.

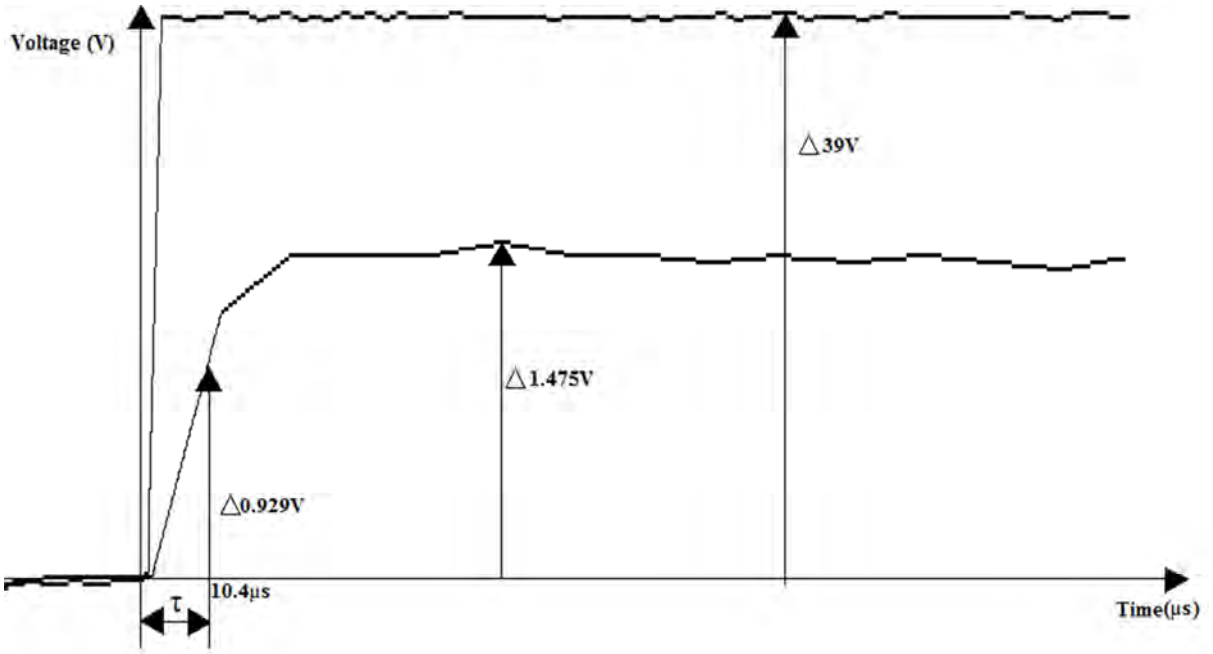

Figure 5-1: The output response of a synthetic-massecuite medium to a step input.

Figure 5-1 shows the step input into a collar filled with synthetic massecuite and the resulting response. The time constant τ was estimated as the time when the response reaches 63% of its final value. The final value was estimated as 1.475V hence the time constant is at 0.929V. The time constant τ was therefore estimated at 10.4μs. Estimating a settling time of 3τ for the response to be at a value which is over 90% of the response's final value. The settling time is approximately 31.2μs. This means that the system should wait at least 31.2μs after a signal has been injected before sampling to be sure that the sampled response will be at a value which is over 90% of its final value. This waiting period will give a frame rate of 154frames/s since 208 data points = 1 frame. However, for a 35Hz sampling frequency the fastest the system can sample the response after the injected signal is 28.57ms or 28570μs which is a long period after the estimated settling time. This is a hardware limitation as the data collection and overall system speeds can be faster.

5.1.2 Number of Frames per Second

An important speed test to consider was how the number of collars simultaneously enabled by the user affects the data collection rate. Each collar's ADC is connected in parallel on the chassis.

Initially one collar was tested, here; the average over ten frames was recorded. This was repeated with two collars and finally with all three collars. The results are shown in Column 2 of Table 5-1.

Table 5-1: Data collection rate for different number of collars

Number of Collars	Average data collection rate (Frames/s)
1	0.557788
2	0.540692
3	0.524942

Theoretically, the data collection speed is affected by capacitive properties of massecuite, i.e. a delay between injected and recorded signal. Therefore objects with minimal capacitive properties will have higher data collection speeds. The result in Table 5-1 shows that adding collars to the system decreases its frame rate. This is because for a fixed sampling frequency, if more collars are added then more data is to be captured simultaneously hence the amount of frames captured per second will decrease. The frame rate obtained when only collar 1 was connected should have halved in value when collar 2 was added but LabVIEW optimises the process to make it faster hence the drop in frame rate is not as significant.

Effect of weighting factor adjustment

Due to non-uniformity of the sensor zones circled by the 16 electrodes, a weighting factor was implemented in order to obtain a more balanced reconstructed image. Naturally this affects the speed at which an image frame is reconstructed since every pixel value in an image must be multiplied by a weighting factor before being displayed. Tests were performed so as to gain further knowledge into the effect of the weight calculations on the speed at which an image is reconstructed. Initially the time it takes for an image to be reconstructed was recorded without any weighting factor. The test was then repeated with the weighting factor included. The image reconstruction rate when no weighting factor is included is 4.211277frames/s. This reduces to 3.825259frames/s when weighting factor is included, which shows that the image reconstruction speed drops when the weighting factor is included. This makes sense as more processing time is needed to multiply each pixel value by its weighting factor before displaying the image. Image reconstruction is independent on the number of collars in the system because data collected from each collar is reconstructed in parallel.

The main problem however is that regardless of medium (capacitive or non-capacitive) the USB version of the cDAQ severely limits the sampling speed. This is evidenced by the fact that there is a large difference between the theoretical data collection rate (154frames/s) calculated for a massecuite medium and the measured data collection rate. The sample on demand option was chosen in the cDAQ-ADC setup but the speed at which data is accessed through the USB port is slow. The speed constraint is therefore hardware related and is fixed to 35Hz for all experiments. This system speed is slow enough to render the settling time required for this capacitive medium irrelevant.

5.2 Image Results

Due to the sugar mill schedule and the cost of shutting down a vacuum pan for testing our tomography system a vacuum pan could not be made available in 2011. Hence a test rig was built in the laboratory to closely mimic the boiling action in a vacuum pan. The collar was filled with 'synthetic massecuite', made up of 65% sugar granules and 35% syrup, until the tomography sensors were submerged. This synthetic massecuite was 'designed' to have a similar conductivity and viscosity at room temperature to that of real massecuite at boiling temperature (65 to70 ℃ at 15 kPa with steam supplied at 150 kPa and 110℃ [**3**]). The rig is fitted with a tube at its base so that air bubbles (steam) can pass from the bottom of the collar to the top and hence simulate the boiling action occurring in a vacuum pan.

The data collected in each session is time stamped and stored on the host PC and can be played at a later time. The reconstructed image is cross sectional (top) view of the collar as shown in Figure 5-2. The reconstructed image uses a colour scale to denote different resistivity values. Data with a low resistance is denoted blue and high resistance is a red colour. Resistance values that fall between these extremes take up different colours within the colour bar shown in Figures 5-2(b) and (c). Images produced from raw data are quantized (Section 3.3.3 of Chapter 3) to indicate bubbles or no bubbles.

Weighted and quantized images appear in two colours only, i.e. either high resistance (vapour) which appears as a red colour or low resistance (massecuite) which appears as a green colour. The requirement for the reconstructed image produced by the system is that it be able to differentiate between different conductivities. The shape of the detected object is of less relevance as long as an object having a different conductivity to the medium is detected. The parameter m introduced to the weighting factor equation (Equation 3.16) was varied to test the conditions under which the system will still function within afore mentioned objectives.

The massecuite, tap water and deionized water tests were conducted for three values of m i.e. $m = 0.1$, $m = 0.325$ and $m = 1$. When $m = 0.1$ the effect of the weighting factor is significantly diminished since m is close to zero hence the result of the weighting factor calculations will tend to one. When $m = 0.325$ and greater, the effect of the weighting factor is more pronounced while $m = 1$ yields the full effect of the weighting factor equation (Equation 3.15). $m = 0.325$ was chosen as the image produced during this setting provides a midpoint between $m = 0.1$ and $m = 1$.The reconstructed image of the homogeneous case is not affected by the weighting factor hence m is not varied for the homogeneous cases of the massecuite, tap water, and deionized water tests. However, m is varied for the non-homogeneous cases i.e. the PVC rod and bubble tests.

5.2.1 Massecuite Test

Figure 5-2a shows a reconstructed image of collar filled with synthetic massecuite. The image was reconstructed from raw data. Figure 5-2 (b) shows the same image after being weighted and quantized. The quantization process is implemented using the pseudo-code provided in Section 3.3.3 of Chapter 3.

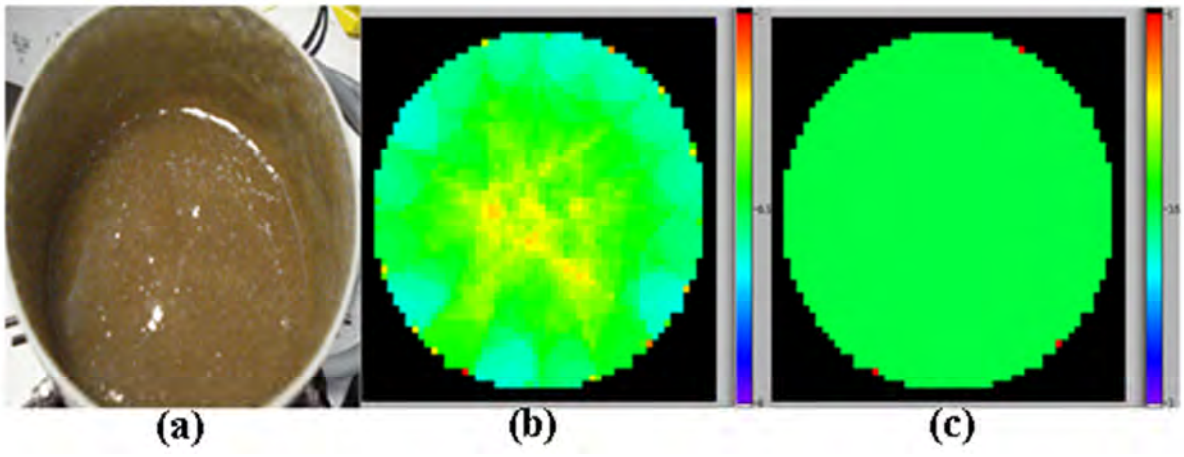

Figure 5-2: (a) Homogeneous condition, synthetic massecuite in collar. (b) Raw back projected image. (c) Weighted and quantized image

Once the homogeneous condition is established further tests were carried out to determine if non-homogeneous conditions can be detected. The image reconstruction method requires that the homogeneous state must first be known. Every measurement is compared to the homogeneous state and the difference is displayed as the reconstructed image. A nonconductive (PVC) rod was placed in the medium to test the sensitivity. Results are shown in Figure 5-3 and Figure 5-4 for different rod positions.

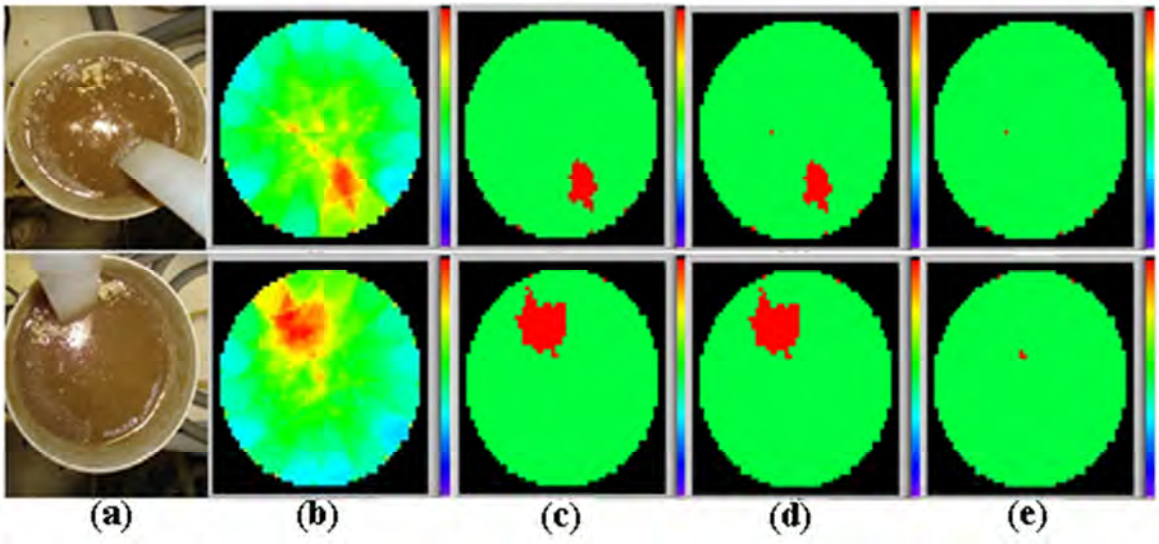

Figure 5-3: (a) Non-conductive rod placed in synthetic massecuite. (b) Raw back projected image. (c) Weighted and quantized raw image with *m*=0.1. (d) Weighted and quantized raw image with *m*=0.325. (e) Weighted and quantized raw image with *m*=1.

In Figure 5-3 the effect of varying *m* is visible. Figure 5-3a shows the position of the PVC rod in the medium. Figure 5-3(b) shows the raw back projected image. Figures 5-3 (c) and (d) shows the weighted and quantized results. The weighting factor's effect in Figure 5-3 (c) is to balance the sensitivity of the sensor zone as explained in Section 3.3.2 of chapter 3. In Figure 5-3 (e) *m*=1 and the change in conductivity caused by the PVC rod is not fully detected. The images show that as *m* is increased the sensitivity at the periphery of the collar is reduced.

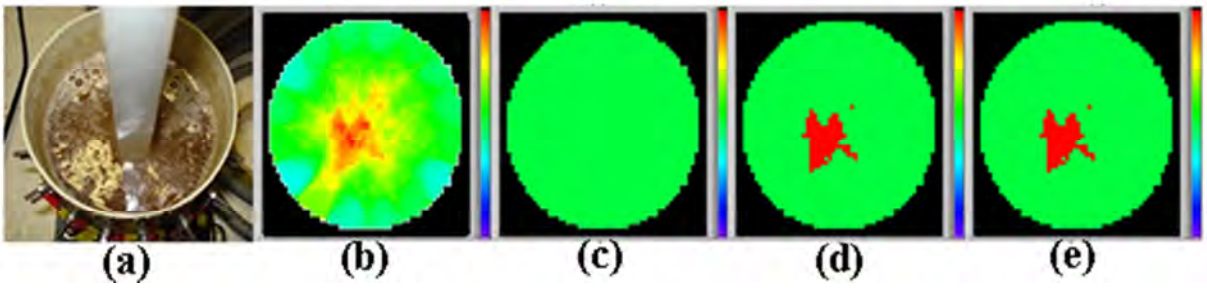

Figure 5-4: (a) Non-conductive rod placed in synthetic massecuite at the centre of collar. (b) Raw back projected image. (c) Weighted and quantized raw image with *m*=0.1. (d) Weighted and quantized raw image with *m*=0.325. (e) Weighted and quantized raw image with *m*=1.

In Figure 5-4 the effect of varying *m* is also visible. Figure 5-4 (a) shows the actual position of the PVC rod in the medium. Figure 5-4 (b) is the raw back projected image. Figures 5-4 (c), 5-4 (d) and 5-4 (e) show the quantized and weighted versions of Figure 5-4 (b). The dampened weighting factor in Figure 5-4(c) caused a reduced sensitivity at the centre of the collar. In Figures 5-4 (d) and (e) the change in conductivity caused by the PVC rod is visible. The images (Figure 5-4) show that as *m* is increased the sensitivity at the centre of the collar is increased. In Figure 5-3 (d) and Figure 5-4 (d) *m*=0.325. The reconstructed images for this value of *m* show that it is possible to have uniform

sensitivity at the centre and the boundary simultaneously. Lower values of *m* i.e. m=0.1 decreases sensitivity at the centre and increases sensitivity at the periphery and higher values of *m* i.e. m=1 have the opposite effect.

To simulate the boiling behaviour expected in the vacuum pan. The collar was fitted with a tube at its base. The tube was connected to a gas cylinder where compressed air was pumped through from the base. Pockets of compressed air would bubble through the synthetic massecuite.

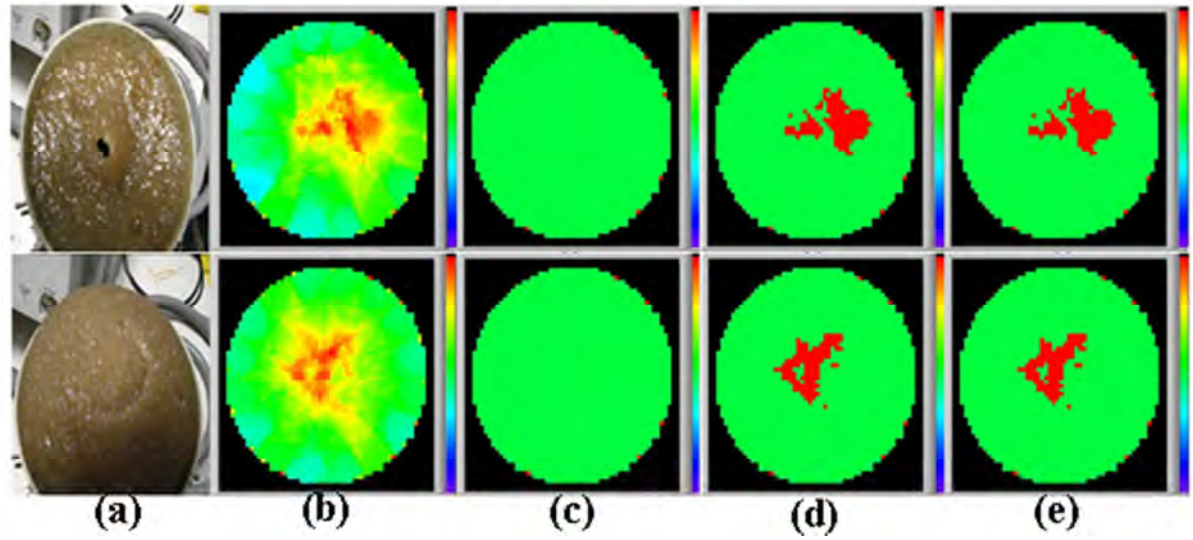

Figure 5-5: (a) Compressed air bubbles travel slowly through synthetic massecuite in collar. (b) Raw back projected image. (c) Weighted and quantized image with *m*=0.1. (d) Weighted and quantized image with *m*=0.325. (e) Weighted and quantized image with *m*=1.

Compressed air bubbles are slowly pumped through the base of the collar. The bubbles increase in size has they travel from the base of the collar to the top. The bubbles should be detected when they pass the region where the electrodes and sensors are located in the collar. When the top part of the bubble reaches the surface it 'deflates' hence the hole in Figure 5-5 (a). Interestingly the tomography image (Figure 5-5 (b)) gives a better representation of the size of the bubble which is hidden under the surface.

When *m*=0.1 bubbles are not shown in the image since they passed through the centre of the collar in this instance, where the sensitivity is low compared to the boundary. Figures 5-5 (d) and (e) detect bubbles indicating improved sensitivity at the centre of the collar for *m*=0.325 and *m*=1. The air bubbles were successfully detected for certain values of *m* as the results in Figure 5-5 clearly show.

The experiment represented in Figure 5-5 supports the fact that real-time mill testing would be possible as the laboratory tests have been done under conditions close to what is expected in the pan i.e. synthetic massecuite has similar conductivity and viscosity.

5.2.2 Tap water test

Tap water was used to test the ability of the system to detect resistance changes when there is a different 'boiling' dynamic due to either a change in viscosity and/or conductivity. Tap water is not as conductive as massecuite and it does not have high capacitive properties as massecuite. Figure 5-6 (b) shows the raw reconstructed image of a homogeneous phantom filled with tap water. Figure 5-6 (c) shows the adjusted image.

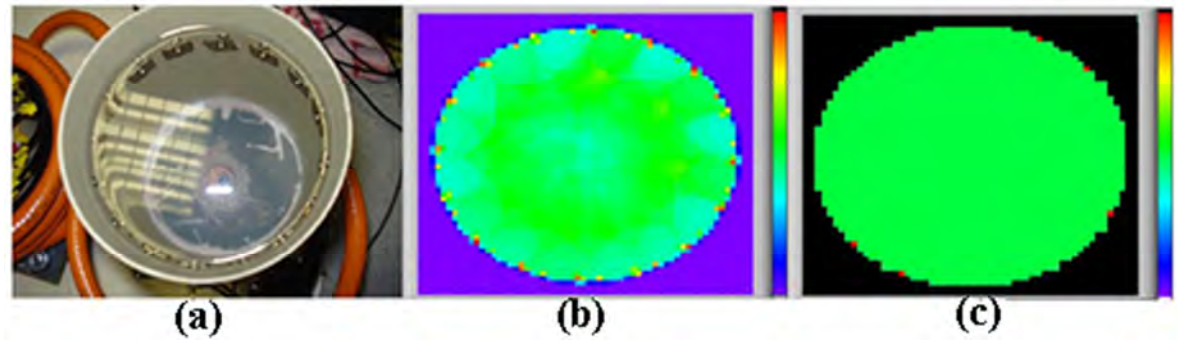

Figure 5-6: (a) Tap water in collar. (b) Raw back projected image. (c) Weighted and quantized image

To test how well a change in resistance can be detected, a non-conductive rod was placed at various positions in the collar. The results are shown in Figure 5-7.

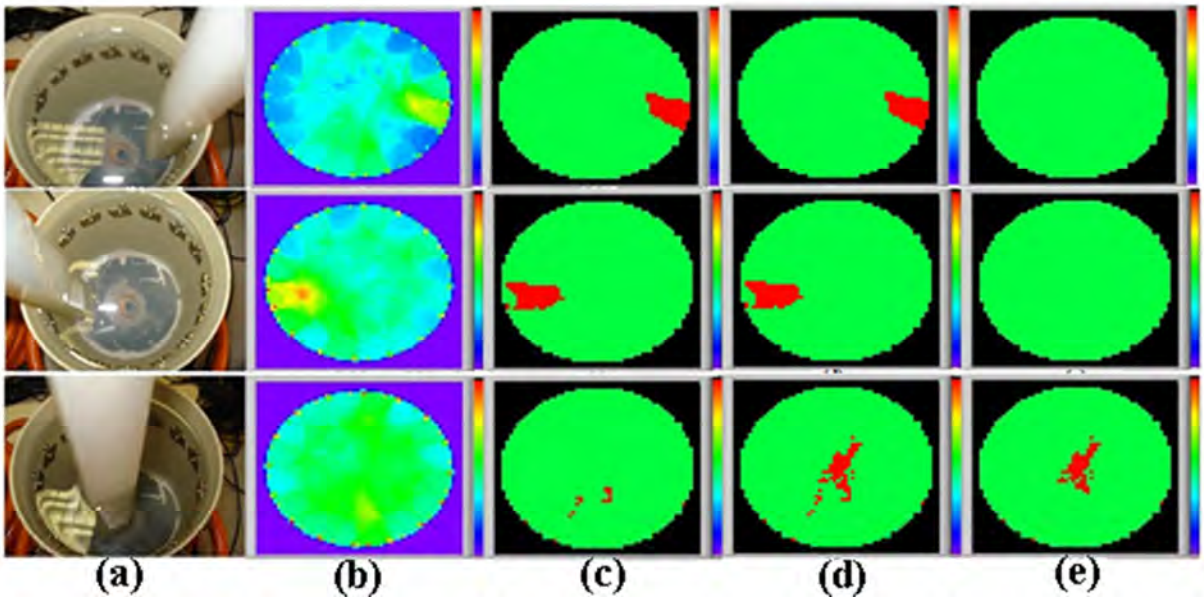

Figure 5-7: (a) Nonconductive rod placed in collar filled with tap water. (b) Raw back projected image. (c) Weighted and quantized image with *m*=0.1. (d) Weighted and quantized image with *m*=0.325. (e) Weighted and quantized image with *m*=1.

Figure 5-7 (a) shows the position of the PVC rod in the medium. Figure 5-7 (b) shows the raw back projected image. Figure 5-7 (c) and (d) shows the weighted and quantized versions of Figure 5-7 (b). The weighting factor in Figure 5-7 (c) is to balance the sensitivity of the sensor zone as explained in

Section 3.3.2 of Chapter 3. In Figure 5-7 (e) m=1 and the change in conductivity caused by the PVC rod is not detected when the rod is on the boundary but is detected when the rod is placed at the centre of the collar. The images show that as m is increased the sensitivity at the periphery of the collar is reduced.

Figure 5-7 shows that the system successfully detects the presence of a non-conductive rod at the boundary of the collar as well as in the centre for all values of m except m = 1. Theoretically, data collection should be faster for this medium as it is not as capacitive as massecuite.

Compressed air bubbles were released into the tap water filled collar. The result is shown in Figure 5-8.

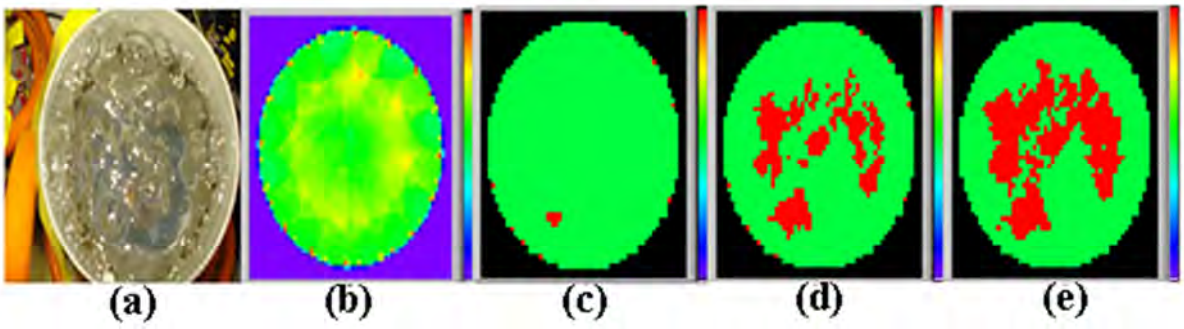

Figure 5-8: (a) Bubbles of compressed air released into tap water filled collar. (b) Raw back projected image. (c) Weighted and quantized image with m=0.1. (d) Weighted and quantized image with m=0.325. (e) Weighted and quantized image with m=1.

Since water is less viscous than massecuite, the bubbles disperse towards the boundary of the phantom a lot easier. When m=0.1 (Figure 5-8 (c)) bubbles are not detected at the centre of the collar. Figures 5-8(d) and (e) detect bubbles indicating an increase in the sensitivity at the centre of the collar for m=0.325 and m=1. The air bubbles were successfully detected at the centre for higher values of m as the results in Figure 5-8 clearly show. This also gives a good basis for mill testing as all bubbles do not have to be accurately imaged since the image reconstruction objective is to detect a change in conductivity.

5.2.3 Deionized water

Tap water was filtered and deionised for a period of 72 hours. This would significantly increase the resistance of the tap water. The purpose of the experiment was to significantly increase the resistance of tap water and test the capability of the system to detect resistance changes in such a case.

Figure 5-9 (b) shows the raw reconstructed image of a homogeneous phantom filled with tap water. Figure 5-9 (c) shows the quantized result of the same image. Higher resistance spots are observed on the boundary of the weighted filtered image. This appears only when deionized water is the medium and is attributed to the highly resistive nature of deionized water.

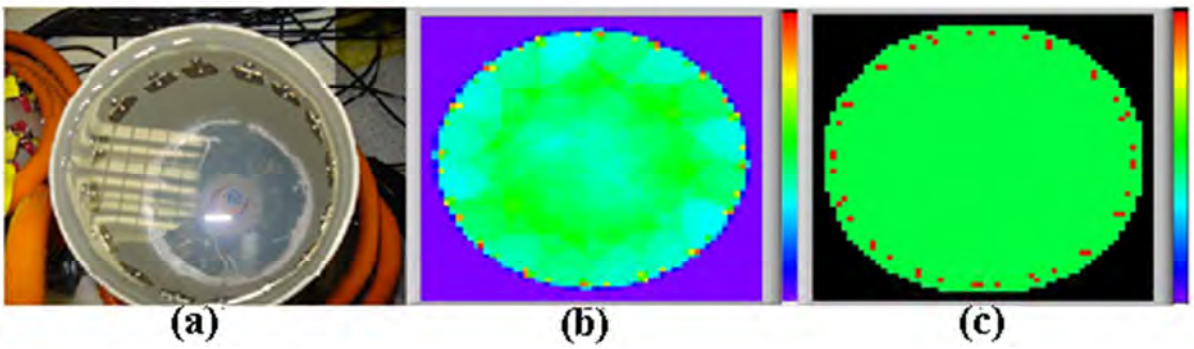

Figure 5-9: (a) Deionized water in collar, (b) Raw back projected image. (c) Weighted and quantized image

A non-conductive rod was also placed in various points in deionized water filled collar. The results are shown in Figure 5-10.

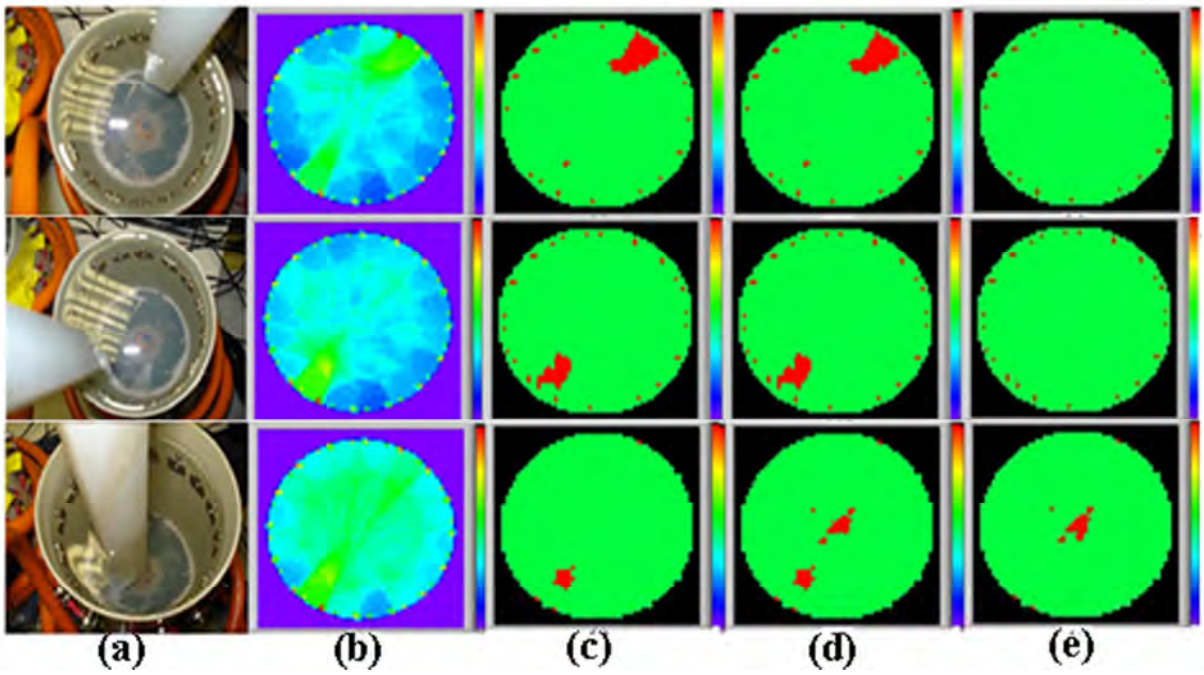

Figure 5-10: (a) Non-conductive rod placed in deionized water filled collar. (b) Raw back projected images. (c) Weighted and quantized image with *m*=0.1. (d) Weighted and quantized image with *m*=0.325. (e) Weighted and quantized image with *m*=1.

Figure 5-10 (a) shows the position of the PVC rod in the medium. Figure 5-10b shows the raw back projected image. Figures 5-10 (c), (d) and (e) are quantized and weighted versions of Figure 5-10(b). The weighting factor in Figure 5-10 (c) is dampened hence the sensitivity on the boundary. Figure 5-10 (d) detects changes at the boundary and at the centre while in Figure 5-10 (e) m=1 and the change in conductivity caused by the PVC rod is not detected when the rod is placed on the boundary. It is however detected when the rod is placed at the centre of the collar. The images show that as m is increased the sensitivity at the periphery of the collar is reduced and the sensitivity at the centre of the collar is increased.

Figure 5-10 shows that a non-conductive rod is successfully detected on the boundary of the collar. When the rod is placed at the centre of the collar the result obtained is less conclusive than in the case of tap water and massecuite as they are more conductive than the deionized water. Higher resistance (red) spots also appear in the Figure 5-10 (b) and (c) which are not present in image results obtained for tap water and massecuite.

Pockets of air bubbles were also passed through the deionized water. The result is shown in Figure 5-11.

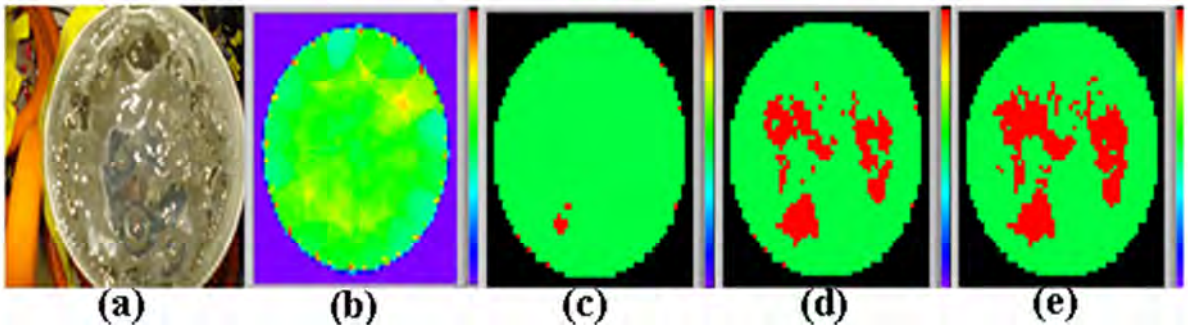

Figure 5-11: Bubbles pumped through deionized water. (a) Raw back projected image. (b) Weighted and quantized image with *m*=0.1. (c) Weighted and quantized image with *m*=0.325 (d) Weighted and quantized image with *m*=0.325. (e) Weighted and quantized image with *m*=1.

When *m*=0.1 (Figure 5-11 (c)) the bubbles at the centre are not detected because the image is sensitive at the boundary than at the centre of the collar. Figures 5-11 (d) and (e) detects bubbles indicating an increase in the sensitivity at the centre of the collar for *m*=0.325 and *m*=1. The air bubbles were successfully detected at the centre for higher values of *m* as the results in Figure 5-11 clearly show.

In conclusion the performance results show that the sampling hardware is responsible for the system's slow operating speed of 0.524942frames/s). The massecuite medium was characterized. This yielded a 3τ settling time of 31.2µs. This could not be tested as the system is not fast enough to sample faster than this settling time. The adjusted image demonstrates that the weighting factor influences the reconstructed image to a more realistic interpretation of the raw data. As *m* is increased there is reduced sensitivity at the boundary of the collar and increased sensitivity at the centre. It is therefore possible to locate an optimum point where sensitivity at the centre and at the boundary can be balanced (This adjusted was manually done and could be automated in the future).

6. Future Work

While the current system achieves the goals initially set out, there are still areas in which the system can be improved. One such area is the speed at which data is sampled. Future improvements to this system must focus on hardware which is able to sample data faster or from which data can be accessed at a greater speed than the USB cDAQ.

6.1 Compact and Faster Solution

The physical size of the current system would be vastly reduced if an application-specific device could be designed to replace both the USFF PC and the cDAQ. The first attempt at implementing a real-time system involved the use of 'compact Reconfigurable Input Output' (cRIO). The cRIO (Figure 6-1) is a NI device running a real-time LabVIEW operating system and would take the place of the USFF PC in this implementation. It is fitted with chassis so that NI modules such as ADCs and digital IOs can be interfaced with it. The cRIO executes LabVIEW applications and has faster access to the modules on the chassis as they are accessed through field programmable gate arrays. This would be a significant improvement on the current implementation as its most major limitation is its slow access to the ADC and digital I/O.

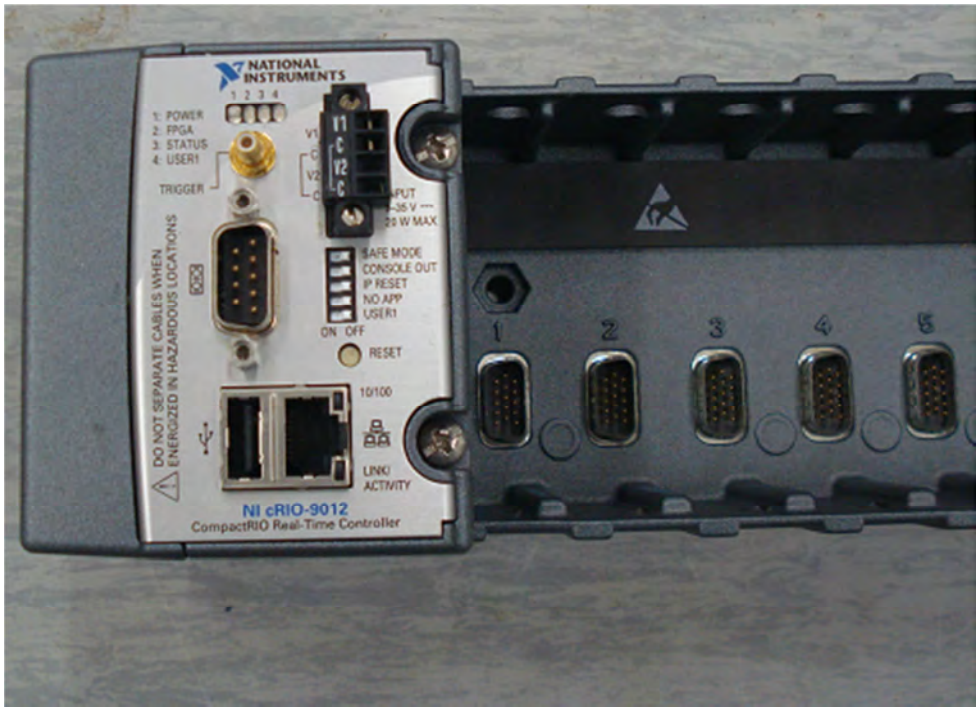

Figure 6-1: NI compact RIO chassis and real-time controller.

However, this implementation was discontinued because the processor speed and on-board memory were not enough to perform real-time tomography. NI Europe has started testing cRIOs with quad core i7 on-board processors in their labs which are due to be available for purchase in the near future. This cRIO model will be able to execute the reconstruction algorithm in real-time as its specifications are more powerful than the USFF PC used in this project. This would reduce the physical size of the

system. It would also be able to perform at speeds where it would be possible to reconstruct multiple frames per second. A major redesign would not be required as the application currently running on the USFF PC would easily be transferred to the improved cRIO for execution.

6.2 Collars

The ring lugs on the outside of the PVC tube (connecting the coaxial cables to the electrodes) is coated with resin, thus insulating the electrodes and hence only injecting current to the interior of the collar (the resin also strengthens the structure of the collar). The resin solution worked well in the laboratory environment but after months of repeated boiling, the massecuite will begin to seep through the resin coat, such as at the point where the cables protrude through the resin (circled in Figure 6-2).

Figure 6-2: Massecuite seep through resin (Weak point circled in red). This is an old collar design with magnets to secure the collar to the pan 'floor'.

A new method of applying the resin, which is yet to be tested, was proposed. This method involves using a resin mould that would better secure the cable and ensure that there are no gaps between the resin and cable at the point where the cable protrudes through the resin. A proposed solution uses a mould shown in Appendix A-10. The mould splits into two parts that can be attached when needed.

There are two holes at the bottom. One is to be used as an outlet for the cables and the other to pour the resin into the mould. Figure A-11 in the appendix shows how the collar would look.

7. Conclusion

The aim of the research was to develop a compact, real-time tomography system to detect the changes in conductivity due to the bubbles formed in the calandria tubes during the boiling of massecuite syrup in a vacuum pan. The images will enhance our understanding and monitoring of the boiling dynamics in a sugar pan. The tomography data can also be used in conjunction with CFD tools to design better sugar pans.

The entire real-time system was successfully designed and implemented. The neighbourhood data collection algorithm was developed in LabVIEW. The image reconstruction was developed in MATLAB during the prototyping stage before being transferred to LABVIEW for the final implementation. A web service application was developed to allow remote users on the same network to control data collection and view the reconstructed image through a browser. The software application is standalone and can be installed on windows PCs running windows XP upwards.

The results demonstrate that capacitive mediums such as massecuite require a settling time before reliable data can be sampled although the bottleneck of the system was found to be well short of this settling time. A faster real-time system could be implemented if a faster sampling hardware is used. The results also show that the system can successfully detect resistance changes in mediums such as synthetic massecuite, tap water and deionized water.

A non-conductive rod and bubbles created from compressed air were successfully detected at multiple regions within the collar in all three mediums. The results show that the best weighting uniformity is achieved when m=0.325. The weighting factor makes it possible to detect changes that occur at the centre of the collar (when m=1) and at the boundary (when m=0.1).

Bibliography

[1] I. Oyvind, "A review of reconstruction techniques for capacitance tomography," *Measurement Science and Technology*, vol. 7, no. 3, pp. 325-337, December 1995.

[2] L.F. Echeverri, P.W. Rein, and S. Acharya, "Measurements and CFD simulations of the flow in vacuum pans," *Proc. Int. Soc. Sugar Cane Technol.*, vol. 26, pp. 1341-1353, 2007.

[3] D. Sanderson, "The application of Electrical Resistance Tomography within a vacuum sugar pan in order to better understand its boiling dynamics," University of Kwazulu Natal, Durban, MSc Dissertation 2010.

[4] E.L. Costa, C.N. Chaves, S. Gomes, and M.A. Beraldo, "Real-time detection of pneumothorax using EIT," *Critical care medicine*, vol. 36, no. 4, pp. 1230-1238, April 2008.

[5] R.W.M. Smith, I.L. Freeston, and B.H. Brown, "A real-time electrical impedance tomography system for clinical use-design and preliminary," *IEEE transactions on biomedical imaging*, vol. 42, no. 2, pp. 133-140, February 1995.

[6] (2010, Oct.) Rapiscan Systems. [Online: September 2010]. http://www.rapiscansystems.com/technologies/real_time_tomography.

[7] N.M. Briggs, N.J. Avis, and F. kleinermann, "A real-time volumetric visualization system for electrical impedance tomography," *Clinical Physics and Physiological Measurement*, vol. 21, no. 1, pp. 27-33, February 2000.

[8] L.M. Heikkinen, J. Kourunen, T. Savolainen, and P.J. Vauhkonen, "Real-time three dimensional electrical impedance tomography applied in multiphase flow imaging," *Measurement science and technology*, vol. 17, no. 8, pp. 2083-2087, February 2006.

[9] A. Hilger, *Electrical Impedance Tomography*, Webster J.G., Ed. Bristol England: IOP Publishing Ltd, 1990.

[10] D.G. Gisser, D. Isaacson, and J.C. Newell, "Current topics in impedance imaging," *Clinical Physics and Physiological Measurement*, no. Supplement A, pp. 39-46, November 1987.

[11] P. Hua, J.G. Webster, and W.J. Tompkins, "Effect of the measurement method on noise handling and image quality of EIT imaging process," in *Annual International conference of IEEE Engineering in Medicine and Biology Society*, 1987.

[12] D.C. Barber and B.H. Brown, "Recent developments in Applied Potential Tomography," in *Information Processing in Medical Imaging*, 1986.

[13] A.D. Seagar, D.C. Barber, and B.H. Brown, "Theoretical limits to sensitivity and resolution in impedance imaging," *Clinical Physics and Physiological Measurement*, pp. 13-31, 1987.

[14] National Semiconductor. Lm317 Datasheet. Document.

[15] R. Bitter, T. Mohiuddin, and M. Nawrocki. LabVIEW Advanced Programming Techniques. [Online: January 2011]. www.physics.utah.edu/~bergman/3620-6620/supp/LV./2049fm.pdf

[16] NI. National Instruments Coporation. [Online: January 2011]. http://www.ni.com

[17] NI. LabVIEW Graphical Programming for Engineers and Scientists. [Online: January 2011]. www.ni.com/

[18] Q Zhu, C McLeod, C Denyer, F Lidgey, and W Lionheart, "Development of a real time adaptive current tomograph," *Physiological Measurement*, vol. 15, pp. A37-A43, 1994.

[19] A. Ross, G.J. Saulnier, J.C. Newell, and D. Isaacson, "Current Source Design for Electrical Impedance Tomography," *Physiological Measurement*, vol. 24, pp. 509-516, 2003.

[20] R. Murugan, "An improved Electrical Impedance Tomography (EIT) Algorithm for the Detection and Diagnosis of Early Stages of Breast Cancer," University of Manitoba, Winnipeg, PhD Thesis 1999.

[21] G.J. Saulnier, R.S. Blue, J.C. Newell, D. Isaacson, and P.M. Edic, "Electrical Impedance Tomography," *IEEE Signal Processing Magazine*, pp. 31-43, November 2001.

[22] Q. Zhu, C. Luo, Z. Zhong, and M. Chen, An Improved Back Projection Algorithm for Electrical Impedance Tomography, 2005.

[23] C. Yossontikul, K. Chitsakul, M. Sangworasil, and Y. Kitjaidure, "An Electrical Capacitance Tomography," King Mongkut's institute of Technology, Bangkok, Progress Report 2005.

[24] E.J. Woo, P. Hua, J.G. Webster, and W.J. Tomkins, "Finite Element Method in Electrical Impedance Tomography," *Medical and Biological Engineering and Computing*, vol. 32, pp. 530-536, September 1994.

[25] J.G. Webster and P. Hua, "Recent North American Progress in Electrical Impedance Tomography," *Clinical Physics and Physiological Measurement*, vol. 9, no. Supplement A, pp. 127-130, 1988.

[26] T. Warren and D.R. Wilcox, "Feasibility Study of Capacitance Tomography," in *The 2006 International Conference on Image processing*, Marietta, 2006.

[27] T.F. Scheussler and J.H. Bates, "Current Patterns and Electrode Types for Single-Source Electrical Impedance Tomography of the Thorax," *Annals of Biomedical Engineering*, vol. 26, pp. 253-259, 1998.

[28] S. OH and R. Sadleir, "Sensitivity Distribution Field of Electrical Impedance Tomography," in *Multiphysics User's Conference*, Boston, Massachusetts, 2005.

[29] J. Kang, M. Kim, and J. Kim, The Modified Newton-Raphson Algorithm Using Region of Interest in EIT, 2008.

[30] R. Guardo, C. Boulay, B. Murray, and M. Bertrand, "An Expermental Study in Electrical Impedance Tomography Using Back Projection Reconstruction," *IEEE Transactions on Biomedical Engineering*, vol. 38, no. 7, pp. 617-627, July 1991.

[31] D.G. Gisser, D. Isaacson, and J.C. Newell, "Theory and Performance of an Adaptive Current Tomography System," *Clinical Physics and Physiological Measurement*, vol. 9, pp. A35-A41, 1988.

[32] M. Cheney, D. Isaacson, J.C. Newell, S. Simske, and S. Goble, "NOSER: An Algorithm for Solving the Inverse Conductivity Problem," *International Journal of Imaging systems and Technology*, vol. 2, pp. 66-75, 1990.

[33] B.H. Brown and A.D. Seagar, "The Sheffield Data Collection System," *Clinical Physics and Physiological Measurement*, vol. 8, no. Supplement A, pp. 91-97, 1987.

[34] B. Blad, K. Lindstrom, L. Bertenstam, B. Persson, and N. Holmer, "A Current Injecting Device for Electrical Impedance Tomography," *Physiological Measurement*, vol. 15, pp. A69-A77, 1994.

[35] D.C. Barber, B.H. Brown, and I.L. Freeston, "Imaging Spatial Distribution of Resistivity Using Applied Potential Tomography," *Electronics Letters*, vol. 19, no. 22, pp. 933-935, October 1983.

[36] R. Apinai, Y. Chanrit, L. Thanakorn, C. Kitiphol, and S. Manas, "Electrical Capacitance Tomography Systems for Industrial Application," National Research council of Thailand, Bangkok, Progress report 2006.

[37] Webster J G and Tompkins W J Hua P, "Effect of the measurement method on noise handling and image quality of EIT imaging process," in *Annual International conference of IEEE Engineering in Medicine and Biology Society*, 1987, pp. 1429-1430.

Appendix

Circuit Boards

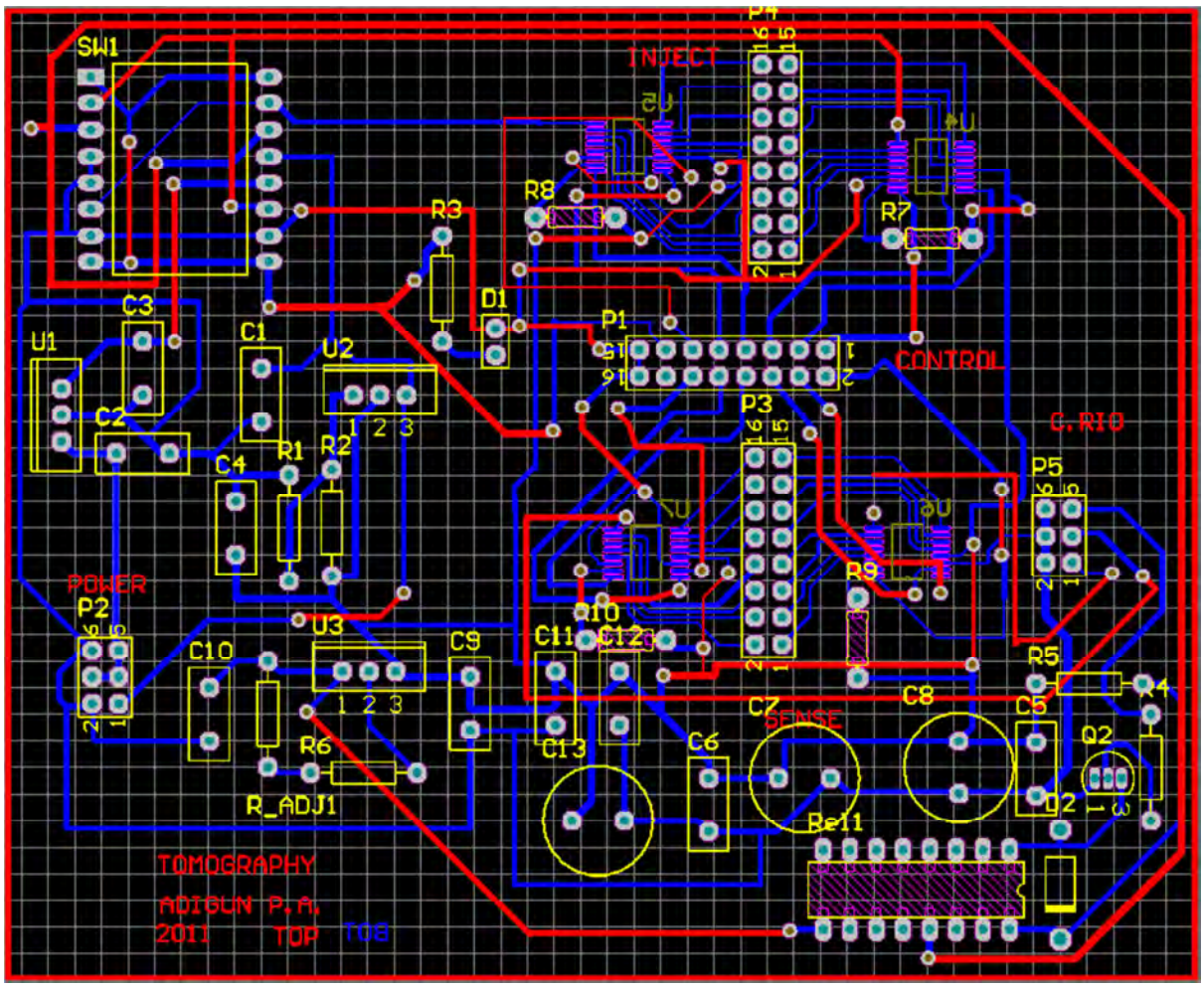

Figure A- 1: Current Control Module PCB Layout

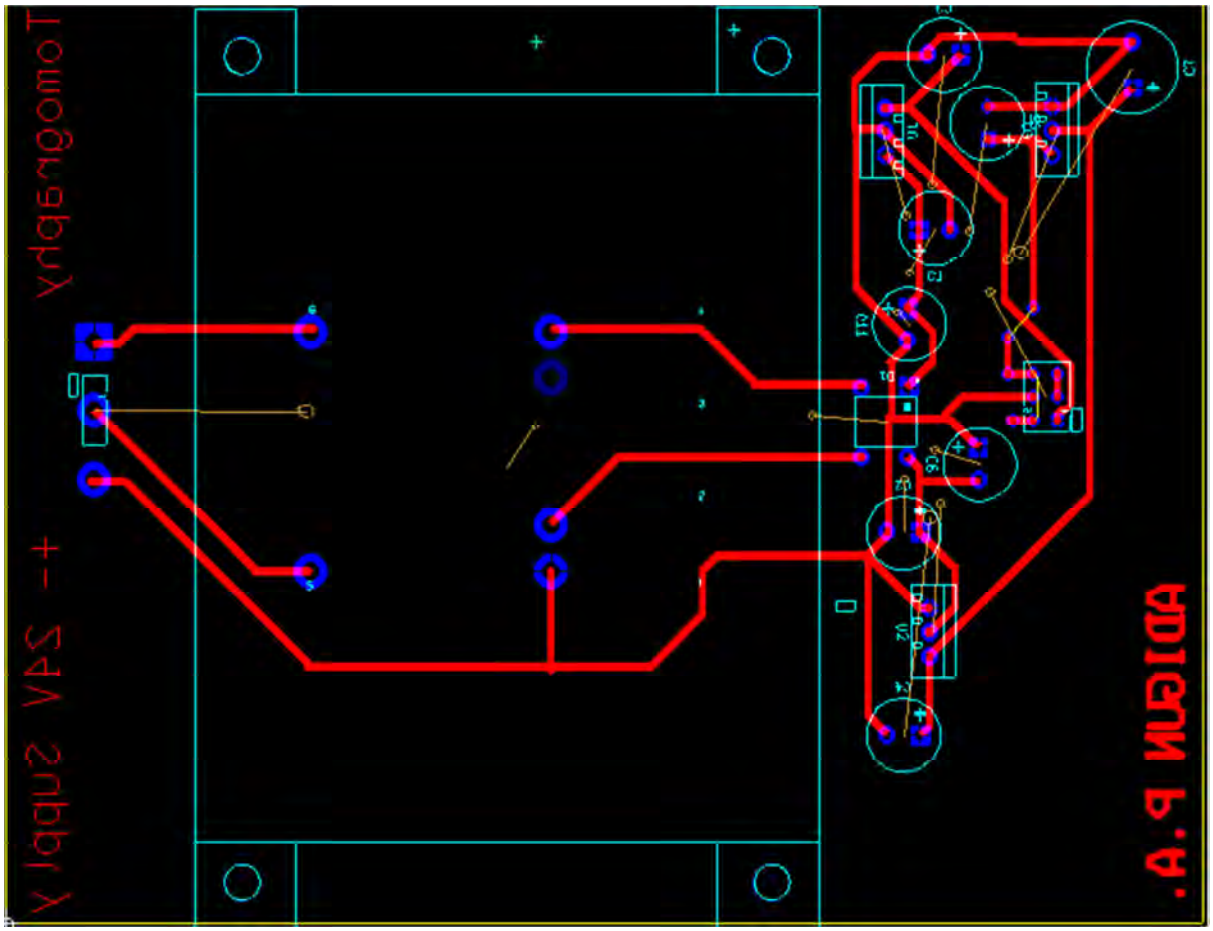

Figure A- 2: Power Supply circuit PCB Layout

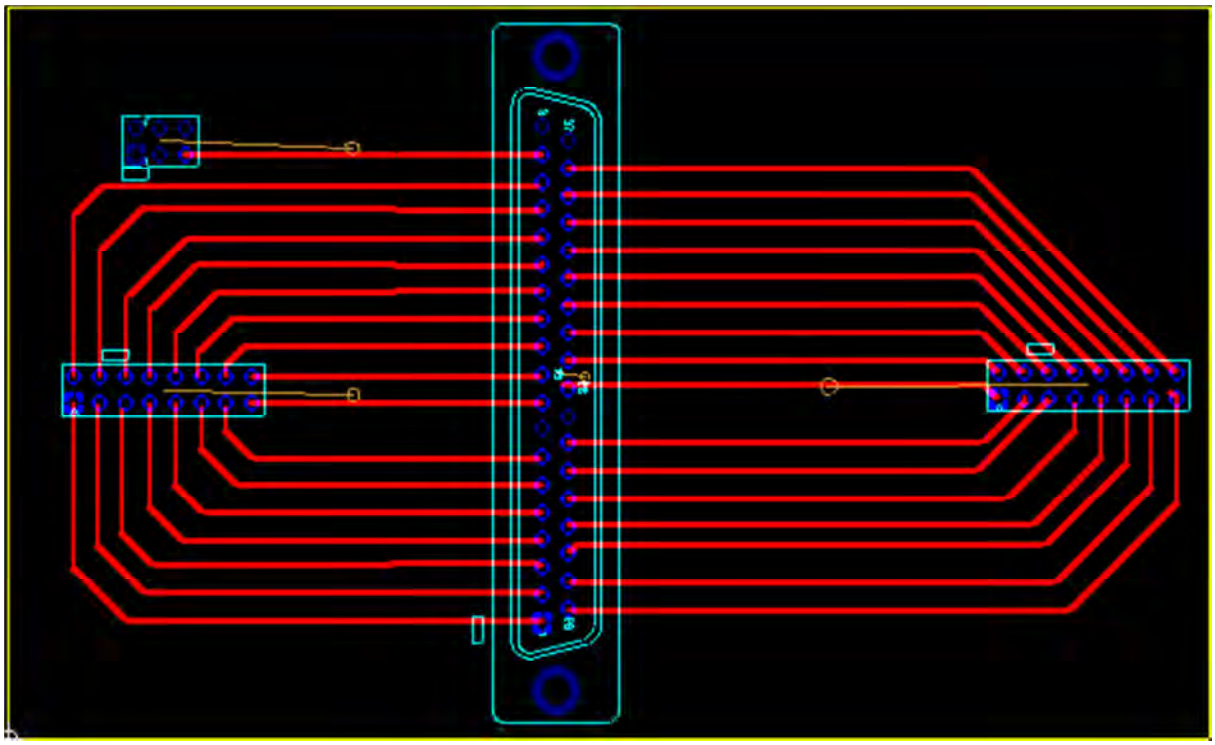

Figure A- 3: Digital interface circuit PCB Layout

MATLAB Code Sample

```
%Draws the Equipotential lines
%Declarations
u=10;
E=zeros(2,16);
V=zeros(1,16);
x=zeros(200);
y=zeros(200);
x1=zeros(200,16);
y1=zeros(200,16);
%For loop to draw Circular region centred at(0,0)
for v=-1:199
        x(v+1)=u/(u^2+v^2);           %Equation 3.8
        y(v+1)=v/(u^2+v^2);           %Equation 3.9
end
%Obtain Coordinates of where Equipotentials cross the circular
boundary
%i.e. Electrode Coordinates
for t=0:pi/8:(2*pi-pi/8)
    m=m+1;
    E(1,m)=0.5*cos(t);
    E(2,m)=0.5*sin(t);                %Equation 3.13
    V(1,m)=E(1,m)/(E(1,m)^2+E(2,m)^2);%Equation 3.12
end
%For loop to obtain x and y Coordinates for equipotential lines
n=0;
for u1=1:0.05:100
    n=n+1;
    for m=1:16
        x1(n,m)=u1/(u1^2+V(1,m)^2);         %Equation 3.8
        y1(n,m)=V(1,m)/(u1^2+V(1,m)^2);     %Equation 3.9
    end
end
```

Collar Manufacturing Specifications

Electrodes

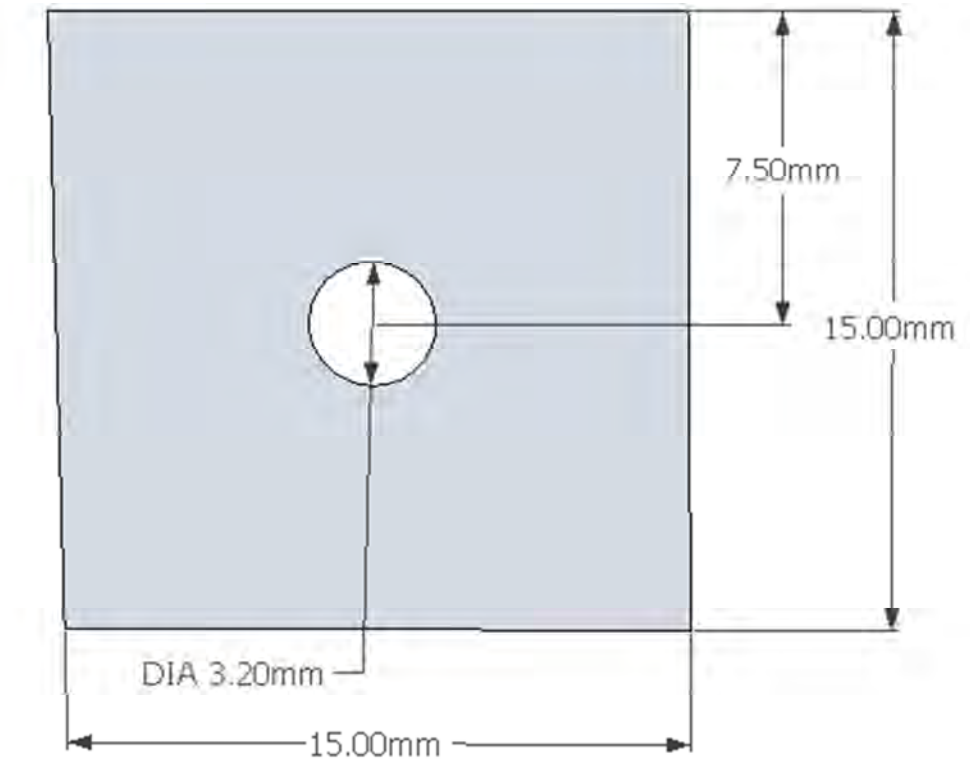

Figure A- 4: Front view of the electrode with dimensions

The Electrode including dimensions is shown above. The electrode material must be conductive but non-corrosive. The hole in the centre of the electrode plate is to fit a 3mm bolt (tight fit) and hence the diameter should be slightly greater than 3mm (approx. 3.2mm). All other dimensions are to remain as shown above. The plate thickness is between 0.5mm and 0.7mm. Each collar contains 16 Electrodes equally spaced apart.

Brackets

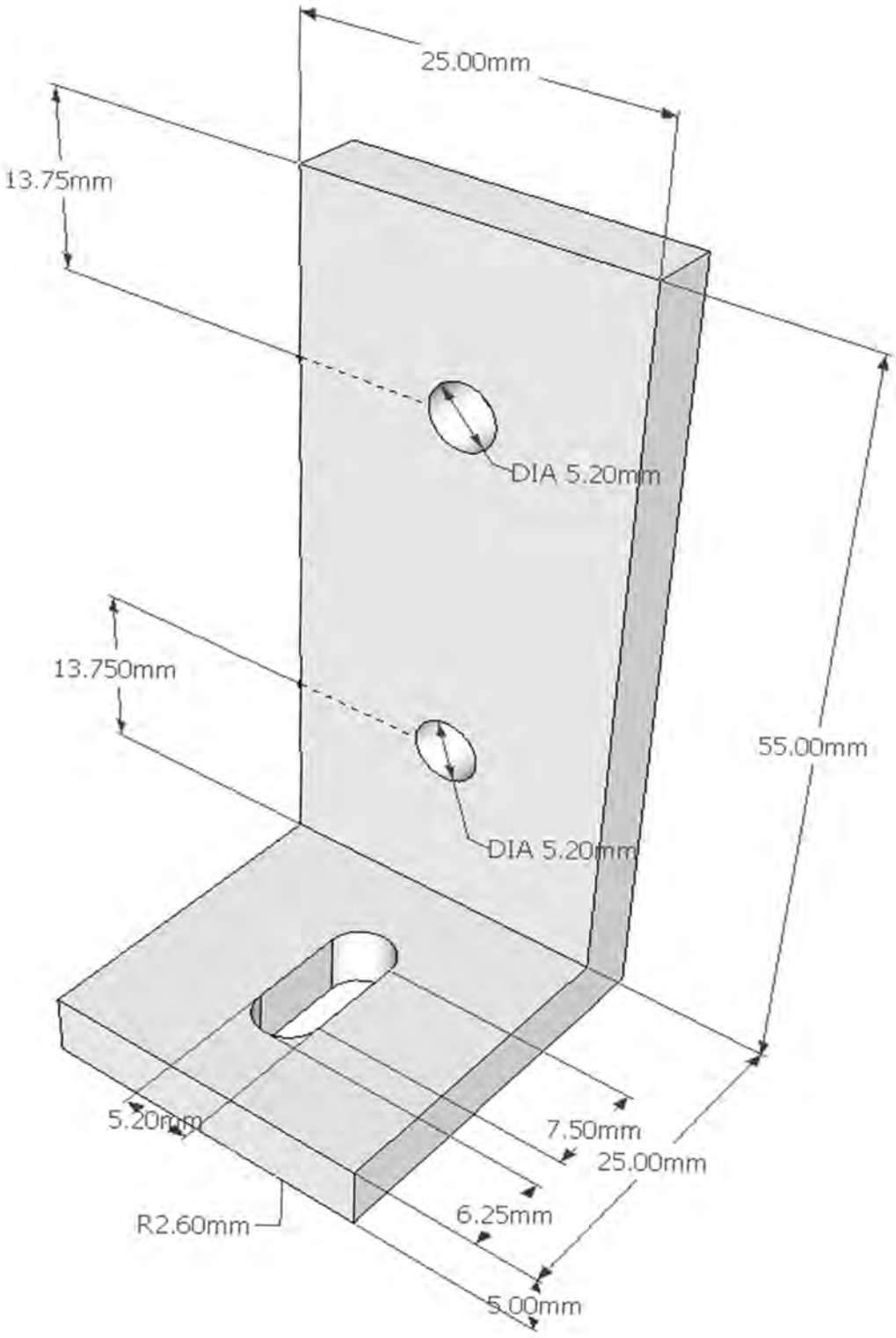

Figure A- 5: Isometric view of the bracket

Each collar contains 3 brackets and they are to be equally spaced (120 degrees apart). The 5mm diameter through holes on the vertical region are to fit 5mm bolts (tight fit) and should thus be slightly larger than 5mm (approx. 5.2mm). The through hole in the horizontal section is also to be slightly larger than 5mm for the same reason. The front and side views of the bracket are shown below. The Bracket is one single piece of metal bent to form an ‘L’ shape.

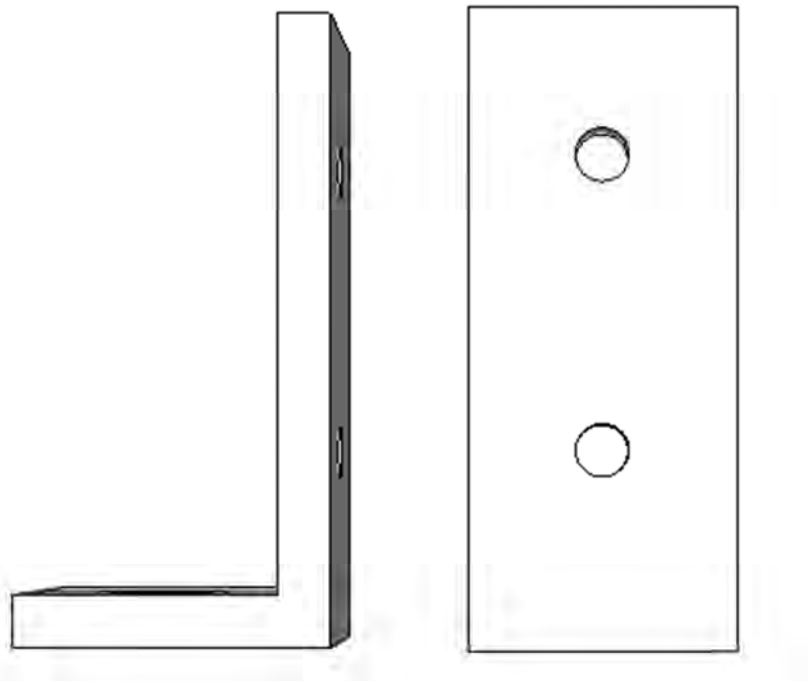

Figure A- 6: Back and side view of bracket.

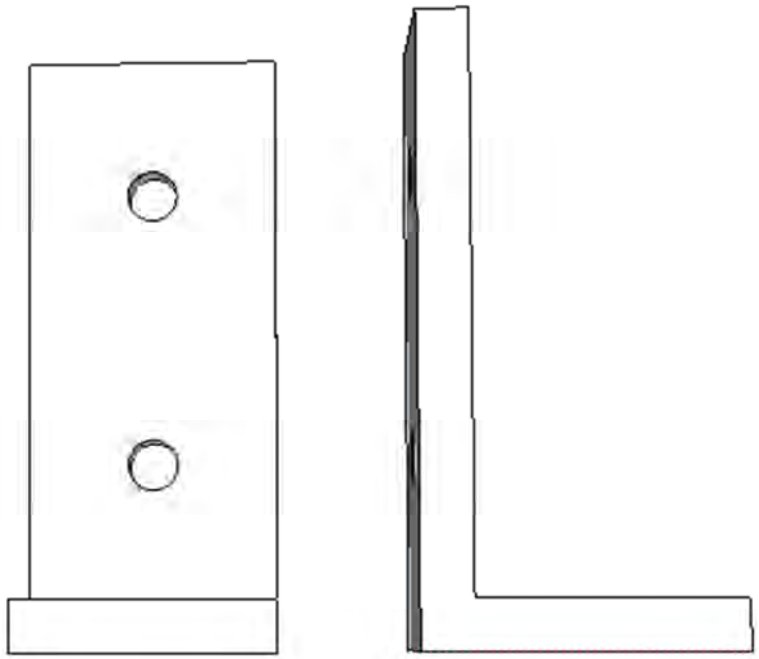

Figure A- 7: Front and side view of bracket

The tube

The tube is made of PVC and is 110mm diameter and 1mm thickness. It contains a row of 16 through holes 3mm in diameter and 50mm from the top of the tube to the centre of the through holes. They will have 3mm bolts passing through them and should thus be slightly larger than 3mm as in the case of the electrode plate. Nearer to the bottom of the tube there are 2 rows of through holes, 5mm in diameter, corresponding to the 5mm through holes on the vertical portion the bracket. They must each be slightly larger than 5mm so that a 5mm bolt tightly fits into it.

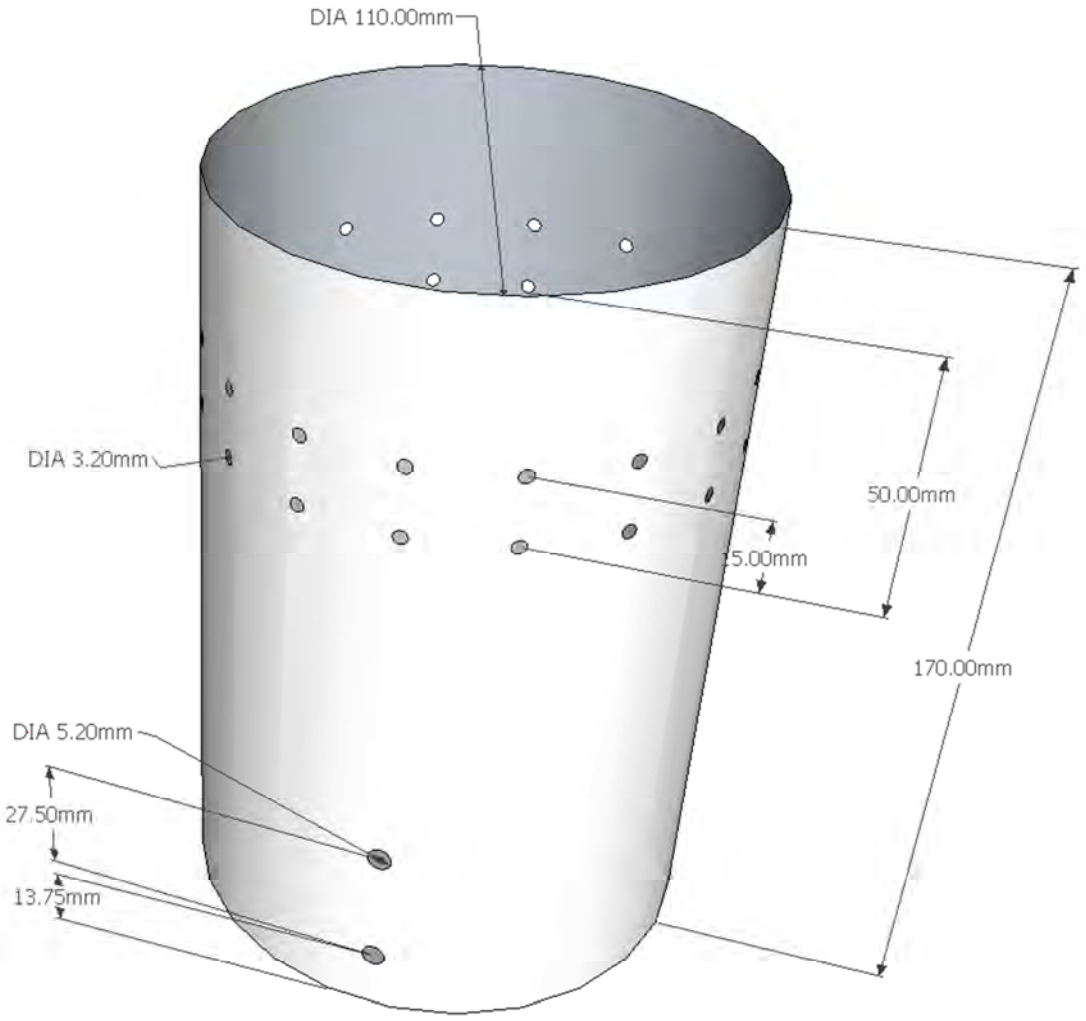

Figure A- 8: Isometric view of the object with dimensions included.

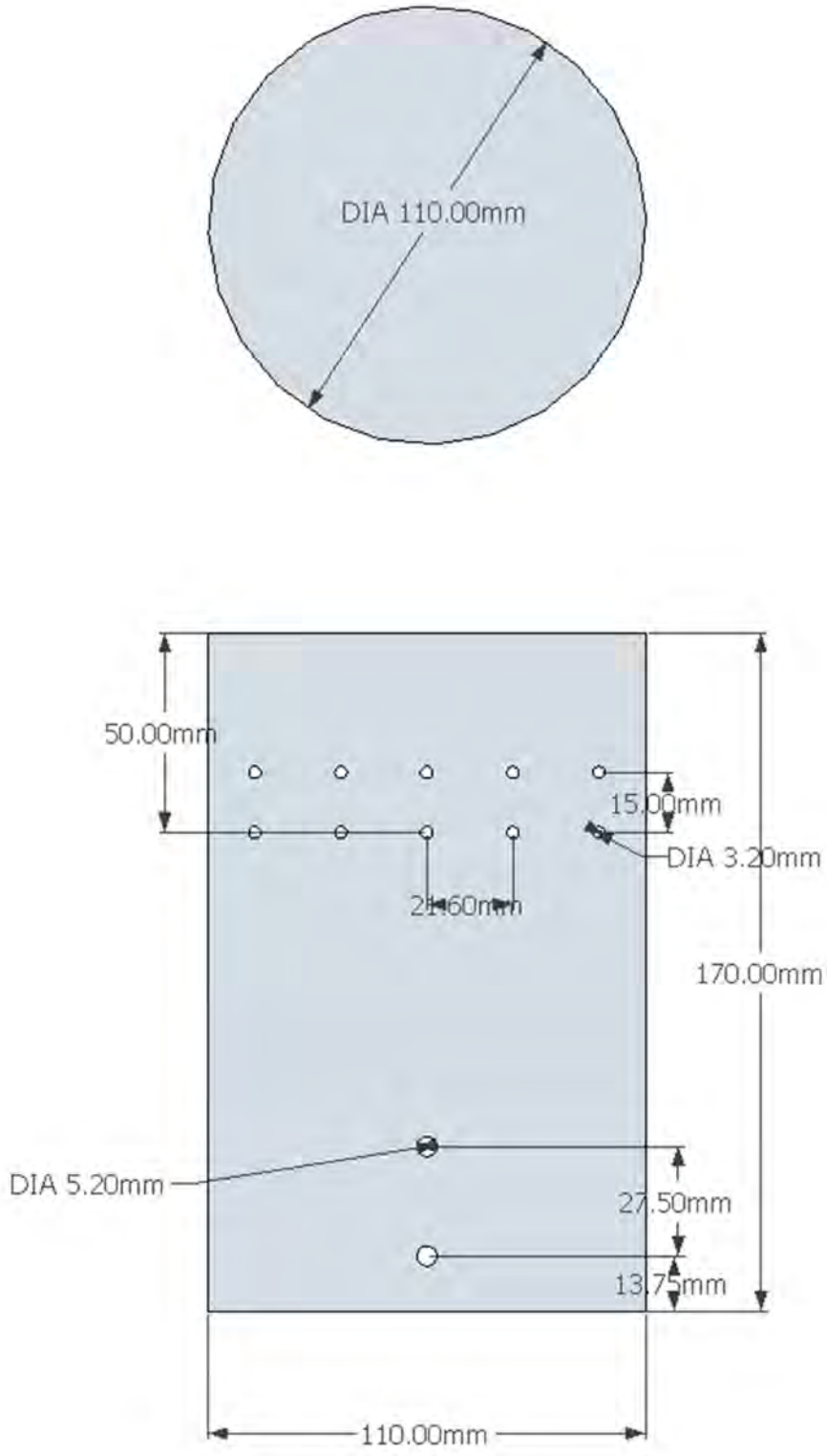

Figure A- 9: Top and front view of the PVC pipe with dimensions included.

Resin Mould

A resin mould is included as a way of better insulating the cable and electrodes. The resin will be poured into the mould through one of the holes on the underside of the mould and the other hole will be used as an outlet for the cables. The mould will be in place while the resin dries off and will be peeled off once the resin is secured around the electrodes and cables. The through holes on the underside of the mould are cantered between the outside and inside layers. They are 22mm from the inside layer and 24mm in diameter. The material used for the resin mould must be such that it will not bond with the resin.

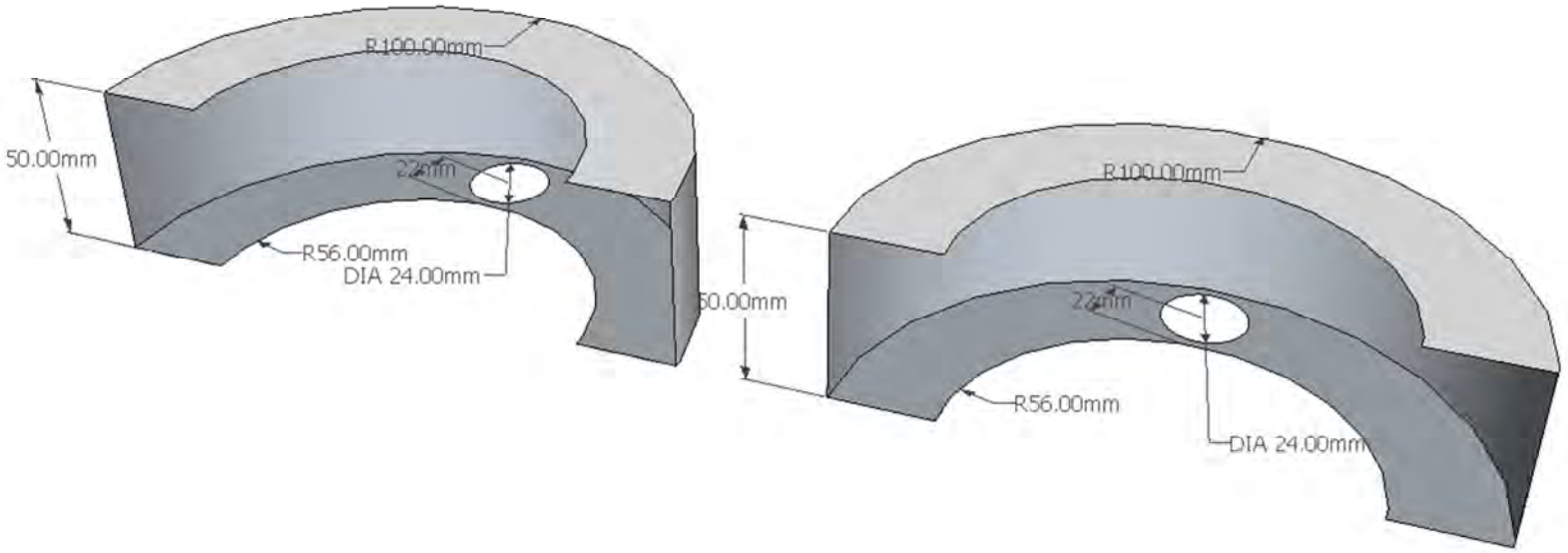

Figure A- 10: Isometric view of the resin mould.

Figure A-11 shows how the components shown above fit together to make up the collar (excluding nuts, bolts and electrode plates).

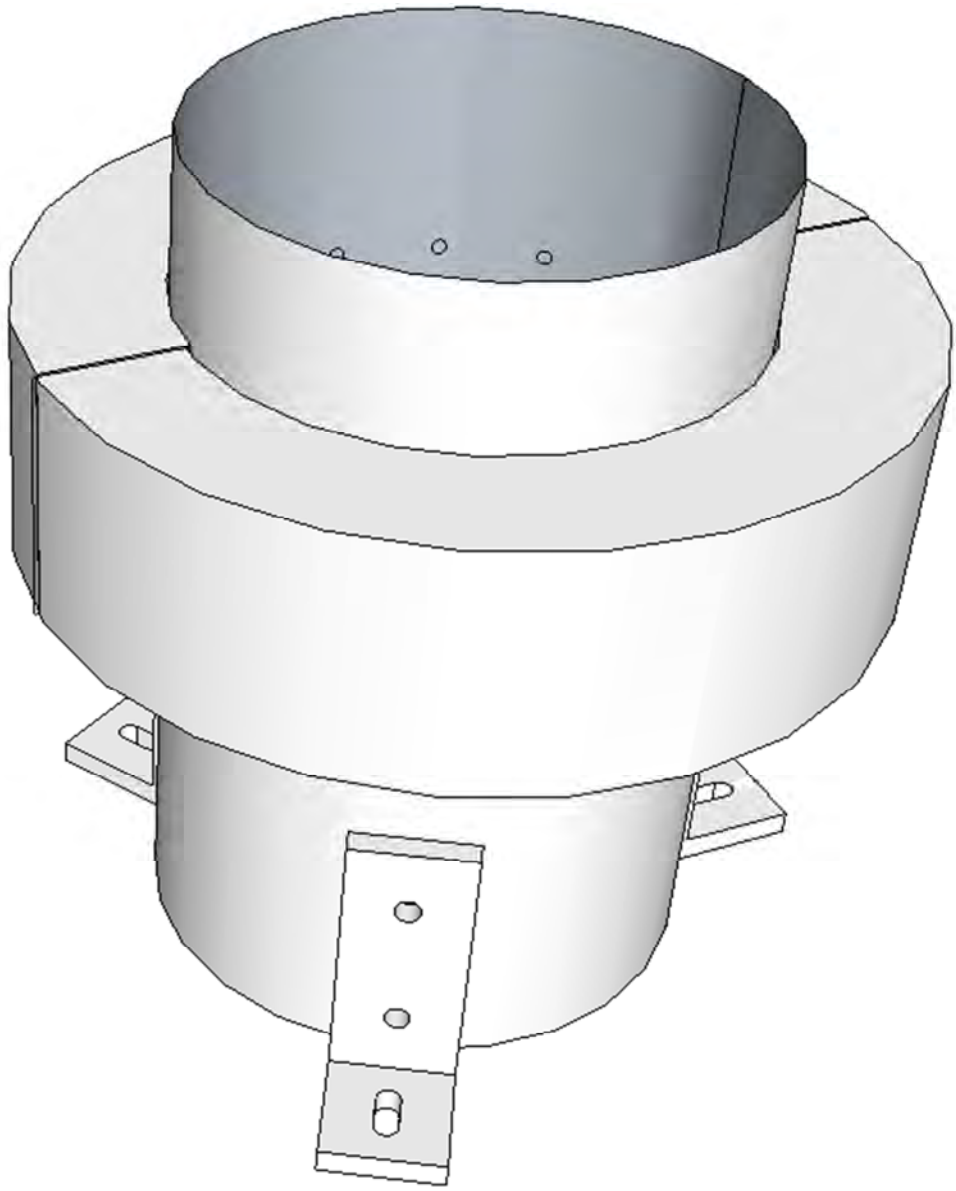

Figure A- 11: Isometric view of all the components

Components List

- ADG5408 x10
- LM317 x10
- 16 pin box headers x20
- 6pin box headers x15
- D_sub 37 Ribbon connector x5
- Relay switch x5
- ADG453BR x5
- LM7815 x5
- LM7915 x5
- LM7824 x5
- LM7924 x5
- 10 to 1 power transformer
- 2.2uF capacitor (electrolytic) x10
- 82 ohm resistor x5
- 220uF capacitor (electrolytic) x5
- 20k ohm potentiometer x5
- 0.33uF capacitor (ceramic) x5
- Ribbon cable 3m
- 3mm ring lugs x50
- 3mm nuts x50
- 5mm nuts x20
- 3mm bolts x50
- 5mm bolts x20

System Manual

DAQ Interface VI

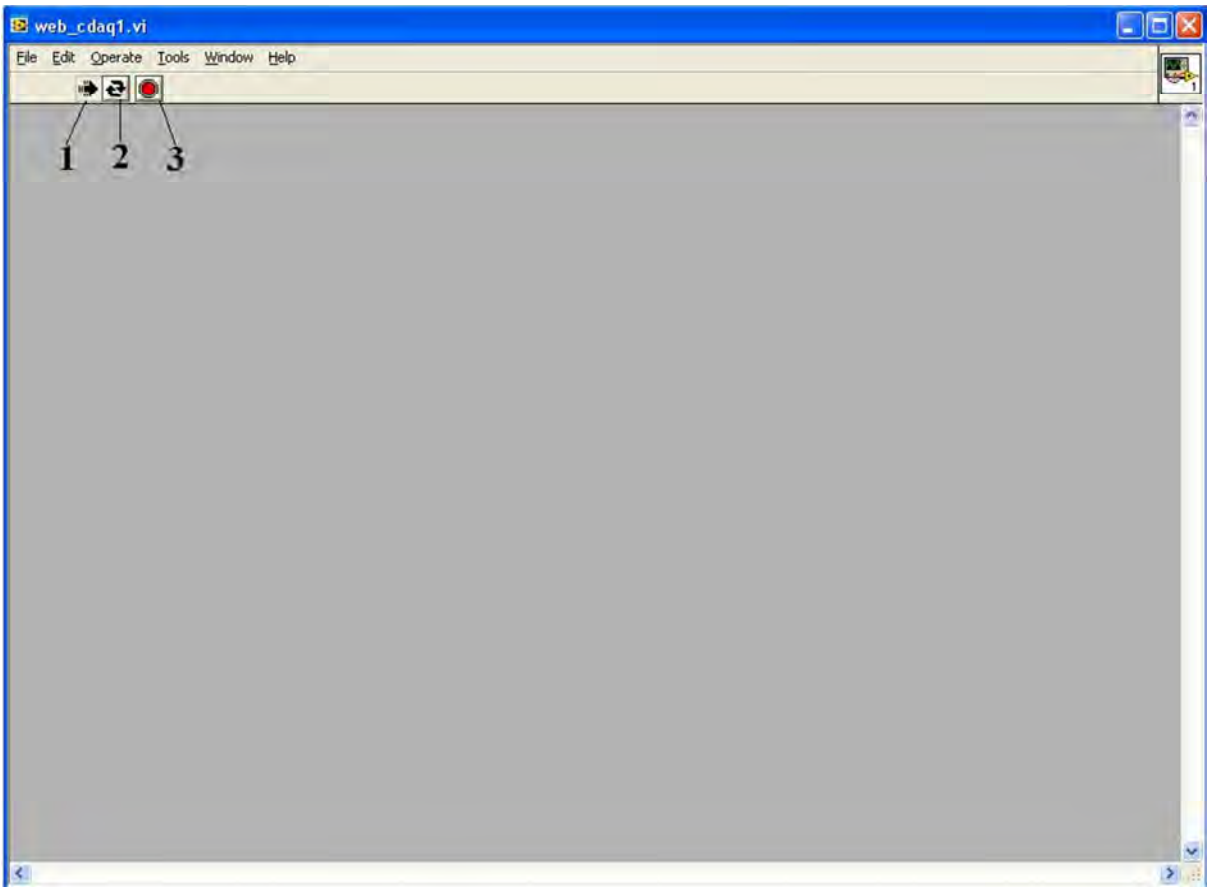

Figure A- 12: Main Application Window

Key:

- Run once
- Run continuously
- Stop

The function of this VI is to interface the cDAQ hardware to the web service and the other VIs. It is important that this VI runs continuously so that the hardware is always accessible; therefore key #2 must be selected in order to control the cDAQ.

Measurements Control VI

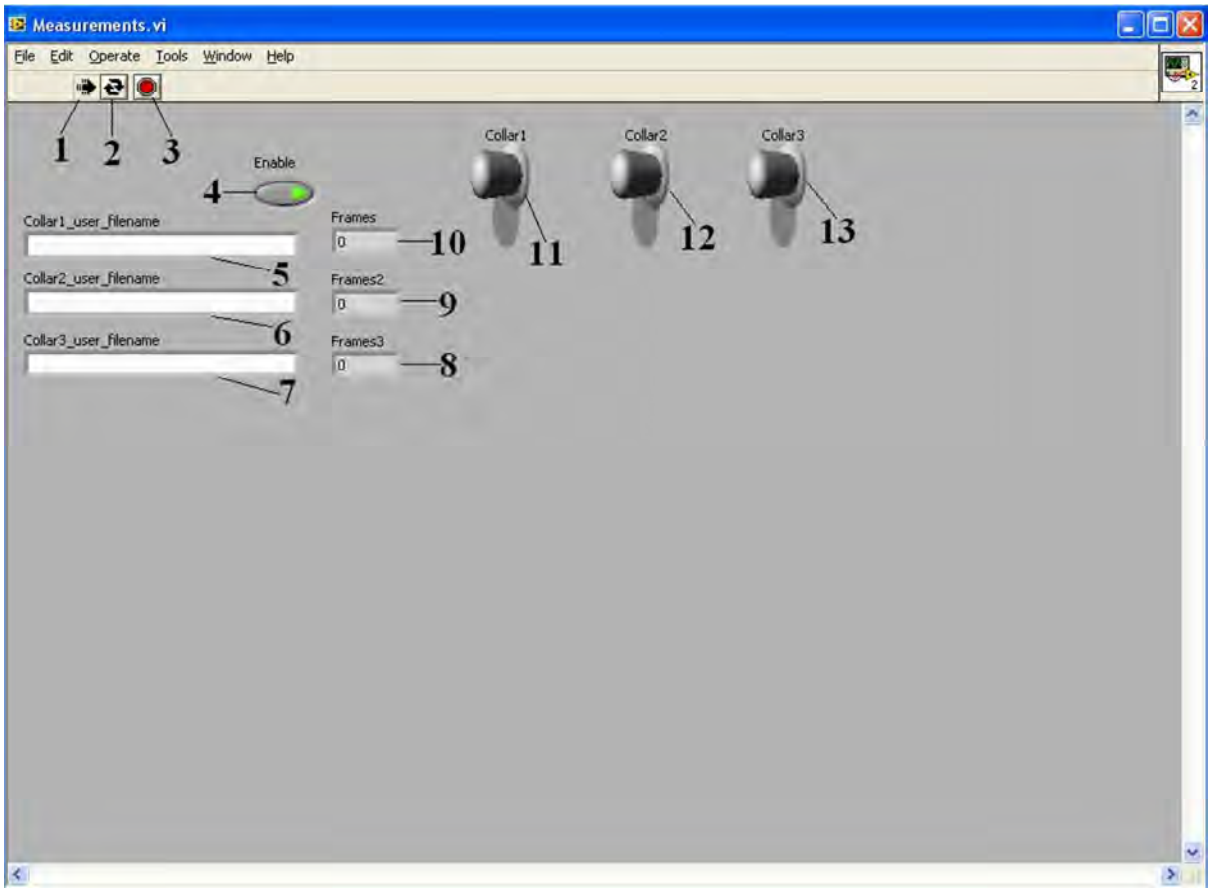

Figure A- 13: Measurements Control Window

Key:

1. Run once
2. Run continuously
3. Stop
4. Enable Switch (green light when True)
5. Textbox: for users to insert a name of their choice as filename for the data collected in Collar 1.
6. Textbox: for users to insert a name of their choice as filename for the data collected in Collar 2.
7. Textbox: for users to insert a name of their choice as filename for the data collected in Collar 3.
8. Frames3: Displays the number frames collected (in Collar 3) for that session.
9. Frames2: Displays the number frames collected (in Collar 2) for that session.
10. Frames: Displays the number frames collected (in Collar 1) for that session.
11. Collar1: Enable switch for Collar 1. Default position is off (Left is Off; Right is on)
12. Collar2: Enable switch for Collar 2. Default position is off (Left is Off; Right is on)

13. Collar3: Enable switch for Collar 3. Default position is off (Left is Off; Right is on)

This VI does not need to be running in other to start and stop measurements from a browser on another PC on the same network. If the user would like to control the measurements by directly using the USFF PC or through remote desktop access to the USFF PC, the following steps should be taken:

1- Check that the Main Application window (web_cdaq1.vi) is running continuously.

2- On the Measurements Window: Click the Enable switch (green light on means enabled)

3- Click on any of the 3 Collar switches to enable them. Refer to key 11, 12 or 13 above to make sure the switch is in the desired state.

4- Type a name of your choice in 5, 6 or 7 if you wish to insert a specific name as the filename of the text file created to store the data collected. Otherwise leave it blank and the filename will simply be a timestamp of the moment the data collection began.

5- Run the application once or continuously. Refer to key 1 or 2 above. Note that if the application is run once, any changes made on the user interface will not be applied unless the run the application once button is clicked after the changes have been made. Running the application continuously immediately applies any changes made to the user interface.

6- To disable all measurements across all collars simultaneously click the Enable switch (green light off means disabled)

7- To stop the recording of data on a specific collar simply click on that collar's switch. Refer to key 11, 12 or 13.

Image Reconstruction VI

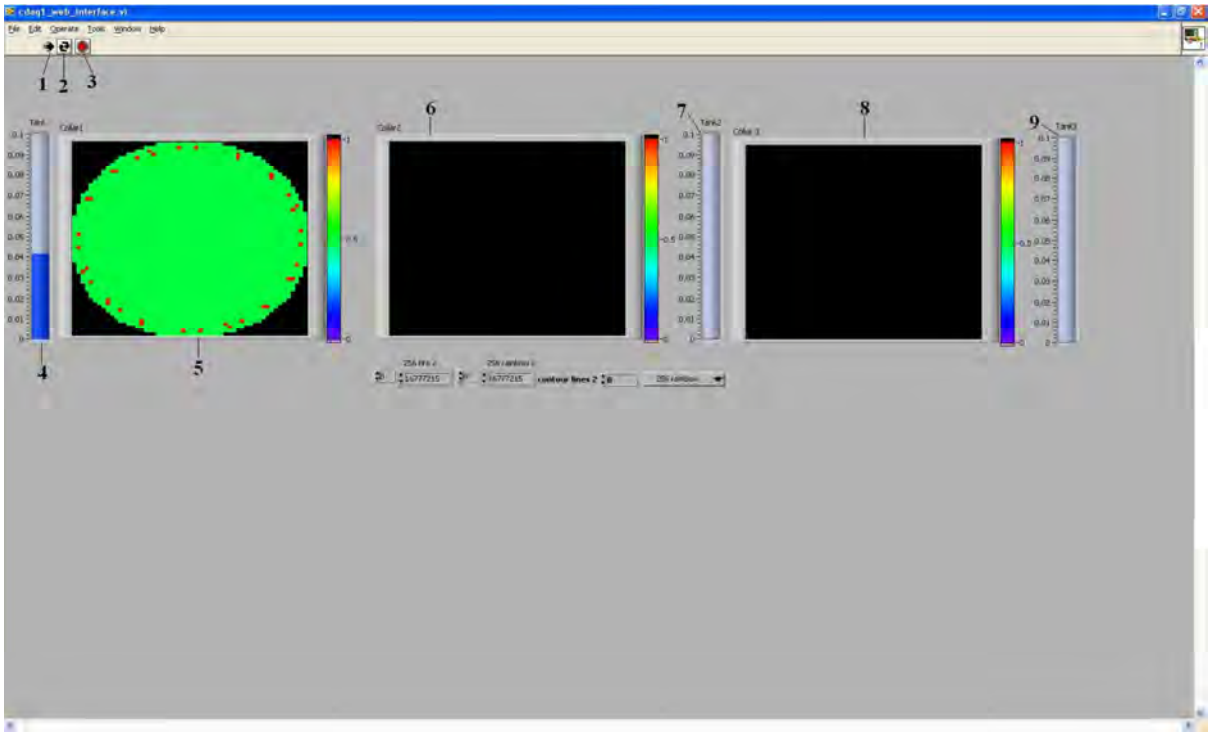

Figure A- 14: Reconstructed image window

Key:

1- Run once

2- Run continuously

3- Stop

4- Tank: To adjust sensitivity level in Collar 1. Also used to supress noise in the system so that changes due to resistance of the massecuite changing is amplified over subtle changes due to noise. Default for massecuite is 0.045

5- Collar1: Reconstructed image of Collar 1 is displayed here

6- Collar2: Reconstructed image of Collar 2 is displayed here

7- Tank 2: To adjust sensitivity level in Collar 2. Also used to supress noise in the system so that changes due to resistance of the massecuite changing is amplified over subtle changes due to noise. Default for massecuite is 0.045

8- Collar3: Reconstructed image of Collar 3 is displayed here

9- Tank 3: To adjust sensitivity level in Collar 3. Also used to supress noise in the system so that changes due to resistance of the massecuite changing is amplified over subtle changes due to noise. Default for massecuite is 0.045

To reconstruct image from the data collected as soon as it is ready, simply run the application continuously. Refer to key 2. If a Collar has been disabled in the Measurements.vi window then no image will be displayed for that Collar.

Live Data VI

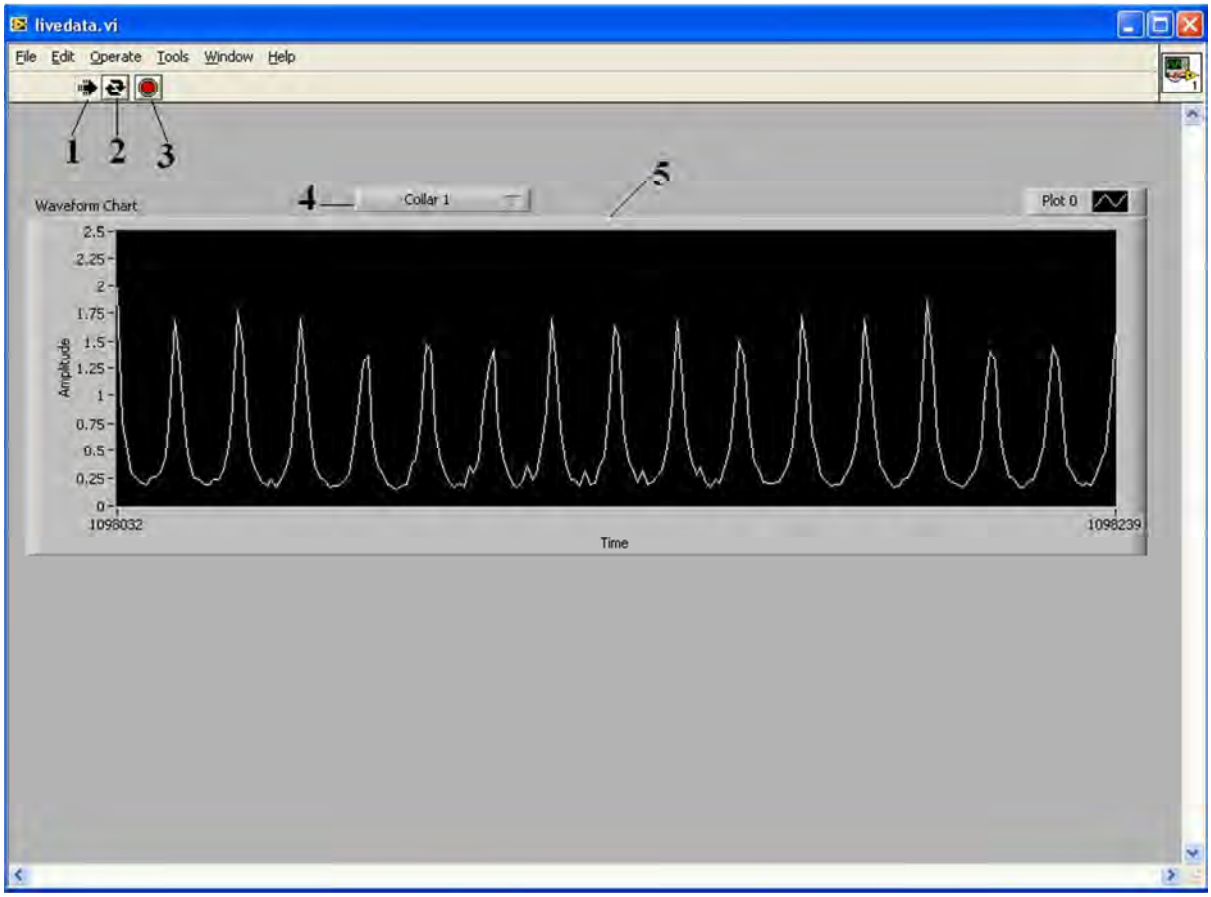

Figure A- 15: Live data window

Key:

1. Run once
2. Run continuously
3. Stop
4. Drop down select: User can select the Collar from which they'd like to view data. There are 3 options: Collar 1, Collar2 and Collar3.
5. Waveform Chart: Displays the Characteristic U-shaped curve when the data collected is not faulty or erroneous.

This VI was created for debugging purposes. To plot data as soon as they have been collected follow these steps:

1- Check that the main window (web_cdaq1.vi) is continuously running
2- Check that the Enable switch (key #4) on the Measurement Control window is enabled (green light on).
3- Check that the Collar whose data you'd like to view is enabled. Refer to key #11, #12 and #13 on measurement control window.
4- Select the desired Collar from key #4 on the Live data window.
5- Select key #2 to run the application continuously. The data collected from the collar will be plotted and will be displayed on the waveform chart (Key #5). The waveform should update approximately every second.

The 208 data points that make up one image frame are seen above as well as the Characteristic U-shaped curves. This live view of the data collected can help to speed up the debugging process if a cable is no longer continuous or an electrode is faulty.

Web Interface

Figure A- 16: Web User Interface

Key:

1- Switch: Start/Stop Measurements

2- Collar 1: User enters filename for Collar 1 text file here.

3- Collar 2: User enters filename for Collar 2 text file here.

4- Collar 3: User enters filename for Collar 3 text file here.

5- Stop button: Terminate session.

6- Frame: Displays the number of frames that have been recorded in the current session.

7- Tomograph of Collar 1: Displays Collar 1's reconstructed image.

8- Switch: Enables/Disables Collar 1.

9- Slider: Sensitivity control for collar 1.

10- Frame Collar 2: Displays the number of frames that have been recorded in the current session.

11- Tomograph of Collar 2: Displays Collar 2's reconstructed image.

12- Switch2: Enables/Disables Collar 2.

13- Slider2: Sensitivity control for collar 2.

14- Frame Collar 2: Displays the number of frames that have been recorded in the current session.

15- Tomograph of Collar 3: Displays Collar 3's reconstructed image.

16- Switch3: Enables/Disables Collar 3.

17- Slider3: Sensitivity control for collar 3.

The Web user interface allows a user on the same network as the USFF PC to start and stop measurements and to also view the reconstructed images as they are being reconstructed. All measurements taken from each collar is stored for later viewing or analysis. The following steps indicate how to go about starting and stopping measurements as well as viewing the reconstructed image:

1- Type the USFF PC's IP address into a web browser of a PC on the same network.

2- The User Interface in Figure A-5 will appear

3- Click the start measurements button (green light is on when measurement has started). Refer to key #1

4- Type the name you wish to call the text files of Collar 1, 2 and/or 3 into the relevant textboxes. Refer to keys #2, #3 and/or #4.

5- Click on any of the Collar switches (refer to keys #8, #12, #16) to switch them from the off position to the on position and enable data collection for that Collar.

6- Once data collection is enabled the Image reconstruction begins and the last image reconstructed is seen on each of the displays. Refer to keys #7, #11, #15

7- When the switches (refer to keys #8, #12, #16) are in the on position; Frame, Frame Collar 2 and Frame Collar 3 display the frame number of the image currently being displayed.

8- To stop data collection on a collar; simply click the relevant switch (refer to keys #8, #12, #16) to switch it to the off position.

9- When any of the switches are transitioned from the off to the on position a new text file is created with the current timestamp and the content of the Collar1, Collar2 and/or Collar 3 textboxes concatenated to be the name of the text file.

10- To stop the entire measurement and image reconstruction process, click the Start/Stop switch (green light is off when measurement is stopped). Refer to key #1.